THE UNIVERSITY OF TULSA
THE GRADUATE SCHOOL

# Assessment of Uncertainty Assessment Methods

by
Ning Liu

A thesis submitted in partial fulfillment of
the requirements for the degree of Master of Science
in the Discipline of Petroleum Engineering
The Graduate School
The University of Tulsa
2001

THE UNIVERSITY OF TULSA

THE GRADUATE SCHOOL

Assessment of Uncertainty Assessment Methods

by

Ning Liu

A THESIS

APPROVED FOR THE DISCIPLINE OF

PETROLEUM ENGINEERING

By Thesis Committee

_____ Chairperson

_____

_____

# ABSTRACT

Ning Liu (Master of Science in Petroleum Engineering)

Assessment of Uncertainty Assessment Methods

(96 pp.-Chapter VIII)

Directed by Dr. Dean S. Oliver

(332 words)

Uncertainty in future reservoir performance is usually evaluated from the simulated performance of a small sampling of reservoir models. Unfortunately, most of the methods for generating reservoir models conditional to production data are known to create distributions of realizations that are only approximately correct. The adequacy of the approximations is unknown, although several previous investigations of the approximate algorithms have suggested that the distributions of realizations could be badly misleading. In this study, I investigated seven sampling algorithms and evaluated the ability of the various sampling methods to correctly assess the uncertainty in reservoir predictions by comparing the distribution of realizations with a standard distribution from a Markov chain Monte Carlo method.

This study compares the ensemble of realizations from seven sampling algorithms for a synthetic, one-dimensional, single-phase flow problem, in order to establish the best algorithm under controlled conditions. The small test problem was chosen in order that a large enough number of realizations could be generated from each method to ensure the statistical validity of the comparisons. The approximate sampling methods evaluated were linearization about the maximum a posteriori model (the square-root of the covariance matrix method), randomized

maximum likelihood, two pilot point methods with six and nine pilot points locations and gradual deformation method. Five thousand realizations were generated from each of the approximate sampling algorithms except for the gradual deformation method. Realizations were also generated by a Markov chain Monte Carlo method with local perturbations and an attempt was made to generate realizations from a rejection sampling algorithm. The distributions of realizations from the approximate methods were compared to the distributions from the exact methods. While the approximate sampling methods performed relatively well for evaluating uncertainty in average reservoir porosity and effective steady-state permeability, most failed to adequately assess uncertainty in some other function of the reservoir model such as the distribution of extreme permeability values or the data mismatch. In general, the method of randomized maximum likelihood performed better than other approximate methods.

TABLE OF CONTENTS

**LIST OF FIGURES** **vi**

**LIST OF TABLES** **xiv**

**CHAPTER 1: INTRODUCTION** **1**

1.1 Background . . . . . 1

1.2 Literature Review . . . . . 3

1.3 Objective Statement . . . . . 9

**CHAPTER 2: MODEL DEFINITION** **11**

2.1 Bayes Theorem . . . . . 11

2.2 The Prior Model . . . . . 12

2.3 The Maximum A Posteriori Estimate . . . . . 13

2.4 Computation of Sensitivity Coefficients . . . . . 15

**CHAPTER 3: ESTABLISHMENT OF A STANDARD DISTRIBUTION FOR COMPARISON** **17**

3.1 Acceptance-Rejection Sampling . . . . . 17

3.2 Markov chain Monte Carlo . . . . . 18

**CHAPTER 4: APPROXIMATE METHODS OF SAMPLING** **23**

4.1 Linearization about the MAP. . . . . 23

4.2 Randomized Maximum Likelihood. . . . . 25
4.3 Pilot Point Methods. . . . . 26
4.4 Gradual Deformation Method. . . . . 27

**CHAPTER 5: EXPERIMENTAL DESIGN** **30**

**CHAPTER 6: RESULTS** **33**

6.1 Rejection . . . . . 34
6.2 McMC-algorithm . . . . . 35
6.3 Linearization about the MAP . . . . . 38
6.4 Randomized Maximum Likelihood . . . . . 38
6.5 Pilot Point methods . . . . . 48
6.6 Gradual Deformation . . . . . 49
6.7 Comparison . . . . . 50

**CHAPTER 7: DISCUSSION** **56**

**CHAPTER 8: CONCLUSIONS** **69**

**APPENDIX A:** **79**

**APPENDIX B:** **84**

**APPENDIX C:** **89**

**APPENDIX D:** **97**

LIST OF FIGURES

3.1 Every 1000th model from the first "short chain" of $10^6$ models was used to generate $f_1$ and $S_m$ (distance from the prior). The chain of values of $S_m$ shows quite long correlation lengths although this might not be guessed from the chain of values of $f_1$. Neither, however, seem to show evidence of a transition period at the beginning of the chain. 21

3.2 The realizations of $k_{\text{eff}}$ in (a) and of $S(m)$ in (b) are from the same chain. The mixing seems to be rapid in (a) but (b) shows a long correlation range. . . . . 21

3.3 A very long sequence of realizations of $S(m)$ showing slow mixing and an apparent correlation length on the order of 100 million iterations. . 22

5.1 The true synthetic permeability and porosity fields, used to generate pressure data to test the sampling algorithms. Well locations are shown by solid bars along the base of the figure. . . . . 31

5.2 The observed pressure drop data at all wells. Random noise added to the true pressure drop causes the nonphysical appearance at low values of $\Delta p$. . . . . 32

5.3 The maximum a posteriori estimates of permeability and porosity. . . 32

6.1 Histograms for properties of 419 realizations from rejection method with $A = C_{\text{M}'}$ and $f(m_{\text{map}})/(c\,h(m_{\text{map}})) = 1$ . . . . . 36

6.2 Histograms for properties of 20 one-million-iteration McMC sequences. 39
6.3 Histograms for properties of 20 two-million-iteration McMC sequences. 40
6.4 Histograms for properties of 20 four-million-iteration McMC sequences. 41
6.5 Histograms for properties of the single forty-million-iteration McMC sequences. The first realization of RML method was used individually as the initial element. . . . . 42
6.6 Histograms for properties of the single forty-million-iteration McMC sequences. The second realization of RML method was used individually as the initial element. . . . . 43
6.7 Histograms for properties of the single eighty-million-iteration McMC sequences. . . . . 44
6.8 Histograms for functionals in McMC with 320 million iterations in one chain. The first realization of RML method was used individually as the initial element. . . . . 45
6.9 Histograms for functionals in McMC with 320 million iterations in one chain. The second realization of RML method was used individually as the initial element. . . . . 46
6.10 The first 10 realizations of the permeability field and porosity field conditioned to pressure data and the true permeability field and porosity field (heavy black line). . . . . 47
6.11 The first 10 realizations of the permeability field conditioned to pressure data and the true permeability field (heavy black line). . . . . 48
6.12 The $Z$ values at the 3rd, the 7th and the 15th gridblocks change with the number of iterations using gradual deformation with global perturbation. . . . . 51

6.13 The $Z$ values at the 3rd, the 7th and the 15th gridblocks change with the number of iterations using gradual deformation with local perturbation. . . . . 52
6.14 Key for interpretation of box plots. P values are percentiles. . . . . 52
6.15 Distributions of conditional realizations of effective permeability, average porosity, and maximum permeability from the approximate sampling algorithms and from the two very long Markov chains starting from the first and the second RML realizations. The unconditional distribution and the true values are shown for comparison. . . . . 54
6.16 Distributions of conditional realizations of squared data mismatch and squared model mismatch from the approximate sampling algorithms and from the two very long Markov chains starting from the first and the second RML realizations. Note that the unconditional realizations of the data mismatch are too large to appear on this plot. . . . . 55

7.1 Distributions of P10, P50 and P90 of the 320 million McMC realizations. The whole distribution is shown for comparison. . . . . 61
7.2 Distributions of P10, P50 and P90 of the 5000 RML realizations. The whole distribution is shown for comparison. . . . . 62
7.3 The posteriori pdf for the single-phase flow problem appears to have a plateau instead of a single peak. The minima shown as black dots are connected by a valley. . . . . 63
7.4 The posteriori pdf for the single-phase flow problem appears to have a plateau instead of a single peak. The minima shown as black dots are connected by a valley. . . . . 64

7.5 Distributions of conditional realizations of squared data mismatch from five different Markov chains. The distribution from randomized maximum likelihood is shown for comparison. McMCVL1 is the very long chain (320 million iterations) starting from the first RML realization; McMCVL2 is the 320 million iterations long chain starting from the second RML realization; McMCMS means multiple short chains (each of which is 2 million iterations in length); McMC80M means one chain of 80 million iterations; McMC40M means one chain of 40 million iterations. . . . . 65

7.6 Distributions of conditional realizations of the maximum permeability from five different Markov chains. The distribution from randomized maximum likelihood is shown for comparison. McMCVL1 is the very long chain (320 million iterations) starting from the first RML realization; McMCVL2 is the 320 million iterations long chain starting from the second RML realization; McMCMS means multiple short chains (each of which is 2 million iterations in length); McMC80M means one chain of 80 million iterations; McMC40M means one chain of 40 million iterations. . . . . 66

7.7 Distributions of conditional realizations of the squared model mismatch about the MAP estimate from five different Markov chains. The distribution from randomized maximum likelihood is shown for comparison. McMCVL1 is the very long chain (320 million iterations) starting from the first RML realization; McMCVL2 is the 320 million iterations long chain starting from the second RML realization; McMCMS means multiple short chains (each of which is 2 million iterations in length); McMC80M means one chain of 80 million iterations; McMC40M means one chain of 40 million iterations. . . . . 67
7.8 The shape of squared data mismatch function at the 1st (left) and 1000th (right) iteration by gradual deformation algorithm. . . . . 68

A.1 Every 40,000th model from the chain of 40 million models was used to generate effective permeability and average porosity. The initial model was a RML realization. No evidence of a transition period is shown at the beginning of the chain. . . . . 80
A.2 Every 40,000th model from the chain of 40 million models was used to generate the maximum permeability and the minimum permeability. The initial model was a RML realization. No evidence of a transition period is shown at the beginning of the chain. . . . . 81
A.3 Every 40,000th model from the chain of 40 million models was used to generate travel time and squared data mismatch. The initial model was a RML realization. No evidence of a transition period is shown at the beginning of the chain. . . . . 82

A.4 Every 40,000th model from the chain of 40 million models was used to generate the squared model mismatch about the prior model and about the MAP estimate. The initial model was a RML realization. No evidence of a transition period is shown at the beginning of the chain. . . . . 83

B.1 The comparison of histograms of maximum permeability from a variety of McMC sequences with different length and number of chains. 85
B.2 The comparison of histograms of minimum permeability from a variety of McMC sequences with different length and number of chains. . 86
B.3 The comparison of histograms of squared model mismatch about the prior model from a variety of McMC sequences with different length and number of chains. . . . . 87
B.4 The comparison of histograms of squared model mismatch about the MAP estimate from a variety of McMC sequences with different length and number of chains. . . . . 88

C.1 Histograms for the properties of 5000 LMAP realizations sampled from the test problem. . . . . 90
C.2 Histograms for the properties of 5000 RML realizations sampled from the test problem. . . . . 91
C.3 Histograms for the properties of 5000 realizations sampled from the test problem by the pilot point method with six pilot point locations in the field and using a full objective function. . . . . 92

C.4 Histograms for the properties of 5000 realizations sampled from the test problem by the pilot point method with six pilot point locations in the field and using the objective function with only squared data mismatch part. . . . . 93
C.5 Histograms for the properties of 5000 realizations sampled from the test problem by the pilot point method with nine pilot point locations in the field and using a full objective function. . . . . 94
C.6 Histograms for the properties of 5000 realizations sampled from the test problem by the pilot point method with nine pilot point locations in the field and using the objective function with only squared data mismatch part. . . . . 95
C.7 Histograms for the properties of realizations sampled from the test problem by the gradual deformation method with global perturbation. 96

D.1 The comparison of histograms of effective permeability from a variety of sampling methods. . . . . 98
D.2 The comparison of histograms of average porosity from a variety of sampling methods. . . . . 99
D.3 The comparison of histograms of travel time from a variety of sampling methods. . . . . 100
D.4 The comparison of histograms of maximum permeability from a variety of sampling methods. . . . . 101
D.5 The comparison of histograms of minimum permeability from a variety of sampling methods. . . . . 102
D.6 The comparison of histograms of squared model mismatch about the prior model from a variety of sampling methods. . . . . 103

D.7 The comparison of histograms of squared model mismatch about the MAP estimate from a variety of sampling methods. . . . . 104
D.8 The comparison of histograms of squared data mismatch from a variety of sampling methods. . . . . 105

LIST OF TABLES

8.1 The true permeability and porosity fields. . . . . 70
8.2 True Pressure data and observed pressure. . . . . 71

# ACKNOWLEDGMENTS

I would like to thank my advisor Dr. Dean Oliver for his support, patience, guidance and insights during my M.S. research in The University of Tulsa. I also would like to express appreciation to Dr. Albert Reynolds and Dr. Richard Redner for serving on my committee. Their instructions, critiques and suggestions are deeply appreciated.

My appreciation extends to all the people in the Department of Petroleum Engineering, who have helped me a lot in different ways, and made my life at TU enjoyable. Special appreciation is extended to all my friends who have provided their encouragement and support since the beginning of my graduate study. I am thankful to Judy Teal for her care and assistance.

This work is dedicated to my parents, Fenghua Liu and Yingqiu Liu, for their guidance and unconditional love.

# CHAPTER I

# INTRODUCTION

## 1.1 Background

Prediction of the reservoir variables is necessary for making appropriate and successful investments and for reducing risk in the development and construction of an oilfield. When forecasting production for a given depletion strategy, when applying an optimization strategy with respect to some recovery criterion, and also when making decisions concerning infill drilling, the essential requirement is being able to predict the underground resource distribution. This is accomplished by running a reservoir simulation program with reservoir models reproducing historic production data given the same operating conditions. In a petroleum reservoir, the most important reservoir model parameters for determining production performance are the gridblock permeabilities and porosities, skin factors, and relative permeabilities of the fluids. Historic production data typically used in this procedure include wellbore pressure, gas-oil ratio and water-oil ratio.

As petroleum reservoirs are generally thousands of feet underground, reservoir parameters can not be measured directly except at well locations. The means to derive reservoir parameters based on historic production data is an inverse procedure. Usually, inverse problems are underdetermined, thus have non-unique solutions. Various algorithms have been developed to estimate the probability density function (pdf) of reservoir property fields based on historic production data.

The future production performance of a gas and oil reservoir is usually evalu-

ated by generating a series of reservoir realizations conditional to historic production data and simulating future performance of each. By simulating the future production from each realization, an empirical distribution of production characteristics is obtained. The validity of the Monte Carlo method for quantifying uncertainty depends on the quality of the distribution of reservoir models generated. Rigorous methods for sampling from the a posteriori probability density function (pdf) of reservoir flow models conditioned to production data have been discussed by Hegstad and Omre (1996), Oliver et al. (1997), Bonet-Cunha et al. (1998), Hegstad and Omre (1999), Holden et al. (2001), and Omre (2001). Most other attempts to quantify uncertainty in reservoir performance are based on approximate sampling algorithms. The purpose of this study is to evaluate the distribution of samples from several of these approximate methods.

The methods evaluated here belong to two types: those that are known to sample correctly and those that are only approximately correct. In the first category, I consider the rejection algorithm (REJ) and a Markov chain Monte Carlo algorithm (McMC). The four approximate methods I consider are linearization about the maximum a posteriori model (LMAP), randomized maximum likelihood (RML), pilot point methods (PP) with six and nine pilot points locations, and gradual deformation method (GD). Each of these methods was used to generate a large number of reservoir realizations from a single-phase, one-dimensional synthetic problem, where the observed data were in the form of dynamic pressure and the unknown reservoir characteristics were the porosity and permeability of each gridblock.

This work contains eight chapters. Chapter 1 provides an overview of theoretical development and states the necessity of carrying out this work. Chapter 2 briefly describes the inverse theory. It includes introductions to Bayes theory, the construction of the MAP estimate, the computation of sensitivity coefficients and the Gauss-Newton and Levenberg-Marquardt algorithms. Chapter 3 presents two standard algorithms, Markov chain Monte Carlo (McMC) and rejection (RJ) sampling

from the posteriori distribution of the objective function. In Chapter 4, I investigate four of the most popular approximate algorithms, the linearization about the maximum a posteriori estimate method, the randomized maximum likelihood method, the pilot point methods and the gradual deformation method. Chapter 5 describes the synthetic test problem designed for this research. Realizations are then generated using each of the sampling methods described in the previous chapter. The results from each of the methods are shown in Chapter 6. In that chapter, I also compare the results from approximate methods with those from the rigorous methods. Chapter 7 presents the analysis of the results based on the methods comparison in Chapter 6. Conclusions are made in Chapter 8 regarding the sampling validity and efficiency of each approximate method.

## 1.2 Literature Review

Characterizing the reservoir variables given well observations and production data is an ill-posed inverse problem. Realistic reservoir problems tend to be quite complex, and the number of parameters is often very large so that methods for solving small problems may not work well for reservoir characteristic problems. Moreover, the connection between reservoir variables and observed production data is highly nonlinear so the partial differential equations can only be solved numerically.

Most approaches in solving this kind of problem belong to one of two categories. One category contains approaches that generate a "rough" property field (an unconditional realization), then add on a smooth correction. Journel and Huijbregts (1978) described this approach for linear problems without accounting for measurement errors in data. When the observations have errors, the approach is similar, except the simulation need not honor the data exactly (Oliver, 1996b). These methods have been applied to nonlinear problems in petroleum engineering and ground

water hydrology by Chu et al. (1995) and RamaRao et al. (1995) among others. In the study by Chu et al. (1995), an unconditional realization was generated from the prior distribution, then a Gauss-Newton procedure was applied to minimize the difference between observed and calculated data, while still remaining close to the unconditional realization. The calibration of each realization requires solving a history matching problem. Justification for the application of this methodology to nonlinear problems was provided by Oliver et al. (1996) and Kitanidis (1995).

The second category contains methods in which "roughness" is added to a smooth, optimal property field. The "roughness" is a stochastic component usually obtained from the square root decomposition of the estimation error covariance. Although the method is quite old (Scheuer and Stoller, 1962), it was first applied to linear problems in petroleum engineering by Davis (1987) and Alabert (1987). Dietrich and Newsam (1995) described a relatively efficient method that uses Chebychev polynomial approximations to calculate the square root of the covariance matrix for large reservoir model problems. This kind of method can be very efficient since only one history matching process is required in the whole process to calculate the optimal estimate, i.e. the maximum a posteriori (MAP) solution. Clifton and Neuman (1982) applied this approach to generate multiple (300) realizations of the 2D transmissivity field of the Avra Valley in Arizona with the square root of the error covariance computed by the Cholesky method. The pressure head was assumed to be linearly related to the transmissivity in this study. Chu et al. (1995) and Oliver (1996a) applied this approach to the generation of conditional permeability realizations for nonlinear single-phase problems in petroleum engineering.

The sampling methods can also be categorized another way: those are known to sample from the true posteriori distribution and those are only approximately correct. The exact methods I discuss in this work are the rejection method and Markov chain Monte Carlo. Both of the two standard methods involve a criterion for accepting or rejecting realizations generated from a stochastic process. The

efficiency of the rejection algorithm depends critically on the ability to find a proposal function that is close to the target probability density function. In practice, however, the posterior density function is difficult to evaluate and sometimes has multiple local minima. Hence, the rejection algorithm is generally slow and inefficient when applied to reservoir history matching problems. General background on rejection algorithm for conditional simulation can be obtained from Ripley (1987) and Gilks et al. (1996b). Hegstad and Omre (1999) and Holden et al. (2001) have applied the rejection algorithm to reservoir characterization problems.

In earlier work, people applied Markov chain Monte Carlo methods by swapping permeability values in two randomly chosen gridblocks (see Farmer (1992), Deutsch (1992), Sagar et al. (1993)). This is an inefficient algorithm for correlated property fields and realizations generated were not realistic. Rather than swapping gridblock values, Oliver et al. (1997) used proposed transitions that were based on the covariance structure and symmetric, then the acceptance is only based on the ratio of the probability of being in the adjacent two states. If the proposed transition is rejected, the old state is repeated in the chain.

In this thesis, I investigate four of the most popular approximate methods: linearization about the maximum a posteriori model (LMAP), randomized maximum likelihood (RML), pilot point methods (PP) and gradual deformation (GD) method.

Linearization about the maximum a posteriori model is a typical method of adding a "rough" correction to the MAP model. Oliver (1996a) used models which are linearized about the maximum likelihood point, to generate multiple realizations of the permeability field that are approximately conditioned to well test data, point measurements of permeability, and the variogram. Chu et al. (2000) used the LMAP method to generate conditional realizations, while improving the method for computing the square root of the a posteriori covariance matrix. Later investigations showed that very few of the approximate realizations from LMAP actually honored the pressure data. The method has also been used to generate candidate

models for Markov chain Monte Carlo algorithms, in which case the candidates with poor pressure matches are rejected. Oliver et al. (1997) found, however, that when the permeability variation is large, the method can be very inefficient for nonlinear problems related to fluid flow in porous media.

The randomized maximum likelihood (RML) method was proposed independently by Kitanidis (1995) and Oliver et al. (1996) for conditional reservoir simulation. It is an approximate algorithm in the general case but can be shown to be rigorous for Gaussian random fields when the data are linearly related to the model parameters and when the errors in the data are normally distributed (Oliver, 1996b). Oliver et al. (1996) originally suggested that this method be used to generate trial states for an McMC algorithm but, because the acceptance criterion was difficult to evaluate and the acceptance rate was very high (approximately 95% for a small highly nonlinear problem), they suggested that the acceptance test be ignored and all trials accepted. Although Oliver et al. (1996) showed that RML did a reasonably good job of sampling a multimodal univariate distribution, the sampling properties for multivariate nonlinear problems was largely unknown. Because the method seeks to minimize the data mismatch and the distance from the unconditional realization, the realizations almost surely honor the data and appear to be from the correct distribution. Similar methods have also been used by RamaRao et al. (1995) and Gómez-Hernández et al. (1997) to condition permeability fields to pressure data. Although the distribution of realizations has been questioned by Floris et al. (2001), the method has been shown to do a good job of sampling from the a posteriori distribution for a highly nonlinear low dimensional problem (Liu et al., 2001).

The pilot point methods are actually methods of parameterization of the reservoir property field. They were developed in order to reduce the dimension of the history matching problem. In pilot point methods, reservoir properties are calculated in a small number of locations and then interpolation is used to assign values to the remaining grid blocks. RamaRao et al. (1995) applied kriging as the interpolation

method. Gómez-Hernández et al. (1997) discussed the method of generating "equally likely" realizations of the transmissivity field that are conditional to transmissivity and head measurements. They used the method of "master points" which, except for the location of pilot points, seems to be identical to the pilot point method described in the RamaRao et al. (1995) papers. They generate a realization that is conditional to transmissivity, then use a kriged interpolation through the pilot points to correct the surface. Using this method, they attempted to find the transmissivity field that is closest to the original and honors the data.

It is not known whether or not the recently developed method of gradual deformation (Roggero and Hu, 1998) is an approximate method or if it actually generates realizations that are distributed correctly. It is a method for gradually deforming continuous geostatistical models to generate reservoir models which honor historic production data. This algorithm has been used by Hu et al. (1999) to incorporate historic production data to reduce uncertainty in production forecasts. Because the gradual deformation algorithm preserves the geostatistical parameters (covariance model and range) while deforming the model to honor the data, it seems intuitive that it might generate realizations from the probability density function (pdf) for model variables conditioned to data.

In addition to the methods described above, several other optimization methods such as simulated annealing and the genetic algorithm have been used to generate conditional realizations. The simulated annealing method has been discussed by Alabert (1989), Deutsch (1993), Hird and Kelkar (1992) and Holden et al. (1995). The genetic algorithm has been discussed by Sen et al. (1992) and Romero et al. (2000) among others. Unfortunately, these methods can be very computationally expensive. They often converge very slowly and require a large number of iterations to achieve an acceptable realization matching production data.

Four comparative investigations of the validity of sampling algorithms for quantifying uncertainty of reservoir performance conditional to flow data have been

reported in the literature. Zimmerman et al. (1998) compared several geostatistical inverse techniques to determine which is better suited for making probabilistic forecasts of solute transport in an aquifer. The comparison criteria were the predicted travel times and the travel paths taken by conservative radioactive tracers if accidentally released from storage at the Waste Isolation Pilot Plant (WIPP) site in New Mexico. The main conclusion achieved by this study was the importance of the appropriate selection of the variogram and "the time and experience devoted by the user of the method."

In a large investigation of uncertainty quantification supported by the European Commission, Floris et al. (2001) applied several methods of evaluating uncertainty to a synthetic reservoir characterization study based on a real field case. Participants received reservoir parameters only at well locations, 'historic' production data (with noise), and a general geologic description of the reservoir. Nine different techniques for conditioning of the reservoir models to the production data were evaluated, and results (production forecast for a certain period) were compared in the form of a cumulative distribution function. Variation in the parameterization of the problem was identified as the main discriminating factor in this study. The differences in the quality of the history matching and the production forecast caused by the distinct approaches to the problem also resulted in major differences in the resulting cumulative distribution functions.

Barker et al. (2001) used the same synthetic test problem as Floris et al. (2001), but focused their investigation of sampling on three methods: history-matching of multiple realizations using a pilot-point approach, rejection sampling, and Markov chain Monte Carlo. They obtained very different distributions of realizations from rejection and Markov chain Monte Carlo methods. The difference was attributed to variations in the prior information used by the participants, but this made evaluation of the results difficult.

Holden et al. (2001) provided an overview of sampling algorithms for Bayesian

history matching. In this paper, the sampling algorithms were divided into three groups; optimization algorithms, rejection algorithms, and Markov chain Monte Carlo algorithms. The theoretical properties for the algorithms were described.

## 1.3 Objective Statement

A test problem is regarded as a linear problem when the relationships between model parameters and conditioning data are linear. We know that for linear test problems, some of these approximate sampling methods, such as LMAP, samples from the true model distribution, thus give similar results about reservoir future performance with those from exact methods. This may make people mistakenly trust the validity of these approximate methods for more realistic nonlinear problems. Unfortunately, this underlying problem was generally ignored in previous research in designing a synthetic test problem. Moreover, we need to be able to generate a large number of realizations. For one thing, the distribution of reservoir realizations should not depend significantly on the random seed. For another, because of the lack of independence of realizations, the Markov chain Monte Carlo method requires a large number of realizations of the model to be generated. Because most of the previous studies are based on complicated synthetic models, they could not afford the huge processing demands required to run the fluid flow simulator millions of times. So a biased conclusion could be made due to lack of sufficient samples. The test problem has to be small enough to reduce the cost of running a large number of numerical fluid flow simulations. One more problem lies in the fact that though sampling from the same reservoir problem, differences in fluid flow simulators and differences in assumptions made by different research groups almost certainly influenced the distributions of future performance from the various algorithms.

In this work, I present our research in evaluating and comparing the abilities of various methods to correctly assess uncertainty in production forecasting.

For each of the methods, a large number of model realizations were generated from a single-phase transient flow problem with highly accurate pressure measurements, fairly large uncertainty in the property field, and a short correlation length. Future production performance of each realization was calculated using the same fluid flow simulator. By comparing realization distributions from these methods, the results indicate that RML is a practical approximate sampling method and produces acceptable results.

# CHAPTER II

# MODEL DEFINITION

The Monte Carlo solution to predict future reservoir performance is to generate many possible reservoir models and to use the ensemble of results to infer the uncertainty in future performance. The uncertainty in prediction depends on the available reservoir observation and production data. Exact simulation algorithms generate reservoirs according to the probability density distribution of the reservoir model.

## 2.1 Bayes Theorem

The conditional probability density for the model variables $m$, given the pressure data $d_{\text{obs}}$, is provided by Bayes rule,

$$f_{\text{M|D}}(m|d_{\text{obs}}) = f_{\text{D|M}}(d_{\text{obs}}|m) f_{\text{M}}(m) / \int f_{\text{D|M}}(d_{\text{obs}}|m) f_{\text{M}}(m)\, dm, \tag{2.1}$$

where $f_{\text{M}}(m)$ is the prior probability density for $m$ before incorporating the observations. $f_{\text{D|M}}(d_{\text{obs}}|m)$ is the probability of $d_{\text{obs}}$ given the model variables $m$. For convenience, I will denote the conditional probability density $f_{\text{M|D}}(m|d_{\text{obs}})$ as $f(m)$, understanding that it is conditional to the data. When the prior pdf for $m$ is Gaussian and the errors in the data (and modeling errors) are Gaussian, the a posteriori pdf for $m$ is

$$\begin{aligned} f(m) \propto \exp\Big(-\frac{1}{2}(g(m) - d_{\text{obs}})^{\text{T}} C_{\text{D}}^{-1} (g(m) - d_{\text{obs}})\Big) \\ \times \exp\Big(-\frac{1}{2}(m-\mu)^{\text{T}} C_{\text{M}}^{-1} (m-\mu)\Big), \end{aligned} \tag{2.2}$$

where $g(m)$ is the vector of theoretical pressure data obtained by running the simulator with log-permeability and porosity values given by the vector $m$. $C_{\text{D}}$ and $C_{\text{M}}$

are the data error covariance and the prior model parameter covariance respectively. Both of these matrices are assumed to be known.

## 2.2 The Prior Model

The reservoir model parameters that can be estimated using inverse procedures include gridblock permeabilities, gridblock porosities, well skin factors, and relative permeabilities (see Li (2001) for details). In the prior model, the parameter variables are assumed to be correlated Gaussian variables with specified mean and covariance. The prior pdf for model parameters $m$ is given by

$$\pi_p(m) = c \exp\Big\{-\frac{1}{2}(m - m_{\text{prior}})^{\text{T}} C_{\text{M}}^{-1}(m - m_{\text{prior}})\Big\}, \tag{2.3}$$

where $c$ is the normalizing constant. $C_M$ is the model covariance matrix. It defines the relationship among the model parameters and can be constructed from the prior information, mainly the variogram model. Eq. 2.4 shows the structure of $C_M$ for a model with only permeability and porosity.

$$C_M = \begin{bmatrix} C_\phi & C_{\phi,k} \\ C_{k,\phi} & C_k \end{bmatrix} \tag{2.4}$$

Matrices $C_\phi$ and $C_k$ are the porosity covariance and permeability covariance among gridblocks respectively. $C_{\phi,k}$ is the cross-covariance between the porosity and the permeability fields.

From Eq. 2.3, the model has the highest probability when $m = m_{\text{prior}}$, so in that sense $m_{\text{prior}}$ is the best estimate of the model based on static data. $m_{\text{prior}}$ is generally set as the expectation of reservoir variables based on the prior knowledge about the reservoir.

## 2.3 The Maximum A Posteriori Estimate

The maximum a posterior (MAP) estimate is the most probable model of the posterior pdf (Eq. 2.2), i.e. it corresponds to the minimum value of the objective function:

$$O(m) = \frac{1}{2}(g(m) - d_{\text{obs}})^{\text{T}} C_{\text{D}}^{-1}(g(m) - d_{\text{obs}}) + \frac{1}{2}(m - m_{\text{prior}})^{\text{T}} C_{\text{M}}^{-1}(m - m_{\text{prior}}). \quad (2.5)$$

The data covariance matrix $C_D$ is based on the accuracy of the data. If the measurement error is small, the data variance should also be small and vice versa. Usually, I assume that all measurement errors are Gaussian with means equal to zero. I also assume all measurement errors are independent so the data covariance matrix is diagonal.

If the relationship of data to model parameters, $d = g(m)$, is not linear, the objective function (Eq. 2.5) may have several local minima. An algorithm that uses derivatives to find a downhill direction will most likely end up getting "stuck" in a local minima.

### 2.3.1 Gauss-Newton and Levenberg-Marquardt Algorithms

If the objective function has continuous second derivatives, the Gauss-Newton and Levenberg–Marquardt algorithms could be used for minimization of the objective function.

In the Gauss-Newton procedure, the model parameters at iteration $l + 1$ are updated by

$$m^{l+1} = m^l + \mu_l \delta m^{l+1}, \quad (2.6)$$

where $0 < \mu_l \leq 1$ is a scalar which controls the size of the step in the direction $\delta m^{l+1}$ and is calculated by the restricted step procedure (see He (1997)). When the number of model variables is not too large, $\delta m^{l+1}$ is computed by

$$(C_M^{-1} + G_l^T C_D^{-1} G_l)\delta m^{l+1} = -C_M^{-1}(m^l - m_{\text{uc}}) - G_l^T C_D^{-1}(g(m^l) - d_{\text{uc}}). \quad (2.7)$$

The term $(C_M^{-1} + G_l^T C_D^{-1} G_l)$ is called the "Hessian" matrix for the Gauss-Newton algorithm.

The Levenberg-Marquardt algorithm can be thought of as modification of the Gauss-Newton algorithm with an extra weighting term in the Hessian:

$$H_l = H(m^l) = (1+\lambda)C_M^{-1} + G_l^T C_D^{-1} G_l, \tag{2.8}$$

where $\lambda$ is a positive number. In Bi (1999), $\lambda$ is initially a large value, and is divided by a factor after each successful iteration in which the value of the objective function is reduced. It is multiplied by the factor if the new parameters lead to an increased value of the objective function. A big value for $\lambda$ indicates a small step along the negative gradient direction. The model changes smoother from the beginning of the algorithm when the $\lambda$ value is big than in the later iterations. For ill-conditioned matrix problems, the Levenberg-Marquardt algorithm is more robust and converges faster than the standard Gauss-Newton method with restricted-step. In this work, the MAP estimate is obtained by running the Levenberg-Marquardt method until the objective function is reduced below a certain criterion. The final reservoir model from the iterations is noted as $m_\infty$, i.e. $m_{\text{map}} = m_\infty$.

### 2.3.2 Posteriori Covariance

After calculating $m_{\text{map}}$, the a posteriori covariance matrix $C_{M'}$ of the model can be estimated as:

$$C_{M'} = (G_\infty^T C_D^{-1} G_\infty + C_M^{-1})^{-1}, \tag{2.9}$$

where $G_\infty$ is the sensitivity coefficient matrix corresponding to the MAP solution, $m_{\text{map}}$.

### 2.3.3 Posteriori Distribution

Assuming that the relation between the observed data and the model parameters can be linearized around the MAP solution, i.e.

$$g(m) \approx g(m_\infty) + G_\infty(m - m_\infty), \tag{2.10}$$

then an approximation to the pdf can be written as:

$$\begin{aligned}
\pi(m) &\propto \exp\Big[-\frac{1}{2}(g(m) - d_{\text{obs}})^{\text{T}} C_{\text{D}}^{-1}(g(m) - d_{\text{obs}})\Big] \\
&\quad \times \exp\Big[-\frac{1}{2}(m - m_{\text{prior}})^{\text{T}} C_{\text{M}}^{-1}(m - m_{\text{prior}})\Big] \\
&\approx \exp\Big[-\frac{1}{2}\Big(g(m_\infty) + G_\infty(m - m_\infty) - d_{\text{obs}}\Big)^{\text{T}} C_{\text{D}}^{-1}\Big(g(m_\infty) + G_\infty(m - m_\infty) - d_{\text{obs}}\Big) \\
&\quad - \frac{1}{2}(m - m_{\text{prior}})^{\text{T}} C_{\text{M}}^{-1}(m - m_{\text{prior}})\Big] \\
&\propto \exp\Big[-\frac{1}{2}(m - m_\infty)^{\text{T}}[C_M^{-1} + G_\infty^T C_D^{-1} G_\infty](m - m_\infty)\Big].
\end{aligned} \tag{2.11}$$

## 2.4 Computation of Sensitivity Coefficients

The computation of the gradient and the approximate Hessian in the Levenberg-Marquardt algorithm requires the sensitivity coefficients matrix $G$. $G$ represents the Fréchet derivative of production data with respect to model parameters. As we know, the relation between data $d_{\text{obs}}$ and model parameters $m$ can be expressed as a function,

$$d_{\text{obs}} = g(m) + \varepsilon, \tag{2.12}$$

where $\varepsilon$ is measurement error. When the model is changed by a small amount, the resulting change in the data is

$$g(m + \delta m) - g(m) = (G, \delta m) + R(\delta m), \tag{2.13}$$

where $R(\delta m)$ is the remainder and equals to zero when $g(m)$ is a linear function. If

$$\lim_{\|\delta m\| \to 0} \frac{R(\delta m)}{\|\delta m\|} = 0, \tag{2.14}$$

then $g(m)$ is said to be Fréchet differentiable.

A sensitivity coefficient $G_{i,j}$ indicates how much the datum $d_i$ is affected by changing a model parameter $m_j$.

$$G_{i,j} = \frac{\partial g_i(m)}{\partial m_j}, \qquad \text{for} \quad 1 \leq i \leq N \quad \text{and} \quad 1 \leq j \leq M, \tag{2.15}$$

where $N$ is the number of data and $M$ is the number of model parameters. The dimension of $G$ is $N \times M$. From Eq. 2.15, it is clear that the Fréchet derivative of "data" can be obtained simply by observing the resulting change of data from model perturbation.

This method of calculating sensitivity coefficient matrix is called the finite difference method or direct method. Given the small size of the test problem in this work, I used the finite difference method to calculate sensitivity coefficients.

# CHAPTER III

# ESTABLISHMENT OF A STANDARD DISTRIBUTION FOR COMPARISON

In order to establish the quality of the distributions of realizations from the approximate methods, it is necessary to establish a standard distribution from a method that samples correctly. Rejection sampling and Markov chain Monte Carlo both satisfy this criterion.

## 3.1 Acceptance-Rejection Sampling

The main idea in acceptance-rejection sampling is to propose samples from some relatively simple distribution, then apply a test to decide whether or not to accept it. In this respect it is similar to the McMC method. One important difference, however, is that in rejection sampling, the test does not depend on the most recent sample, so all accepted samples are truly independent.

To generate samples (realizations) from the target probability density $\pi(m) = f(m)/K$ where $f(m)$ is the un-normalized density (i.e. $\int f(m)\,dm \neq 1$) and $K$ is the unknown normalizing constant, let $h(m)$ be a probability density that can be easily sampled (e.g. multivariate Gaussian) and suppose that there is some constant $c$ such that $f(m) \leq c\,h(m)$ for all $m$.

Random samples from $\pi(m)$ can be obtained in the following procedure (Ripley, 1987):

1. Generate a candidate sample $m^*$ from pdf $h(\cdot)$.

2. Generate a decision variable $u$ from the uniform distribution on $(0, 1)$.

3. If $u \leq f(m^*)/(c\,h(m^*))$ then accept the proposal and return $m = m^*$, else reject $m = m^*$.

4. Return to step 1.

The key to the efficiency of the rejection algorithm is selecting a proposal density that is a close approximation to the target density, in which case the acceptance rate is close to one. Unfortunately, it can be very difficult to find a simple distribution for the proposal of trial realizations that leads to an efficient algorithm, especially when the number of model variables is large. In this study, I tried proposing from several Gaussian pdfs centered on the maximum a posteriori model. The proposal pdfs were of the form

$$h(m) = B \exp\Big[-\frac{1}{2}(m - m_{\text{map}})^{\text{T}} A^{-1} (m - m_{\text{map}})\Big] \tag{3.1}$$

and $A$ was either chosen to be proportional to the prior covariance or to be the model covariance based on the linearization of the simulator relationship at the maximum a posteriori model, see Eq. 2.10.

## 3.2 Markov chain Monte Carlo

Markov chain Monte Carlo methods also are capable of generating sequences of realizations that are samples from a target probability density. One advantage of the McMC methods is that it is unnecessary to know the normalization constant to have a valid sampling algorithm. The algorithm that I used to obtain random samples from $f(m)$ is quite simple:

1. Initialize the chain with $m_1$ and $i = 1$.

2. Generate a candidate sample $m^*$ from pdf $q(\cdot|m_i)$.

3. Generate a decision variable $u$ from $\mathcal{U}(0, 1)$.

4. If $u \leq \alpha(m^*, m_i)$ then set $m_{i+1} = m^*$, else set $m_{i+1} = m_i$.

5. $i \rightarrow i + 1$, return to step 2.

Numerous possibilities are available for the acceptance criterion. I chose to use the Metropolis-Hastings criterion,

$$\alpha(x, y) = \min\Big[1, \frac{f(x)q(y|x)}{f(y)q(x|y)}\Big]. \tag{3.2}$$

Aside from some fairly general requirements on $q(\cdot|\cdot)$ that are easy to satisfy (Chib and Greenberg, 1995), the primary concern with the choice of the proposal distribution $q(\cdot|\cdot)$ is that the chain mix rapidly and have a relatively high acceptance rate (Gilks et al., 1996a). Previous experiments with the use of McMC for reservoir characterization from pressure data (Oliver et al., 1997) led to the conclusion that for highly nonlinear problems it is more effective to make local perturbations to the model parameters than to perturb all parameters at once. In that study, it was also concluded that perturbations that were based on linearization of the data relationship improved the efficiency substantially. The characterization problem that I treat in this paper is more highly nonlinear than that treated by Oliver et al. (1997), so not all of the conclusions of that paper were valid for our current problem.

In this paper, all proposed transitions are of the form

$$m^* = m_i + LZ^* \tag{3.3}$$

where $L$ is a "square root" of the prior model covariance matrix (that is $LL^{\mathrm{T}} = C_{\mathrm{M}}$) and $m_i$ is the current state of the model. At each iteration, I set all elements of $Z^*$ to zero, then randomly selected one element to perturb. The value of the perturbation is chosen from the normal distribution with mean 0 and variance 1.

There is some debate in the literature concerning the relative desirability of running one long Markov chain versus several shorter sequences. Gelman and Rubin (1992) argue that generating multiple independent Markov chains reduces the risk of

basing conclusions on a slowly mixing chain whose variability is less than the actual variability. Geyer (1992) argues that all inference should instead be based on one long run of the Markov chain, that doing so reduces the dependence on the starting value.

Although McMC sampling results will be shown in Chapter 6, I present preliminary results here, as they impacted choices in the implementation of the McMC algorithm. My first analyses were based on multiple "short" chains, each of which contained one million iterations. Fig. 3.1 shows every 1000th realization of $S_m = 0.5(m-\mu)^{\mathrm{T}} C_{\mathrm{M}}^{-1}(m-\mu)$ from the total sequence. The 20 short chains have been placed in sequence. It is disconcerting to observe large differences in mean values between the individual chains. In particular, note that the mean for the third chain is approximately 17, while the mean for the twentieth chain is approximately 27. Clearly, these chains of one million realizations are too short for the distributions to be independent of the starting values.

It is often difficult or impossible to tell by looking at the sequence of realizations from the Markov chain whether or not the chain is mixing well. Fig. 3.2 shows two sequences of functionals of the model realizations from the same Markov chain of one million realizations. Examination of the sequence of values of effective permeability seems to indicate that the sequence is mixing rapidly, i.e. that the realizations that are separated by 1000 iterations are independent. The sequence of values of $S(m)$, on the other hand, shows a correlation range that is at least 200 thousand in length.

Unfortunately, when larger chains were run, it was observed that the mixing is much slower even than indicated by Fig. 3.2. The sequence of 320 million realizations shown in Fig. 3.3 shows some correlation of values of $S_m$ over distances as large as 100 million iterations.

Several alternative proposal mechanisms were tried in order to increase the efficiency of sampling, but none were more successful than the local perturbations

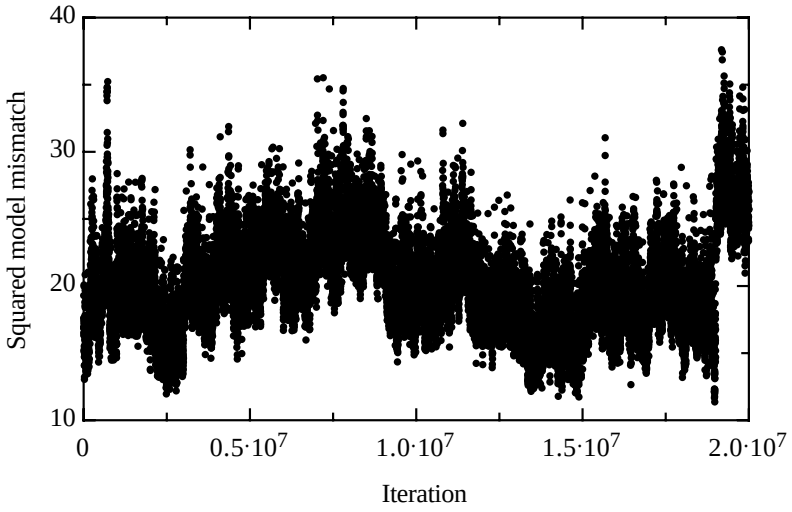


Figure 3.1: Every 1000th model from the first "short chain" of $10^6$ models was used to generate $f_1$ and $S_m$ (distance from the prior). The chain of values of $S_m$ shows quite long correlation lengths although this might not be guessed from the chain of values of $f_1$. Neither, however, seem to show evidence of a transition period at the beginning of the chain.

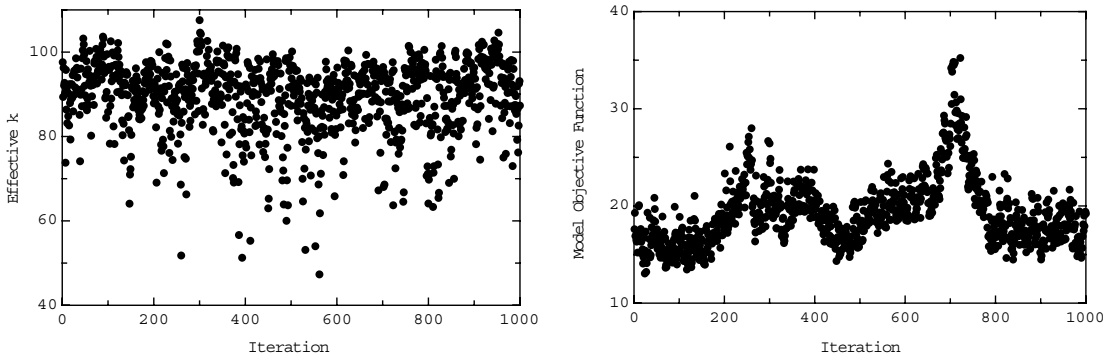


(a) Effective permeability.

(b) Squared distance from the prior model.

Figure 3.2: The realizations of $k_{\text{eff}}$ in (a) and of $S(m)$ in (b) are from the same chain. The mixing seems to be rapid in (a) but (b) shows a long correlation range.

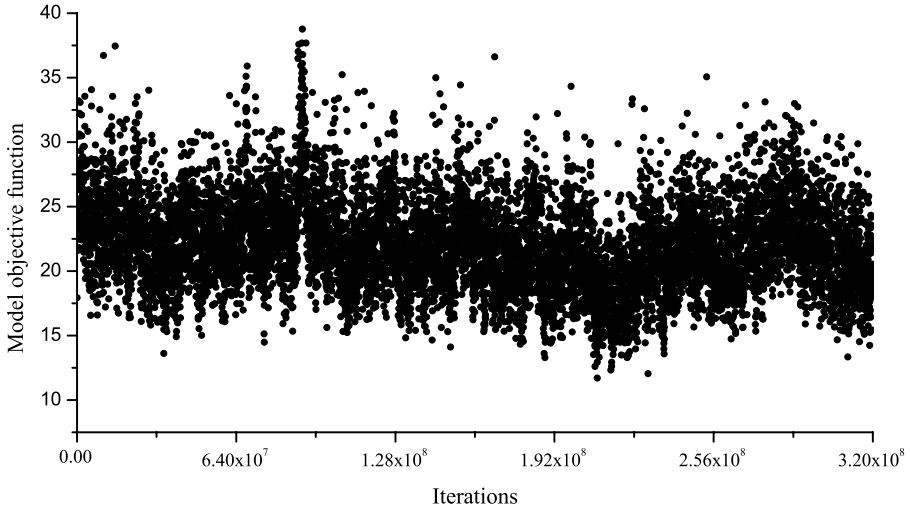


Figure 3.3: A very long sequence of realizations of $S(m)$ showing slow mixing and an apparent correlation length on the order of 100 million iterations.

from the prior covariance, so all McMC results in this paper used local perturbations.

# CHAPTER IV

# APPROXIMATE METHODS OF SAMPLING

Here I describe the sampling algorithms for which the distribution of realizations generated are known to be only approximately correct when the data relationship is nonlinear.

## 4.1 Linearization about the MAP.

For variables that are multivariate Gaussian, it is possible to generate realizations from the square root of the covariance (Rao, 1973). This method has been applied to the problem of generating realizations of Gaussian random fields in petroleum engineering by Davis (1987) and Alabert (1987). Even when the data relationship is not linear, it is possible to use the square-root method for generating conditional realizations by computing an approximation to the a posteriori covariance based on linearization of the data relationship at the maximum a posteriori point. Once the most probable model $m_{\text{map}}$ is computed, the a posteriori covariance matrix $C_{\text{M}'}$ of the model can be estimated as:

$$C_{\text{M}'} = \left(G_{\infty}^{\text{T}} C_{\text{D}}^{-1} G_{\infty} + C_{\text{M}}^{-1}\right)^{-1} \tag{4.1}$$

where $G_{\infty}$ is the sensitivity coefficient matrix corresponding to the MAP solution. From a square root of $C_{\text{M}'} = LL^{\text{T}}$, it is possible to generate models that approximately honor the production data as

$$m_i = m_{\infty} + LZ_i. \tag{4.2}$$

$Z_i$ is a vector of independent normal random deviates $Z_i \rightarrow N[0,1]$ and $L$ is the square root of $C_{\text{M}'}$ obtained with the Cholesky method.

The following are the steps of calculation in LMAP code.

1. Read geostatistical parameters and other data.

2. Read the observed pressure data $d_{obs}$ from the given file *d_observ*.

3. Read the MAP model, $m_{map}$, from the file *map_model*. This is the best estimate of $\phi$ and $lnk$ in every grid block.

4. Generate the vector $m_{prior}$ by:

$$m\_prior[1 : n\_grid] = \bar{\phi} \tag{4.3}$$

$$m\_prior[n\_grid : 2 \times n\_grid] = \overline{\ln k} \tag{4.4}$$

5. Compute the sensitivity matrix of pressure to model parameters $G_\infty$ by calling the subroutine *senscoef*.

6. Generate the transpose of $G_\infty$ as $G_\infty^T$.

7. Generate the prior model covariance matrix, $C_M$, by calling the subroutine *covmat*, which need input the value of $\delta x$, variance of $\phi$, variance of $\ln k$, correlation coefficient for porosity and $\ln k$, and the range of the variogram.

8. Compute the inverse of the posteriori covariance model by

$$C_{M'}^{-1} = (C_M^{-1} + G_\infty^T G_\infty / \sigma_D^2) \tag{4.5}$$

(We might see this as $C_M^{-1} + G_\infty^T C_D^{-1} G_\infty$.) $\sigma_D^2$ in this equation is the variance of the observed data.

9. Then compute $C_{M'} = (C_{M'}^{-1})^{-1}$, the corresponding command is CALL matinverse .

10. Compute Cholesky decomposition of $C_{M'} = L_p L_p^T$. Here we get $L_p$ as output.

11. By now, both $m_{\text{map}}$ and $L_p$ are known, the rest work is to generate $z_i$ and produce a series of realizations (samples) in a loop. In my fortran code, $i = 1$ to 5000.

    - Generate random normal deviates to construct the vector $z_i$.
    - Compute $m_i = m_{\text{map}} + L_p \cdot z_i$ .
    - Compute the functionals of the sample generated ($f_1, f_2, \ldots, f_5, Sm1i, Sm2i$, and $Sd1i$). And write out the results.

This algorithm requires not much computer resources once $L$ is computed. The advantage of this method over the following two approximate sampling methods is that only one minimization (i.e. one history match) is required.

## 4.2 Randomized Maximum Likelihood.

Kitanidis (1995) and Oliver, He, and Reynolds (1996) proposed that unconditional realizations from a Gaussian random field could be used to generate realizations conditional to nonlinear data by a process of minimization. If the prior covariance of the model parameters and the variance of the observed data are known, samples can be generated in the following way:

1. Generate an unconditional realization of the model parameters, $m_{\text{u}} \leftarrow N[m_{\text{pr}}, C_{\text{M}}]$.

2. Generate a realization of the data, $d_{\text{u}} \leftarrow N[d_{\text{obs}}, C_{\text{D}}]$.

3. Compute the set of model variables, $m$, that minimizes the function:

$$S(m) = \frac{1}{2}(m - m_{\text{u}})^{\text{T}} C_{\text{M}}^{-1}(m - m_{\text{u}}) + \frac{1}{2}(g(m) - d_{\text{u}})^{\text{T}} C_{\text{D}}^{-1}(g(m) - d_{\text{u}}) \quad (4.6)$$

The minimization step is similar to the computation of the maximum a posteriori estimate, with the difference that the regularization is with respect to unconditional realizations of the model and the data instead of the prior model and the observed data. This method requires much more computation than the LMAP method as a minimization problem must be solved for each realization.

## 4.3 Pilot Point Methods.

The pilot point method can be considered an approximation to the RML method, in which perturbations to the model parameters are made only at selected locations (the pilot points). The system of equations to be solved in a Newton iteration step for minimization is typically smaller than in the randomized maximum likelihood method because the number of parameters is reduced. In the pilot point method, the columns of $C_{\mathrm{M}}$, associated with pilot point locations, are used as basis vectors for computation of corrections to the model parameters. One widely used implementation of the algorithm is as follows:

1. Generate an unconditional realization of the model parameters, $m_{\mathrm{u}} \leftarrow N[m_{\mathrm{pr}}, C_{\mathrm{M}}]$.

2. Generate an unconditional realization of the data, $d_{\mathrm{u}} \leftarrow N[d_{\mathrm{obs}}, C_{\mathrm{D}}]$.

3. Minimize the function:

$$J_{\mathrm{D}}(\delta m) = \big(d_{\mathrm{u}} - g(m_{\mathrm{u}} + \delta m)\big)^{\mathrm{T}} C_{\mathrm{D}}^{-1} \big(d_{\mathrm{u}} - g(m_{\mathrm{u}} + \delta m)\big) \tag{4.7}$$

   where $\delta m = \sum C_{\mathrm{M,i}} \alpha_i$ and the summation is only over the values of $i$ corresponding to gridblocks containing pilot points.

Pilot points, and the related master points, have been used in history matching by de Marsily et al. (1984), Bréfort and Pelcé (1990), and LaVenue and Pickens (1992). The application to conditional simulation was made by RamaRao et al.

(1995) and Gómez-Hernández et al. (1997) among others. In practice, it is usually unclear how many pilot points should be used to represent the correction in the property fields. For our study, the PP algorithm was evaluated with six and nine pilot point locations (33% and 45% of the model parameters) distributed nearly uniformly over the study region. As Oliver et al. (2001) point out, the use of Eq. 4.7 seems to be based on a mistaken belief that the regularization term (model mismatch squared) is not necessary when using the pilot point method. In a Bayesian context, the correct alternative is to minimize

$$J(\delta m) = \big(d_{\mathrm{u}} - g(m_{\mathrm{u}} + \delta m)\big)^{\mathrm{T}} C_{\mathrm{D}}^{-1} \big(d_{\mathrm{u}} - g(m_{\mathrm{u}} + \delta m)\big) + (\delta m)^{\mathrm{T}} C_{\mathrm{M}}^{-1} \delta m. \tag{4.8}$$

I evaluated the distribution of conditional realizations for both formulations of the pilot point method.

## 4.4 Gradual Deformation Method.

The principal idea of the gradual deformation method is that new realizations of a random field $Z$ with mean $\mu$ and covariance $C_Z$ can be written as the linear combination of a set of independent random Gaussian fields with expected mean $\mu$ and covariance $C_Z$, i.e.

$$Z(K) = \sum_{i=1}^{n} k_i (Z_i - \mu) + \mu \tag{4.9}$$

If the coefficients $k_i$ satisfy:

$$\sum_{i=1}^{n} k_i^2 = 1 \tag{4.10}$$

then it is easy to show that the expected mean and covariance of the random vector $Z$ is also $\mu$ and $C_Z$. In this study, each of the $Z_i$ is a vector of independent deviates from the same Gaussian distribution with expectation 0 and variance 1.

I tested the most basic form of the gradual deformation algorithm in which pairs of vectors are combined:

$$Z(\rho) = Z_1 \cos(\pi\rho) + Z_2 \sin(\pi\rho) \tag{4.11}$$

where $\rho$ is the deformation parameter with the range from 0 to 2. The procedure for generating a realization conditional to $d_{\text{obs}}$ is as follows:

1. Generate an initial vector $Z_1$ of independent normal deviates.

2. Generate a second vector of independent normal deviates $Z_2$.

3. Search the optimum $\rho$ value which gives a reservoir realization minimizing the objective function $S_d$ of Equation (4.14).

   Reservoir model realizations are calculated by:

   $$m(\rho) = m_{\text{prior}} + LZ(\rho) \tag{4.12}$$

   where

   $$LL^T = C_M. \tag{4.13}$$

   Note that the objective function to be minimized contains squared data mismatch only:

   $$S_d(\rho) = \frac{1}{2}[g(m(\rho)) - d_{\text{obs}}]^T C_D^{-1}[g(m(\rho)) - d_{\text{obs}}]. \tag{4.14}$$

4. If the minimum value of the objective function is sufficiently small, then stop the procedure. Otherwise, replace $Z_1$ with the optimal $Z(\rho)$ and return to step 2.

Because the gradual deformation algorithm involves minimization, the convergence or stopping criterion is important. Hu et al. (1999) refer to a convergence criterion, $S_d \leq n_d$, where $n_d$ is the number of data used for matching. In this study, we were unable to attain that value in a reasonable number of iterations (10,000), so I used $S_d = 1.6n_d$ as a stopping criterion in step 3.

Local Perturbation

When the historic production data are scattered spatially in the reservoir, adding an independent vector $Z$ is likely to improve the fit in some gridblocks while deteriorating the fit in other locations. This led Hu et al. (1999) to develop a procedure for modifying the values of $Z$ only within a limited region for which the data mismatch was large. Because it is not clear how to choose a limited region for interference tests, I examined the extreme case in which the region of change was limited to a single gridblock. The location of the gridblock to be modified was randomly chosen in each iteration. In this case, the $Z$ vector in Equation (4.12) is calculated as:

$$z_i(\rho) = \begin{cases} z_{1,k} & \text{for } i \neq k, \\ \cos(\pi\rho) z_{1,i} + \sin(\pi\rho) z_{2,i} & \text{for } i = k. \end{cases} \tag{4.15}$$

where $k$ is a randomly selected perturbation location. $z_{2,i}$ is a realization of a random variable sampled from the Gaussian distribution with mean 0 and variance 1. $z_{1,i}$ is the $i$th element of the vector $Z_1$.

# CHAPTER V

# EXPERIMENTAL DESIGN

Because my objective is to compare the distribution of the realizations of reservoir predictions generated by approximate sampling methods with the distribution generated by methods that are known to assess uncertainty correctly, it was important to choose the test problem carefully — it is known that some of the approximate methods sample correctly when the relationships between the conditioning data and the model parameters are linear, so I designed the test problem to be highly nonlinear. I also needed to be able to generate large numbers of realizations so that the resulting distributions do not depend significantly on the random seed. By choosing a single-phase transient flow problem with highly accurate pressure measurements, fairly large uncertainty in the property field, and a short correlation length, I was able to obtain a problem with multiple local maxima in the likelihood function, yet for which a flow simulation required only 0.02 seconds.

My test problem is a one-dimensional heterogeneous reservoir whose permeability and porosity fields are shown in Fig. 5.1. The reservoir is discretized into 20 gridblocks, each of which is 50 feet in length. Both the log-permeability ($\ln k$) and porosity fields were assumed to be multivariate Gaussian with exponential covariance and a range of 175 ft. The prior means for porosity and log-permeability are 0.25 and 4.5, respectively. The standard deviation of the porosity field is 0.05 and the standard deviation of the log-permeability field is 1.0. The correlation coefficient between porosity and log-permeability is 0.5. The flow is single phase with an oil viscosity of 2 cp and a total compressibility of $4 \times 10^{-6}$ psi$^{-1}$. The initial reservoir pressure is 3500 psi.

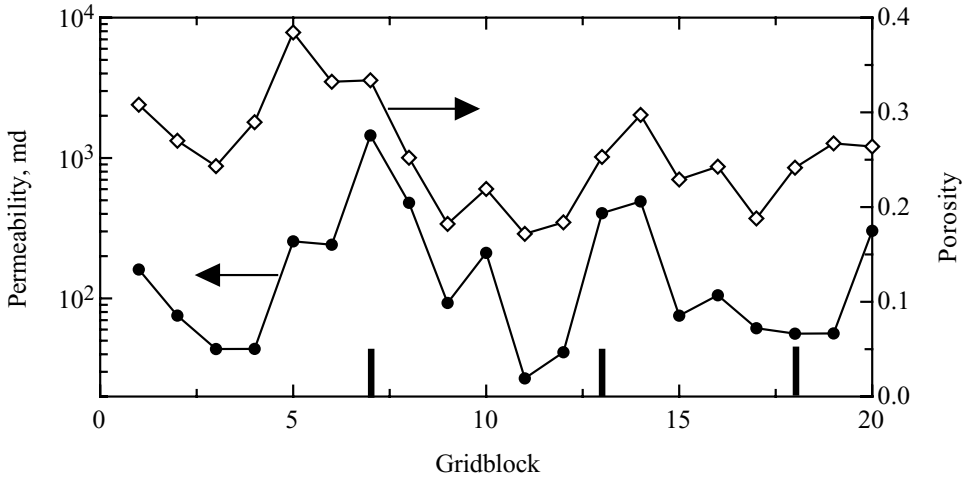


Figure 5.1: The true synthetic permeability and porosity fields used to generate pressure data to test the sampling algorithms. Well locations are shown by solid bars along the base of the figure.

The well located in gridblock 13 produces at a constant rate. Observation wells are located in gridblocks 7 and 18. Gaussian random noise with a standard deviation of 0.5 psi has been added to the data generated from the true reservoir model. The observed pressure data for all three wells are shown in (Fig. 5.2). Although there are 10 measurements of pressure drop at each well, the first three measurements at the observation wells are below the noise level. Porosity measurements at well locations were not included in this study as their introduction would have made the posteriori (conditional) pdf for model variables more nearly Gaussian.

The model that maximizes the probability density for model parameters conditional to pressure data, $f(m)$, is shown in Fig. 5.3. It is clearly much smoother than the true model but matches the observed pressure data better than the true model.

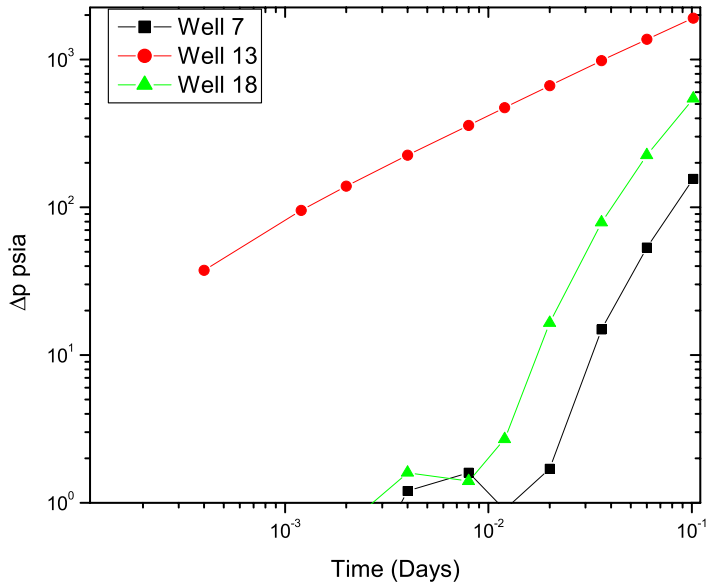


Figure 5.2: The observed pressure drop data at all wells. Random noise added to the true pressure drop causes the nonphysical appearance at low values of $\Delta p$.

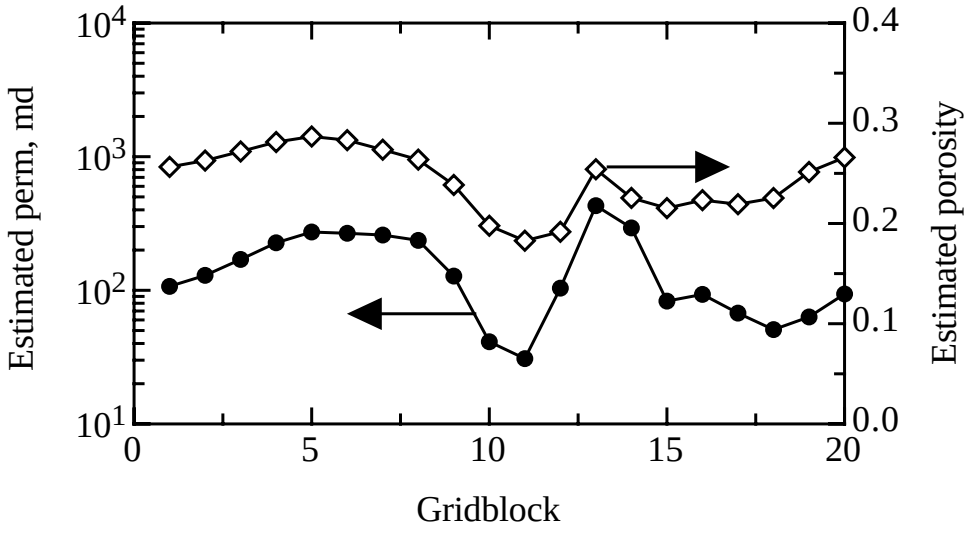


Figure 5.3: The maximum a posteriori estimates of permeability and porosity.

# CHAPTER VI

# RESULTS

I calculated eight properties of each conditional reservoir realization. Histogram plots were used to show the distributions of those properties from different methods. By comparing the distributions of reservoir realizations from approximate methods with those from the standard methods, we are able to evaluate the validity of each approximate method. The average porosity and effective permeability ($k_{\text{eff}} = 20(\sum_{i=1}^{20} k_i^{-1})^{-1}$) for each realization were then computed as prediction of the uncertainty in these quantities would be important for assessing oil-in-place and recovery. I computed the water front travel time in the reservoir, i.e. the breakthrough time because it is an important parameter to predict future production. I also computed the maximum permeability and the minimum permeability for each realization because it had been argued previously (Oliver et al., 2001) that the pilot point method tends to produce extreme values in the property fields, and this would provide a check on the validity of that conjecture. Finally, I computed the squared data (pressure) mismatch, the squared model mismatch about the prior model and the squared model mismatch about the MAP estimate. The model mismatch about the prior model provides an indication of the probability that the realization could be a sample from the prior distribution (a Gaussian random field with known covariance). The model mismatch about the MAP estimate indicates the probability that the realization could be a sample from the local Gaussian approximation to the a posteriori distribution. The data mismatch provides a measure of the likelihood of the model given the data. If the realizations do not approximately honor the data, they are unlikely to be valid samples from the conditional distribution and little

confidence could be placed in predictions of future performance.

For simplicity, the properties are denoted as follows:

- f1 —— Effective permeability $(\frac{1}{20}\sum(\frac{1}{K_i}))^{-1}$
- f2 —— Average porosity
- f3 —— Travel time
- f4 —— Maximum permeability
- f5 —— Minimum permeability
- Sd1 —— $\frac{1}{2}[g(m) - d_{\text{obs}}]^T C_D^{-1}[g(m) - d_{\text{obs}}]$
- Sm1 —— $\frac{1}{2}(m - m_{\text{prior}})^T C_M^{-1}(m - m_{\text{prior}})$
- Sm2 —— $\frac{1}{2}(m - m_{\text{MAP}})^T C_{M'}^{-1}(m - m_{\text{MAP}})$

## 6.1 Rejection

Proposals were made from several Gaussian pdfs centered on the maximum a posteriori model. The form of proposal pdfs is repeated here:

$$h(m) = B \exp\Big[-\frac{1}{2}(m - m_{\text{map}})^{\text{T}} A^{-1}(m - m_{\text{map}})\Big]. \tag{6.1}$$

$A$ was either chosen to be proportional to the prior covariance or to be the model covariance based on the linearization of the simulator relationship at the maximum a posteriori model. Despite considerable experimentation, I was unable to obtain an acceptable number of valid samples using rejection.

In the first and the second case, I chose $A = 1.2C_{\text{M}}$ and $A = 0.8C_{\text{M}}$ respectively, and selected $c$ such that the ratio $f(m_{\text{map}})/(c\,h(m_{\text{map}})) = 1$. In the first

case, only one realization was accepted among 0.4 million proposals. Three out of 0.4 million proposals were accepted in the second case.

In the third case, I chose $A = 0.01C_{\mathrm{M}}$ and selected $c$ such that the ratio $f(m_{\mathrm{map}})/(c\,h(m_{\mathrm{map}})) = 1$. Preliminary experimentation had shown that if we did not reduce the covariance significantly, we obtained very few acceptances. Even with $A = 0.01C_{\mathrm{M}}$ we accepted only 152 of the first 5 million proposals. In each case, however, the requirement that $f(m) \leq c\,h(m)$ was violated so the sampling was not from the correct distribution.

In the final case, I chose $A = C_{\mathrm{M}'}$ and selected $c$ such that the ratio $f(m_{\mathrm{map}})/(c\,h(m_{\mathrm{map}})) = 1$. With this proposal function, we accepted approximately 400 of the first 240 million proposals. In approximately half of the cases, the requirement that $f(m) \leq c\,h(m)$ was violated. Fig. 6.1 shows the property distributions of all the 419 realizations accepted in this case. Although we could create a valid sampling algorithm by increasing the value of $c$, the efficiency was already so low that this approach seemed unlikely to succeed in generating a sufficient number of valid samples.

## 6.2 McMC-algorithm

Since there has been debate about the benefits of several short chains versus one long chain (Gelman and Rubin, 1992; Geyer, 1992), investigations were made in both cases.

Case 1: I elected to run 20 independent chains to reduce the possibility of remaining stuck in one region. Three different chain lengths, 1 million, 2 million and 4 million iterations in each chain, have been applied to investigate the chain-length effect in McMC sampling. The initial element of each chain was a model realization generated using the method of randomized maximum likelihood, so I did not expect a transition period at the beginning of the chain. I confirmed the lack of a transition

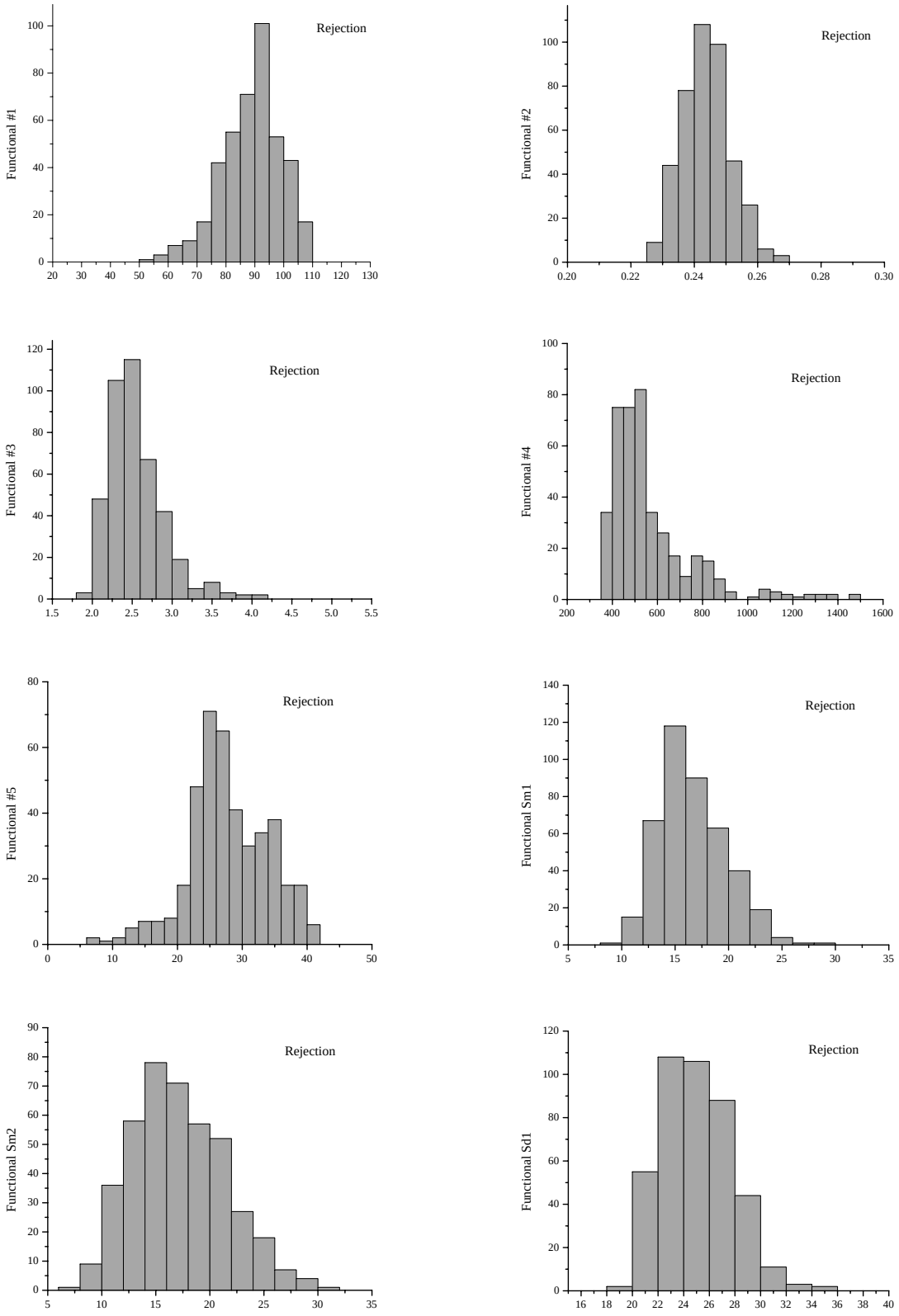


Figure 6.1: Histograms for properties of 419 realizations from rejection method with $A = C_{\mathrm{M}'}$ and $f(m_{\mathrm{map}})/(c\,h(m_{\mathrm{map}})) = 1$

period by examining plots of the eight McMC sequences of the 40 million realizations Markov chain (see Appendix A, Fig. A.1– A.4). Eight properties of each realization from the three chains with different lengths were calculated, and the distributions of these properties from each sequence are shown in Fig. 6.2, 6.3 and 6.4. The number of realizations included is labeled in each histogram, for example, $20E6$ means twenty million realizations. All of the three figures look similar, though differences do exist in values of local maxima and the ranges of distributions.

Case 2: As a contrast with the first case, we ran single long chains with lengths of 40 million and 80 million iterations each. For the 40 million iterations single long chain, the first and second realizations of RML method were used individually as the initial element, as shown in Figs. 6.5 and 6.6. The label "2nd" on each histogram in Fig. 6.6 indicates that the initial element is the second RML realization. The difference between the two figures confirms our suspicion that the sequence of 40 million realizations is not long enough to have the distributions independent of the initial state. Fig. 6.7 shows the properties of the single 80-million-iteration McMC sequence. The histograms for functionals 4, 5 and $Sm2$ have distinct difference with those in Fig. 6.5 and 6.6. Finally, we ran a very long chain consisting of 320 million iterations. The histograms of this long chain are shown in Fig. 6.8. To make better comparison, histograms of the maximum permeability, the minimum permeability, the model mismatch about the prior model and the model mismatch about the MAP estimate from each of the six Markov chains are put together for comparison (see Appendix B).

To make a clear comparison on the effect of chain length and starting model to the resulting distributions, histograms of the values of the properties from each case are shown in Fig B.1, B.2, B.3 and B.4. Where 20E6, 40E6 and 80E6 stand for the number of the total iterations in 20 chains, and 4E7 means one chain with 40 million iterations. "4E7 2nd" means start from the second realization of RML method.

Because of the apparent dependence on the starting model, even for fairly long chains (compare Fig. 6.5 and 6.6), I decided to run another long chain starting from the second RML realization. The histograms for the second 320 million realizations long chain are shown in Fig. 6.9. Although most of the histograms from the two very long chains are similar, obvious difference still exist in the distribution of maximum permeability and the model mismatch about the MAP estimate.

## 6.3 Linearization about the MAP

The first 10 realizations of the permeability field and the porosity field conditioned to pressure data are plotted together with the true permeability field and the true porosity field, as shown in Fig. 6.10. The spread of LMAP realizations of permeability at the producer seems reasonable. Although the LMAP realizations also seem to reproduce the true porosity at the producer location, the scatter is large at two observation well locations as the data is not sensitive to observation well porosity. Analysis of the LMAP realizations reveals that LMAP realizations do not honor production data. Histograms for the properties of 5000 LMAP realizations sampled from the test problem are shown in Appendix C Fig. C.1. Though other distributions of properties seem similar with McMC distributions, the histogram of squared data mismatch is severely skewed and most of the squared data mismatch values are over 10,000.

## 6.4 Randomized Maximum Likelihood

As the randomized maximum likelihood method seeks to minimize both the data mismatch and the distance from the unconditional realization, the realizations almost surely honor the data and appear to be from the correct distribution. Fig. 6.11 shows 10 realizations of the permeability field generated using the randomized maximum likelihood method together with the true permeability model.

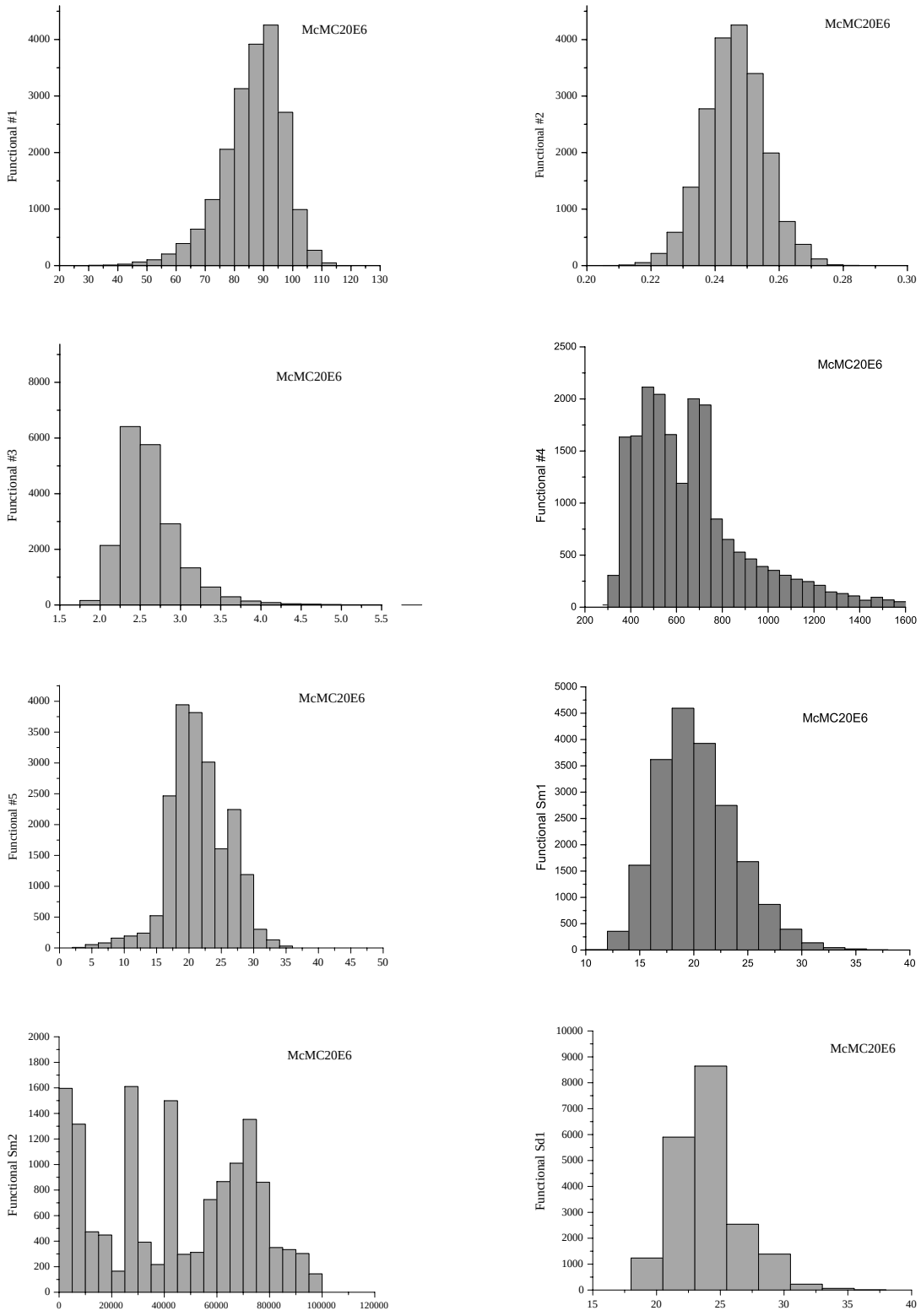


Figure 6.2: Histograms for properties of 20 one-million-iteration McMC sequences.

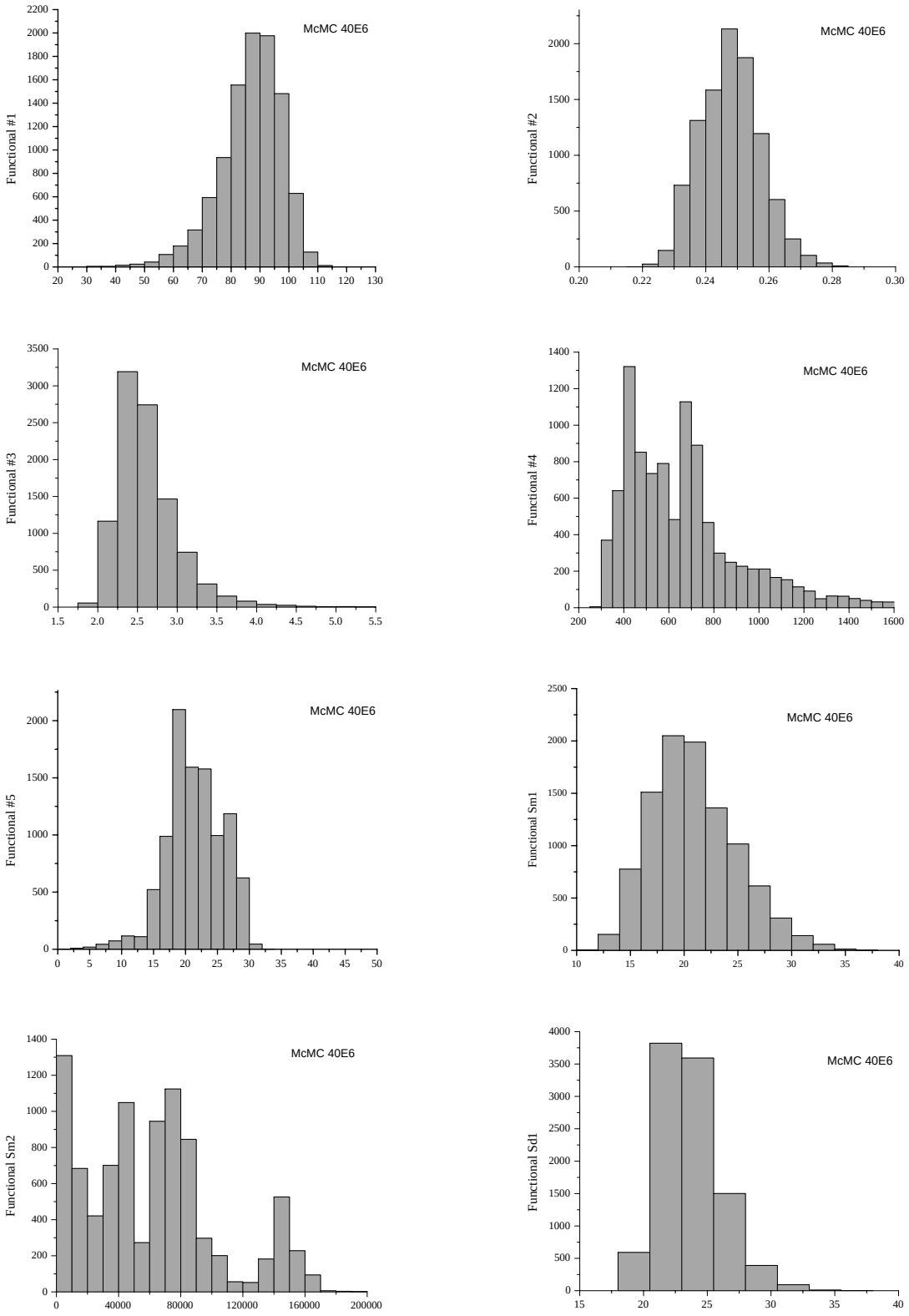


Figure 6.3: Histograms for properties of 20 two-million-iteration McMC sequences.

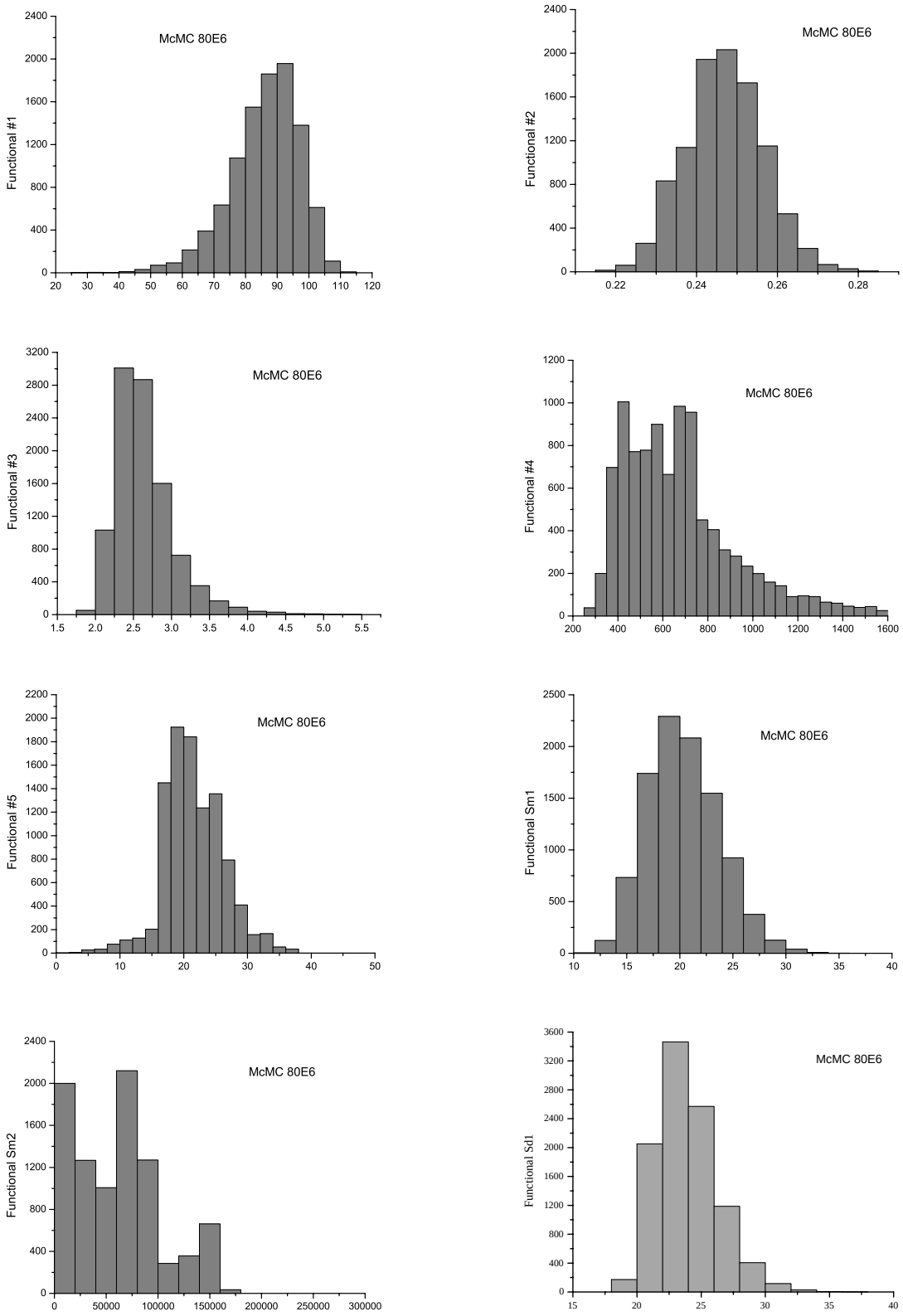


Figure 6.4: Histograms for properties of 20 four-million-iteration McMC sequences.

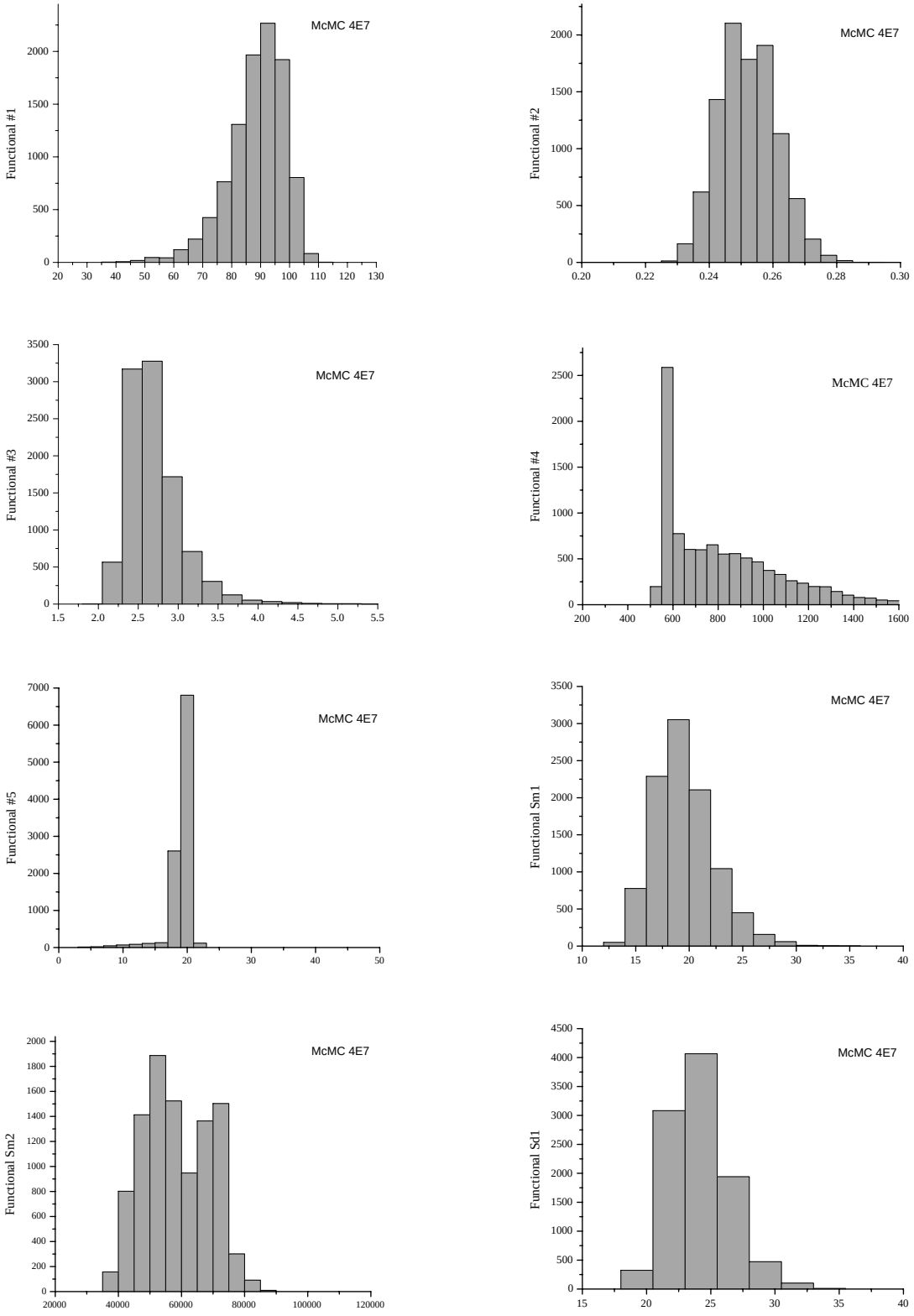


Figure 6.5: Histograms for properties of the single forty-million-iteration McMC sequences. The first realization of RML method was used individually as the initial element.

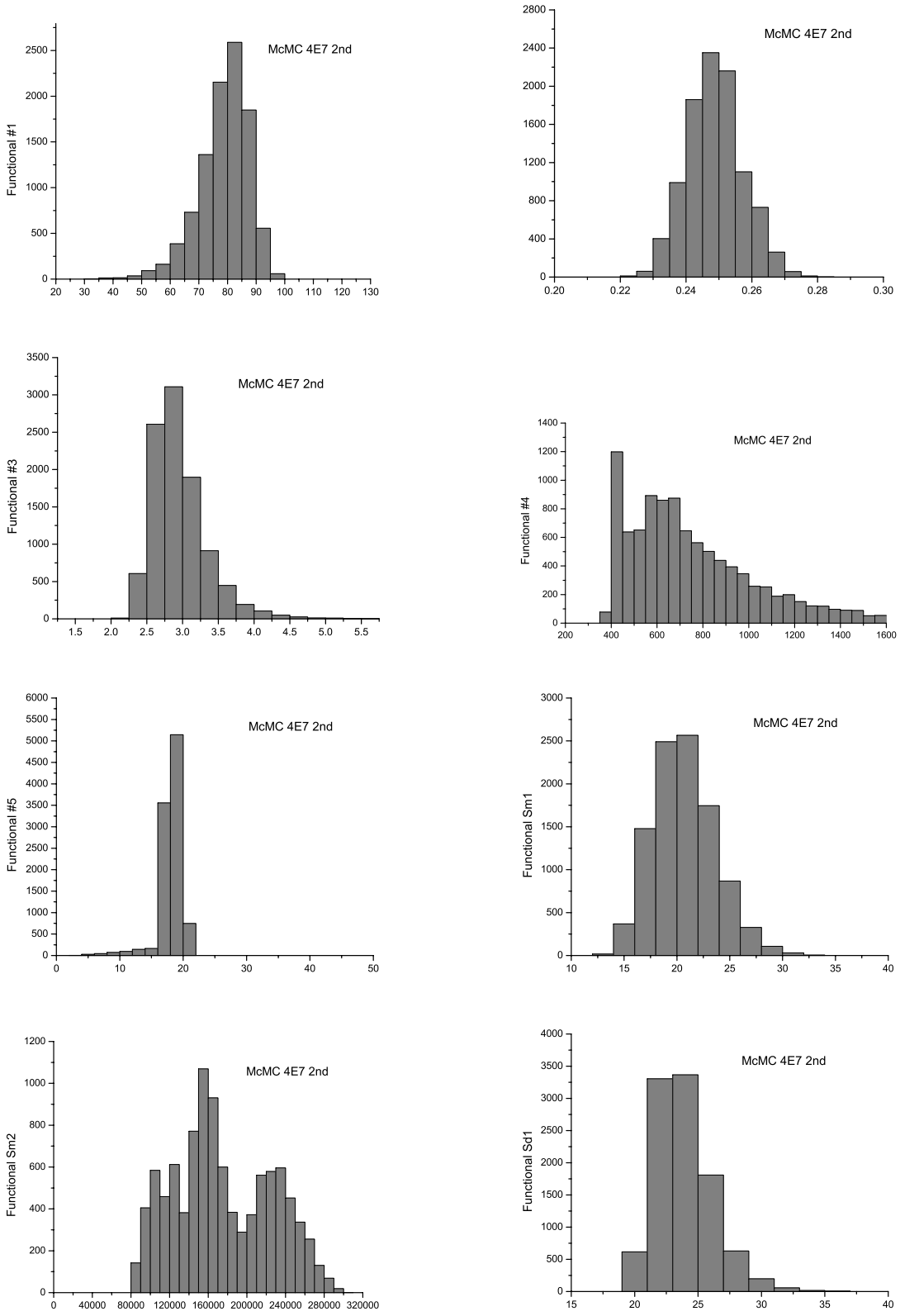


Figure 6.6: Histograms for properties of the single forty-million-iteration McMC sequences. The second realization of RML method was used individually as the initial element.

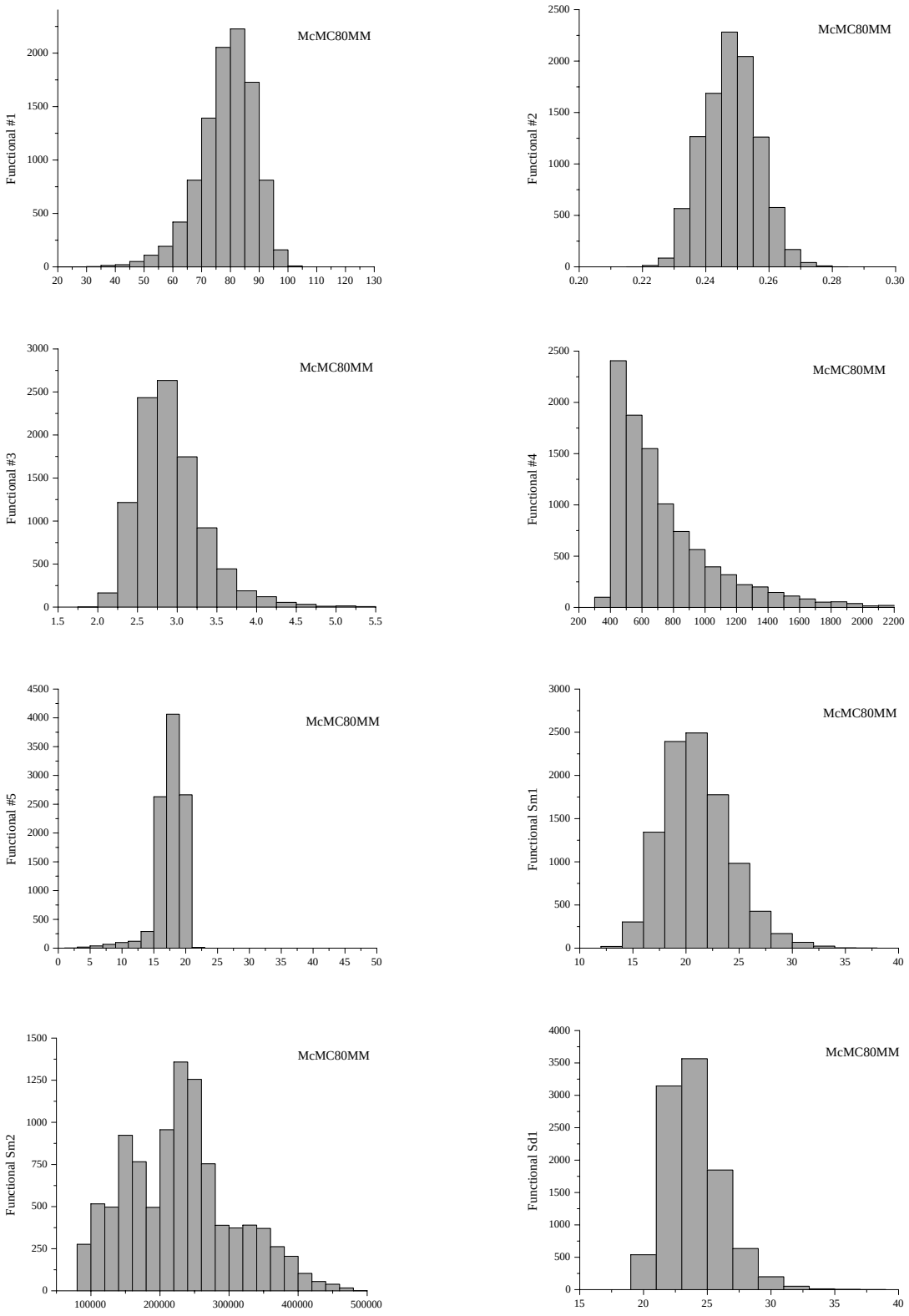


Figure 6.7: Histograms for properties of the single eighty-million-iteration McMC sequences.

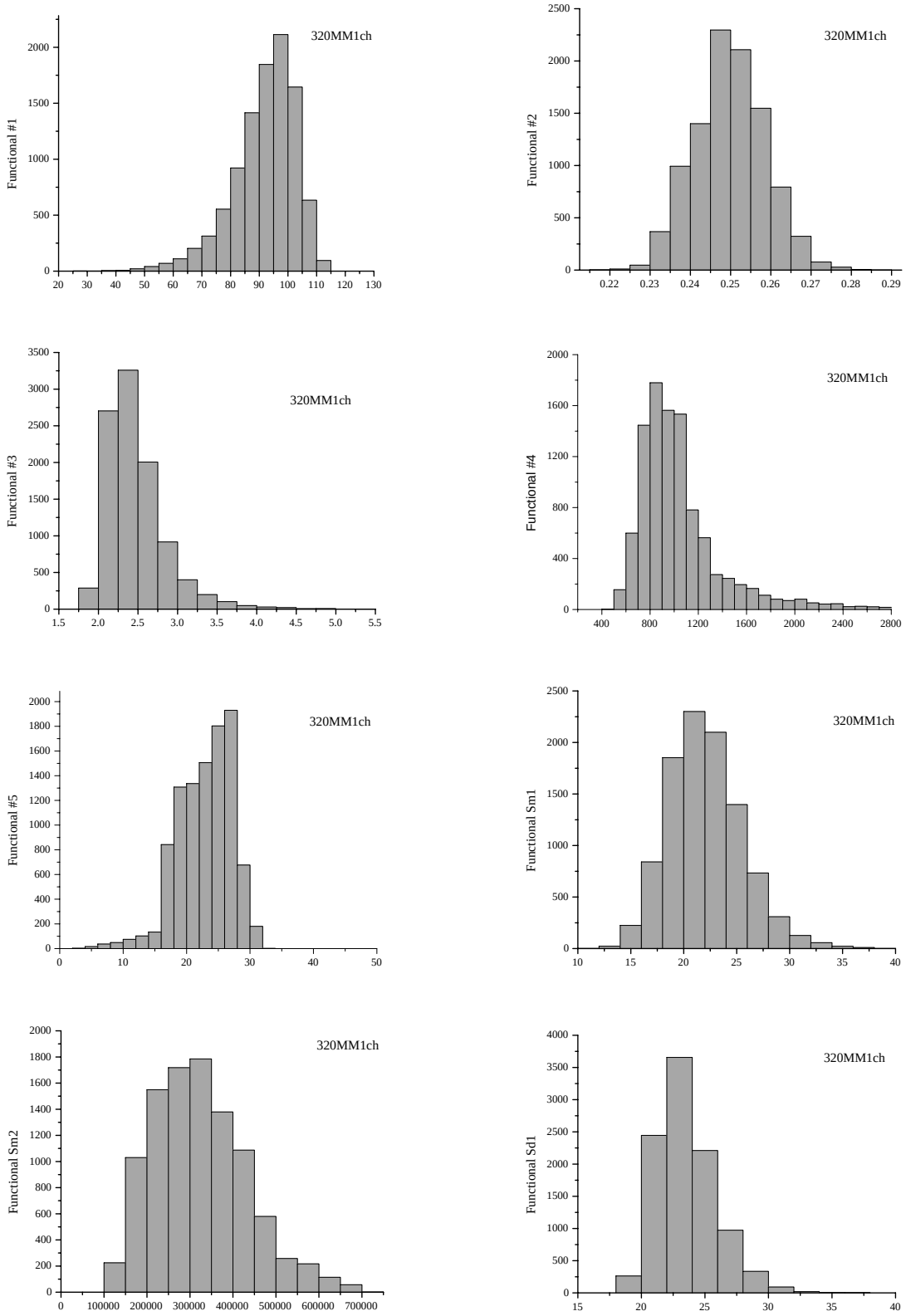


Figure 6.8: Histograms for functionals in McMC with 320 million iterations in one chain. The first realization of RML method was used individually as the initial element.

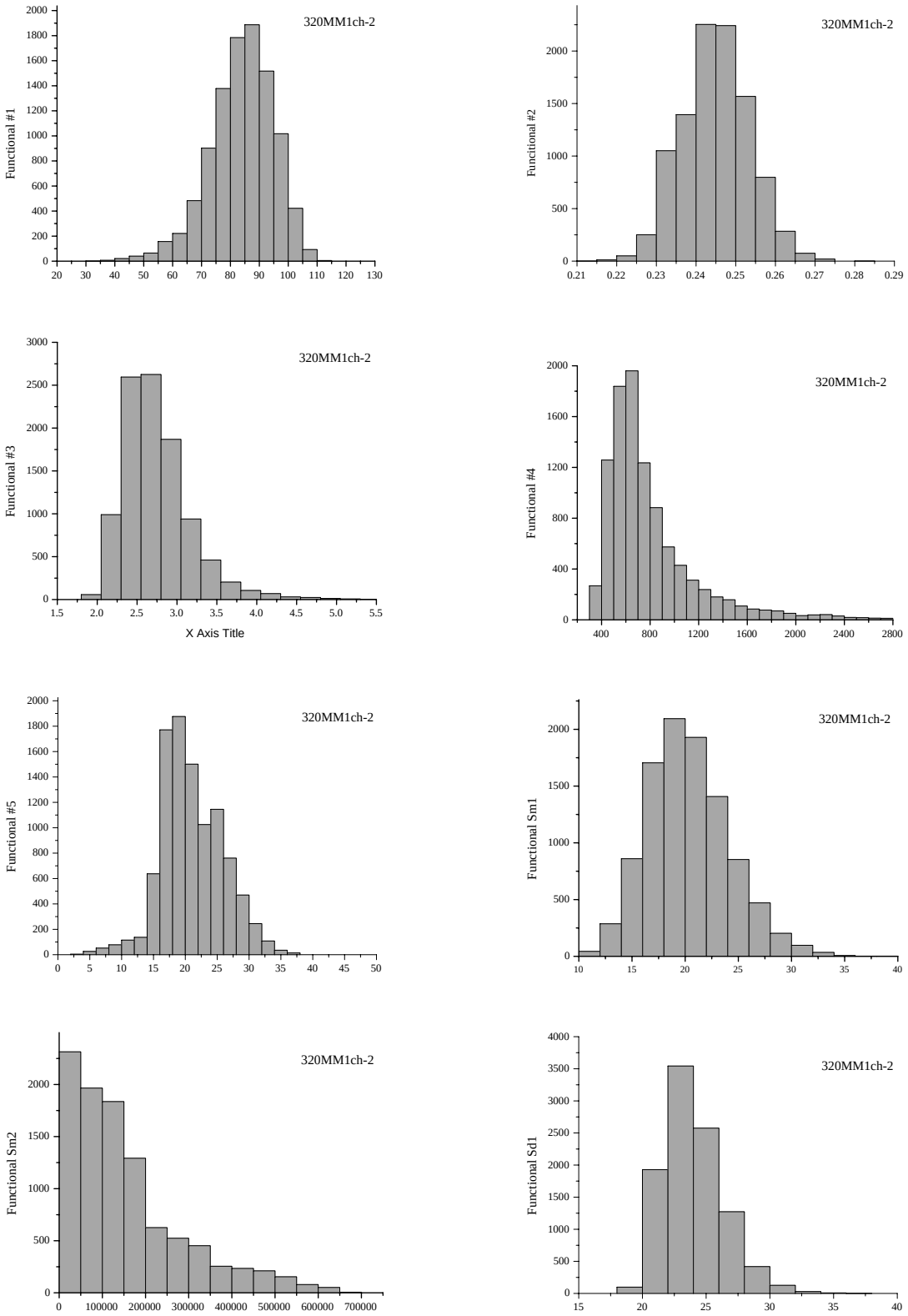


Figure 6.9: Histograms for functionals in McMC with 320 million iterations in one chain. The second realization of RML method was used individually as the initial element.

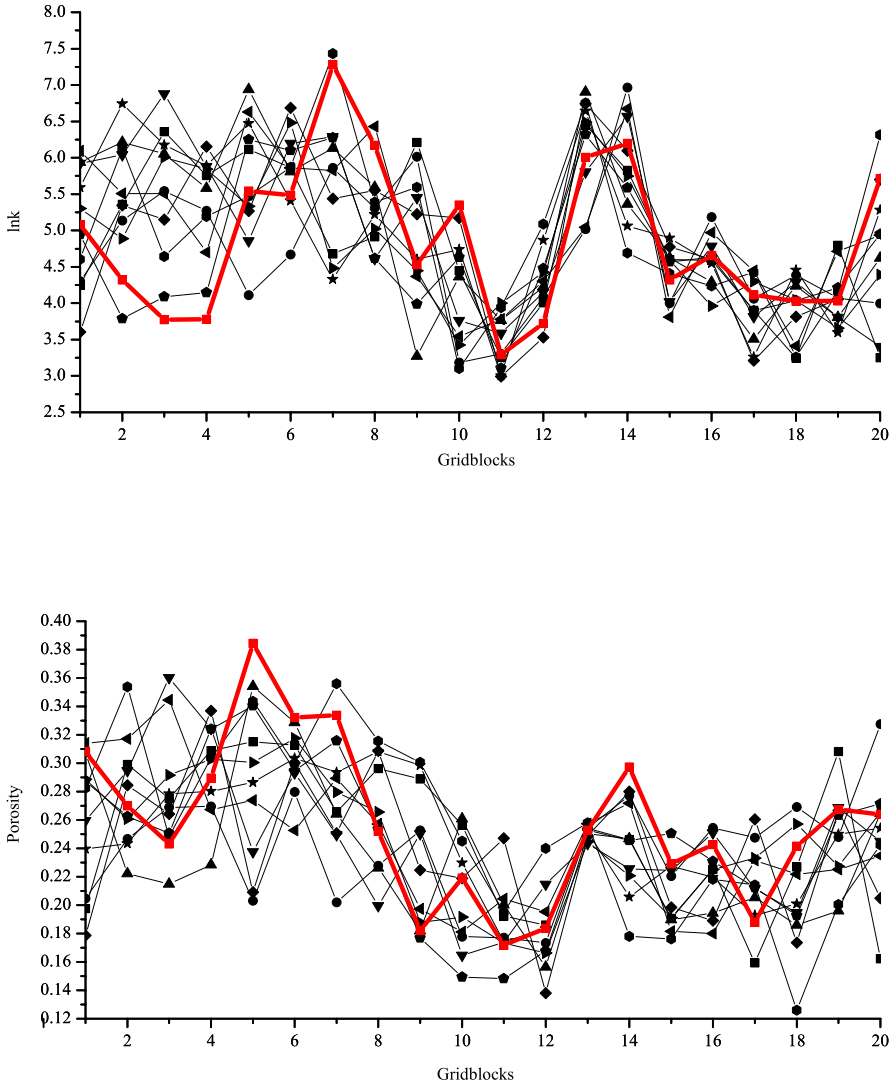


Figure 6.10: The first 10 realizations of the permeability field and porosity field conditioned to pressure data and the true permeability field and porosity field (heavy black line).

All of the RML models have similar shape with the "true" model, and seem to be

distributed appropriately. Histograms for the properties of 5000 RML realizations sampled from the test problem are shown in Appendix C Fig. C.2. They are very similar to histograms from McMC methods.

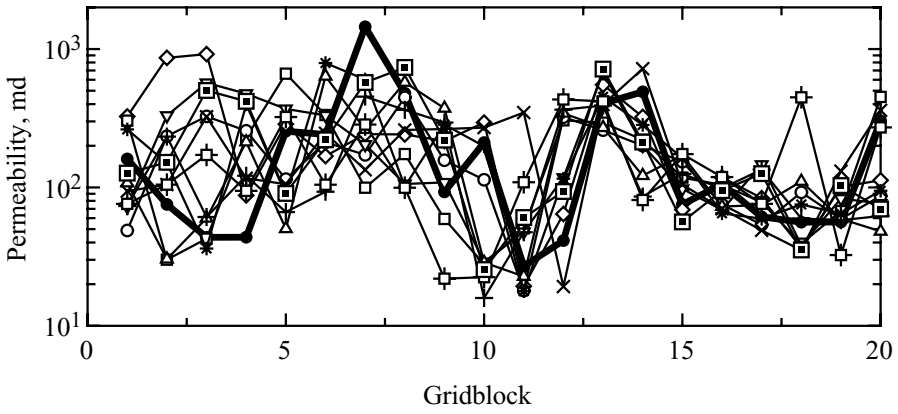


Figure 6.11: The first 10 realizations of the permeability field conditioned to pressure data and the true permeability field (heavy black line).

## 6.5 Pilot Point methods

There are many varieties of pilot point methods in application. The number of pilot points used is adjustable, so I evaluated the performance with pilot points at 6 locations and at 9 locations. When six locations are used, the pilot points are located at gridblocks 4, 7, 10, 13, 15, and 18. When nine locations are used, the pilot points are located at gridblocks 1, 4, 7, 10, 11, 13, 15, 18, and 20. Because there are two model variables per gridblock, we actually use 12 and 18 pilot points: two in gridblock 4, two in gridblock 7, etc. For each pilot point number, we evaluated the distribution of realizations using the whole objective function and the distribution of realizations using only squared data mismatch in the objective function. Histograms of all the eight properties of the 5000 realizations generated from the test problem

by each of the four pilot point methods are shown in Fig C.4, Fig C.3, Fig C.6 and Fig C.5.

Comparing the four sets of histograms, distributions of realizations using 6 pilot points generally have a wider span than those using 9 pilot points, especially in the case based on the objective function with only squared data mismatch and using 6 pilot points, the histograms are obviously flatter than those from other cases. But the results from the pilot point method with 9 pilot points and incomplete objective function were surprisingly similar to those obtained when the prior pdf was used.

The histograms in Fig. C.5 were not substantially different from the histograms in Fig. C.6 although it seems apparent that the maximum likelihood method should give rise to an ill-posed problem. I believe that the explanation for the similarity is that we used Levenberg-Marquardt to find the minimum and, even at the final iteration, the regularization term was sufficiently large to prevent the problem from being ill-posed or even much different from the full problem. In fact, the value of $\lambda$ in Eq. 6.2 at the final iteration was never smaller than 0.4 and in most cases it was 1.5 or greater. It is likely that most papers that report results for maximum likelihood methods actually use some type of regularization in the minimization so that the result is often similar to that obtained by minimizing the full objective function.

$$[A^T(\lambda C_M^{-1} + G^T C_D^{-1} G)A]\alpha = -A^T G^T C_D^{-1}[g(m_{\text{uc}}) - d_{\text{uc}}] \tag{6.2}$$

## 6.6 Gradual Deformation

In this study, we ran the gradual deformation algorithm until the objective function (see Eq. 4.14) was reduced to 50 or less. If the objective function was not reduced to 50 by the 10,000th iteration, it was discarded. For comparison, over 99% of the McMC realizations have squared data mismatch values less than

50, so 50 is a relatively loose tolerance on the data mismatch. In each iteration, a line search is required to find the optimum $\rho$ value, so 10,000 is a sensible maximum number of iterations. For the global perturbation method, 86 realizations were generated out of 1000 gradual deformation sequences. The local perturbation method performed slightly better with 11% of the sequences reaching the convergence criterion before the 10,000th iteration. Histograms for the properties of the 86 realizations sampled from the test problem by the gradual deformation method with global perturbation are shown in Fig. C.7. Instead of showing functional $Sm2$, i.e. $\frac{1}{2}(m - m_{\text{MAP}})^T C_{M'}^{-1}(m - m_{\text{MAP}})$, I show the number of iterations taken by each accepted realizations before reaching the acceptance criterion. The histogram of iteration numbers indicates that most of the realizations generated from the gradual deformation method with global perturbation reached the acceptance criterion after more than 6000 iterations. The histogram of the squared data mismatch $Sd1$ is like a $\delta$ function in that 90% of the values fall between 49 and 50.

The gradual deformation method we applied is very inefficient. Figures 6.12 and 6.13 show the log-permeability value in the 3rd, 7th and 15th gridblock after every 100th perturbation for global and local perturbation respectively. From these two figures, the squared data mismatch is seen to decrease even slower by local perturbation than by global perturbation. Part of the reason is that some of the local perturbations are applied in regions for which a change in property values has no effect on the data mismatch.

## 6.7 Comparison

The distributions of realizations are summarized in the form of box plots. A key for interpreting the box plots is shown in Fig. 6.14. The method of generation of realizations is identified by an acronym along the bottom axis beneath each box. The meaning of the acronyms should be obvious with the possible exception that the

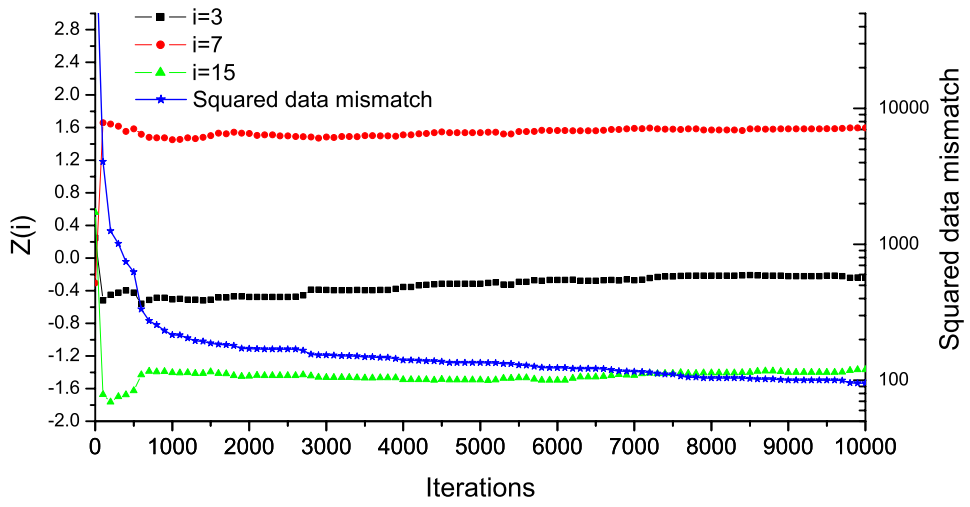


Figure 6.12: The $Z$ values at the 3rd, the 7th and the 15th gridblocks change with the number of iterations using gradual deformation with global perturbation.

several pilot point methods (PP) are identified by number of pilot point locations (6 or 9) and by the objective function that was minimized (D if the objective function minimized the data mismatch only). The two very long Markov chains starting from the first and the second RML realizations are combined to create a better estimate of the true distribution, and the resulting distributions of the properties are labeled as "McMC". The true value of each property and the distribution of realizations unconditional to production data are shown for comparison.

Fig. 6.15 shows comparisons of the distributions of summary reservoir properties from each of the methods. All of the approximate methods in this case seem to generate reservoir realizations whose effective permeability distributions have been shifted to lower values than the distribution obtained from McMC (top of Fig. 6.15). The differences among the methods do not seem to be large, except that the pilot point methods that used 6 locations tend to predict greater uncertainty in effective

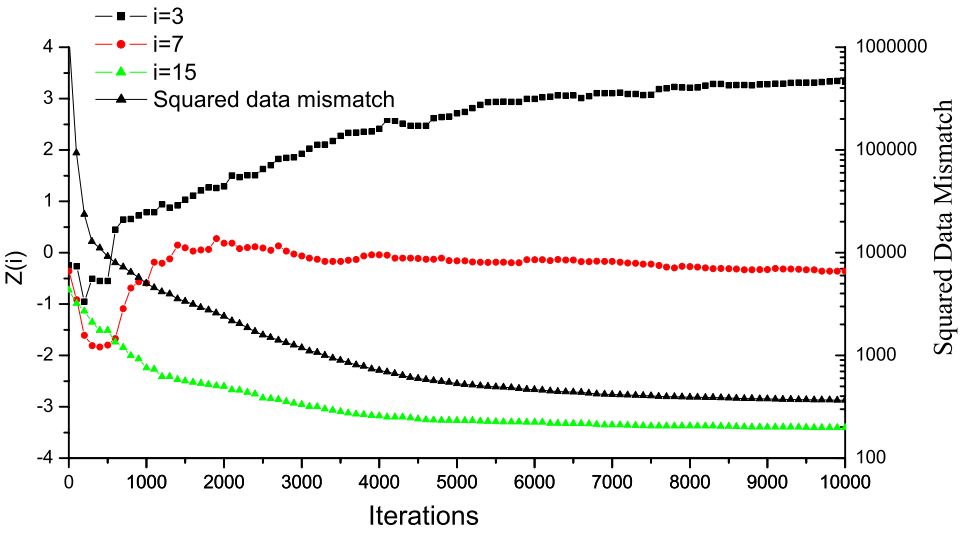


Figure 6.13: The $Z$ values at the 3rd, the 7th and the 15th gridblocks change with the number of iterations using gradual deformation with local perturbation.

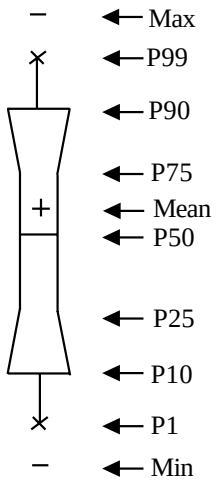


Figure 6.14: Key for interpretation of box plots. P values are percentiles.

permeability than the other methods. All sampling methods also gave similar results for the distribution of average reservoir porosity. Interestingly, the average reservoir

porosity of the true reservoir was 25.8%, while the median values from the ensembles of realizations were all between 24.5 and 25.0% (middle of Fig. 6.15). One might be tempted to conclude that any method would be acceptable for assessing uncertainty in average porosity, but the good agreement between methods seen here may be due to the fact that the conditional mean is nearly the same as the unconditional mean. Again, the pilot point methods with small numbers of pilot points tend to substantially overestimate the uncertainty in average reservoir porosity.

The distributions of maximum reservoir permeability in the bottom plot of Fig. 6.15 show considerably greater variability. Randomized maximum likelihood and linearization about the MAP both give distributions of realizations that are wider and slightly shifted, but otherwise similar, compared to McMC. The pilot point methods, on the other hand, generate reservoir realizations for which very large permeability values occur frequently. This tendency to produce realizations with extreme values has been one of the primary objections to the use of pilot points in reservoir characterization (Oliver, 1999).

Because the square of the mismatch between data computed from a reservoir model and the observed data is an indication of the likelihood of a model being correct, it is extremely important that the squared data mismatch values be relatively small. The upper plot in Fig. 6.16 shows that realizations generated by the LMAP method have very large data mismatch values and are thus unlikely to be realizations conditioned to the observed data. At the bottom of Fig. 6.16, the model mismatch distributions appear similar to the distributions of maximum permeability, reflecting the frequent occurrence of extreme values in the property fields generated by the pilot point methods.

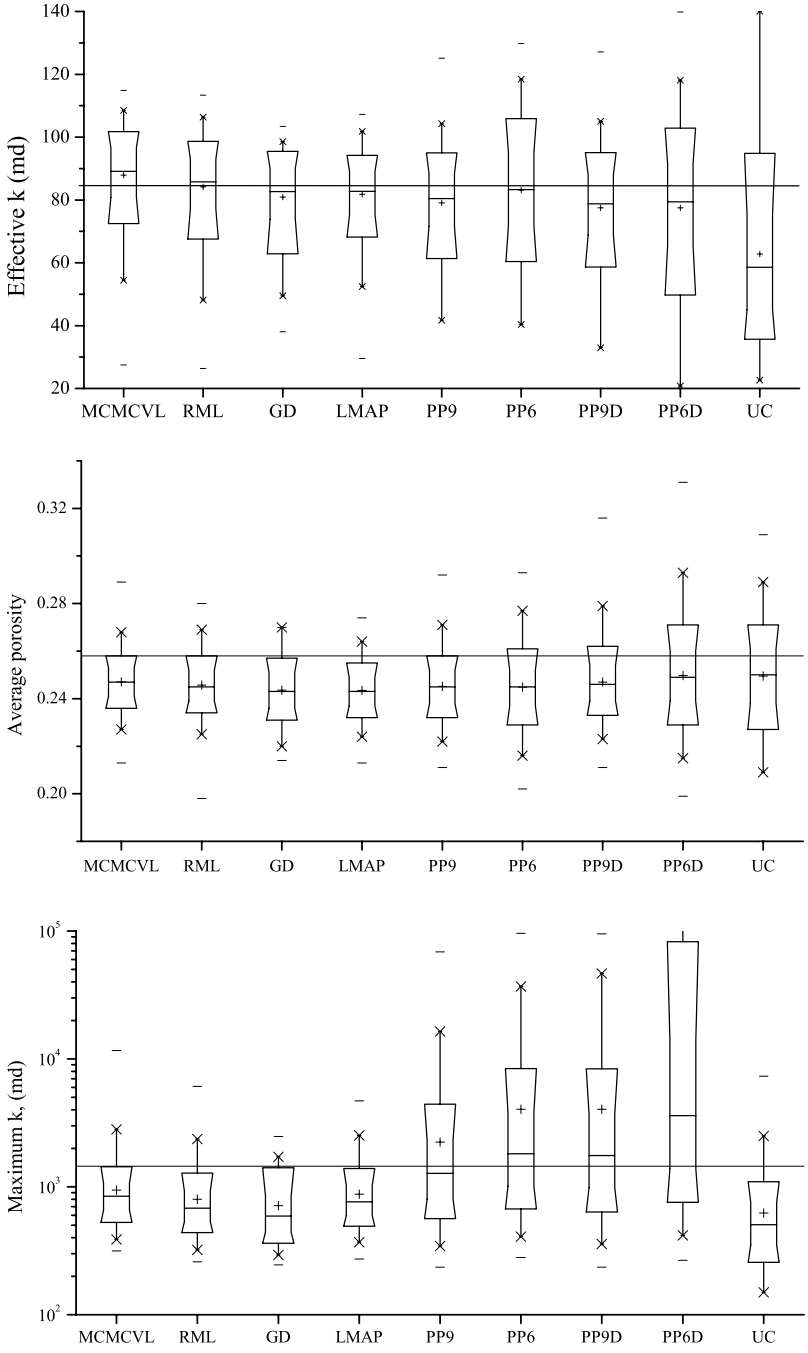


Figure 6.15: Distributions of conditional realizations of effective permeability, average porosity, and maximum permeability from the approximate sampling algorithms and from the two very long Markov chains starting from the first and the second RML realizations. The unconditional distribution and the true values are shown for comparison.

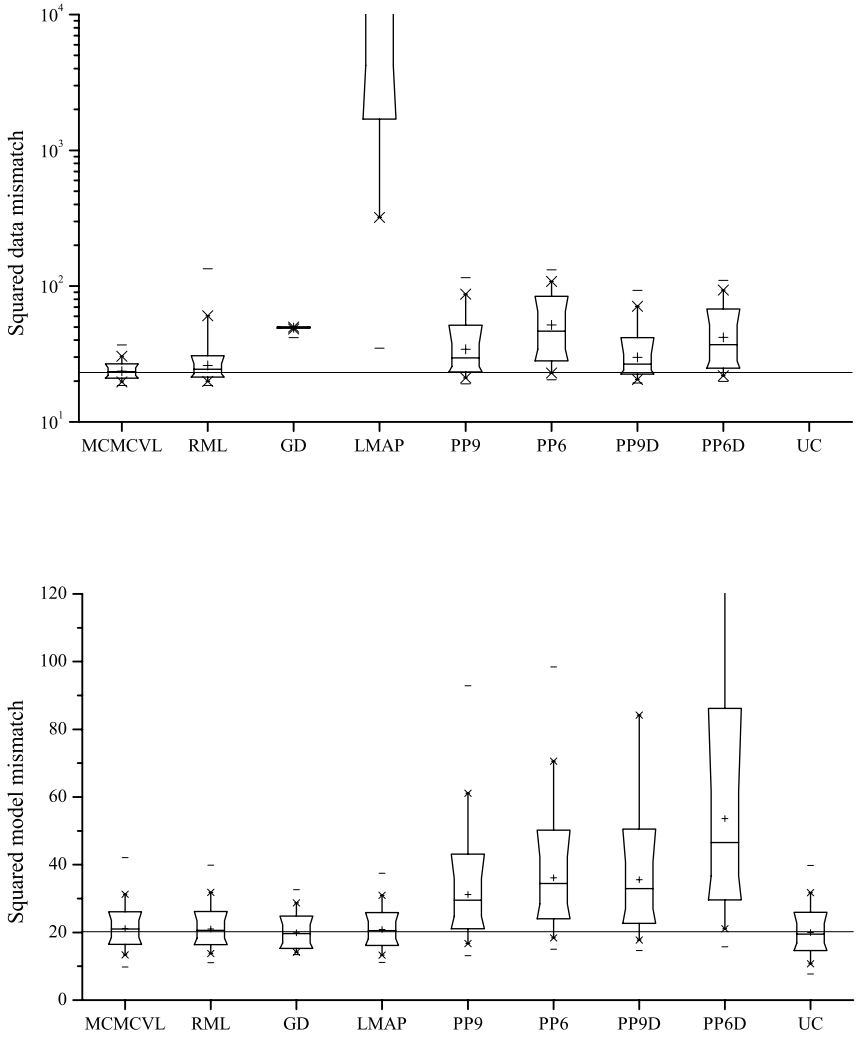


Figure 6.16: Distributions of conditional realizations of squared data mismatch and squared model mismatch from the approximate sampling algorithms and from the two very long Markov chains starting from the first and the second RML realizations. Note that the unconditional realizations of the data mismatch are too large to appear on this plot.

# CHAPTER VII

# DISCUSSION

It is difficult to rectify some of the results that we observed in this study with published results by other authors. Barker et al. (2001) reported accepting 15 of 700 trial realizations from the prior distribution in the rejection algorithm for a reservoir characterization problem with multiphase production data. In contrast, we were unable to obtain any valid realizations using rejection sampling in our problem. Although Barker et al. (2001) do not state the details of their McMC application, they appear to have based their results on the final realizations from 10 chains each of which was 1000 iterations in length. We were unable to obtain any useful information from chains that were that short. The high acceptance rate of proposals obtained from the prior distribution seems to imply that the conditional pdf for the PUNQ-S3 problem is nearly Gaussian. If this is the case, it is difficult to explain the large differences in distributions from the various methods, unless each method was sampling from a different target distribution because of differences in the prior models.

As only around nine realizations were generated from the huge PUNQ-S3 model by each method, and distributions were drawn based on the several realizations, the values of individual samples have great impact on the conclusions. To quantify the effect of small sample size, we randomly drew 9 realizations each time from the 320 million realizations long Markov chain for 1000 times, and saved the maximum, the minimum and the median values among the nine realizations as $P90$, $P10$ and $P50$ respectively. The distributions of $P90$, $P10$ and $P50$ values are shown in the form of box plots in Fig. 7.1. The same experiment was repeated with the 5000

RML realizations, and results are shown in Fig. 7.2. As the 80% confidence intervals for $P90$, $P10$ and $P50$ are larger than the differences between sampling methods, we can conclude that the differences between RML and McMC are insignificant if uncertainty estimates are based on nine Monte Carlo samples. Unfortunately, because of the computational expense of generating the realizations, it seems unlikely that the number of independent conditional realizations will be greater than nine or ten for at least the next few years.

In this work, we chose a highly nonlinear problem to ensure that the conditional pdf was not approximately Gaussian. Even with fairly careful investigation, it is difficult to understand the shape of the pdf (or the objective function). Previous studies have many local minima, especially for problems with discontinues material properties (Zhang et al., 2000). In our synthetic problem, it has been shown by Oliver (2000) that the objective function contains a long curved valley (see Fig. 7.3), as well as multiple local minima. We tested several approximate methods under strictly controlled conditions so that the same assumptions were used for all methods. We also generated enough realizations that we are confident that our conclusions are not affected by the size of our sample. Although the method that we call linearization about the MAP is a valid sampling technique for Gaussian distributions (resulting from linear data relationships), the LMAP realizations produced for this problem did not even approximately honor the data. The failure of the LMAP method in this example is almost certainly related to the poor fit of the pdf to a Gaussian (Fig. 7.4). The pilot point methods performed somewhat better, but they tended to produce realizations with property values much larger and smaller than expected. Increasing the number of pilot points reduces the frequency of occurrence of extreme values. The PP9 examples, for which 45% of the gridblocks are occupied by pilot points, still show a clear excess of extreme values, however, so the potential for computational savings with the pilot point method seem small.

The distributions of the squared model mismatch about the MAP estimate

(function $Sm2$) for the two very long chains were quite different. It seems that even 320 million realizations is not long enough to generate distributions that are independent of the starting point. As $Sm2$ measures the distance from the MAP model to the current realization, it seems to be a good indicator of the tendency for the chain to remain trapped in a region of the model space. The second very long chain (McMCVL2) shows indications of better mixing than the first chain. So even though McMC is a valid method of generating realizations, and these chains were extremely long, conclusions based on distribution from an individual chain could be questionable. For this problem, it seems that the recommendation to assess uncertainty with multiple short chains (Gelman and Rubin, 1992) is reasonable, although multiple long chains would be better. For the properties I evaluated in this research, the distributions were not very sensitive to the starting point (except for $Sm2$ and, to a lesser extent, maximum permeability). So it is reasonable to use the distributions from McMC as a basis for comparison with the approximate methods.

The method of randomized maximum likelihood produced distributions of reservoir properties that were generally quite similar to the presumably correct distributions from McMC (see Figs. 6.15 and 6.16). In Fig. 7.5, distributions of conditional realizations of squared data mismatch from the five different Markov chains are shown together with the distribution from RML. The RML method seems to have overestimated uncertainty of the squared data mismatch. The reason lies in the fact that realizations could be accepted when the changing in the value of the objective function was less than 1%, which was a loose acceptance criterion. If we tighten the criterion, the distribution of the squared data mismatch would certainly be narrowed down. Figs. 7.6 and 7.7 show distributions of the maximum permeability and the squared model mismatch from the five different Markov chains together with the distribution from RML. The first very long chain appears to be stuck in a region of model space. RML realizations give distributions of maximum

permeability and squared model mismatch about the MAP estimate very similar to McMCVL2. The significance of the difference between the RML distribution and the McMC distributions is difficult to evaluate, but it appears to be very small. If it was necessary to limit the results of a study to a small number of realizations, the RML method would probably provide better results than the McMC method for highly nonlinear problems because of the correlation among McMC realizations. From this study, it appears that, of the methods considered here, generating realizations using the Randomized Maximum Likelihood method is the only practical alternative that provides acceptable assessment of uncertainty.

The gradual deformation algorithm also does an excellent job of sampling the squared model mismatch distribution (shown in Figure 6.16), even though this algorithm does not have squared model mismatch term in the objective function. The only distribution from gradual deformation that is poor is the squared data mismatch. Instead of being distributed approximately as $\chi^2$, it is nearly a delta function at $S_d = 50$. The fact that the mean of the squared data mismatch distribution from the gradual deformation algorithm is larger than expected is simply a result of our choice of stopping criterion. If we had chosen a smaller criterion, such as that suggested by Hu et al. (1999), we would have had better agreement in the mean with the correct distribution. Estimates of uncertainty in near future pressure predictions would be in error, however, and it is unclear how that aspect could be corrected.

Although our focus was not on efficiency, it was clear that the gradual deformation method is inefficient compared, for example, to the method of randomized maximum likelihood. One reason for the inefficiency is that the new vector in each iteration of the gradual deformation method provides a random direction for minimization, instead of a downhill direction. At early iterations, a reduction in the mismatch can be achieved in almost any direction, but at later iterations, the likelihood that a reduction in the mismatch can be obtained in a randomly chosen

direction is small. Figure 7.8 shows the data objective function as a function of $\rho$ for the first and the 1000th iterations. In the first iteration, a large reduction is obtained by choosing $\rho = 0.88$. At the 1000th iteration, on the other hand, no reduction was possible. From the squared data mismatch curve in Figures 6.12 and 6.13, it is clear that the rate of improvement in the data match is slow at late iterations. It does seem very likely that the rate of convergence would improve dramatically if multiple independent realizations were used at each step in the deformation. Instead of a line search for an optimal $\rho$, it would be necessary to perform a multidimensional search for the coefficients of the expansion. It appears that the objective function to be minimized for Gradual Deformation can be multimodal, even when the data constraints are linear, so gradient-based search methods may not be effective for gradual deformation.

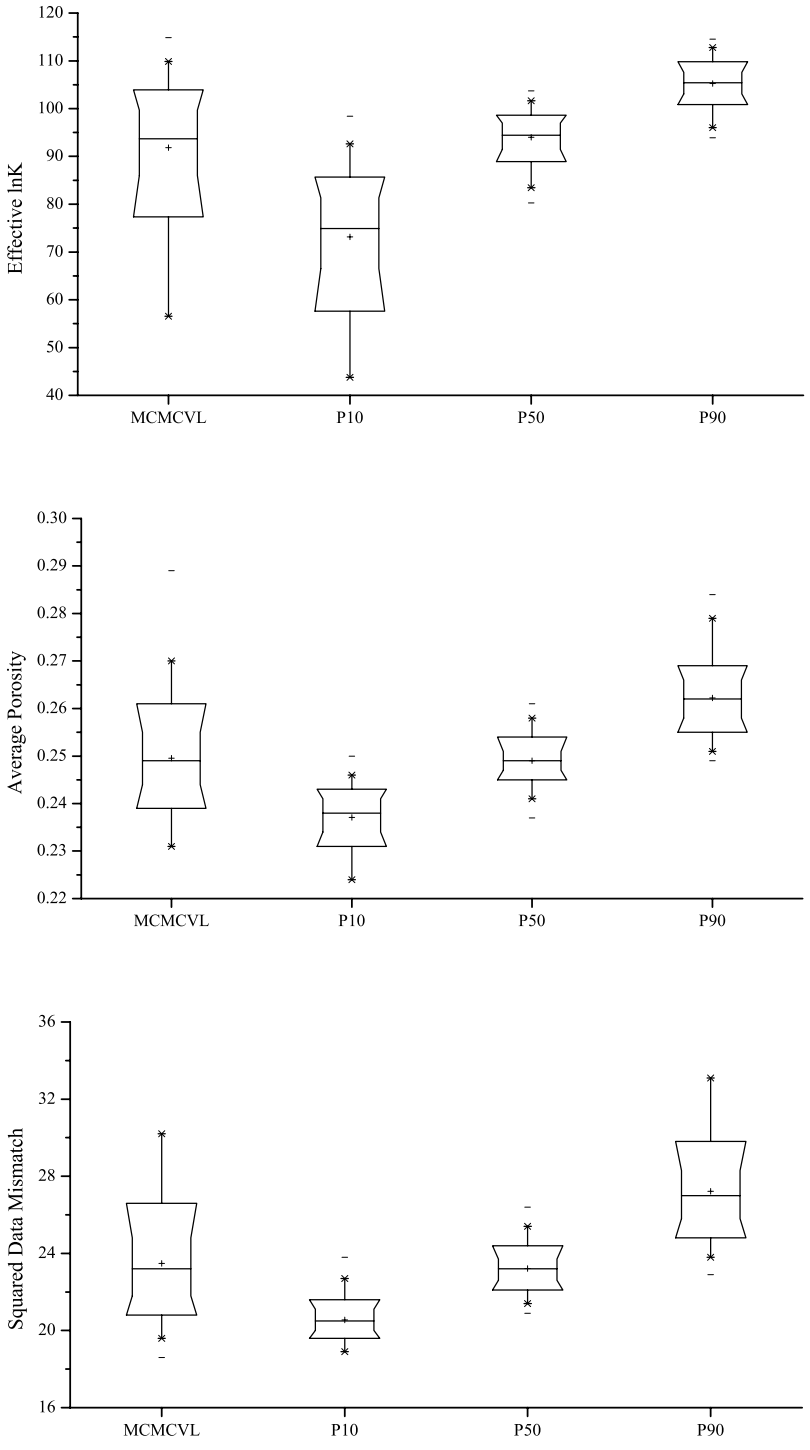


Figure 7.1: Distributions of P10, P50 and P90 of the 320 million McMC realizations. The whole distribution is shown for comparison.

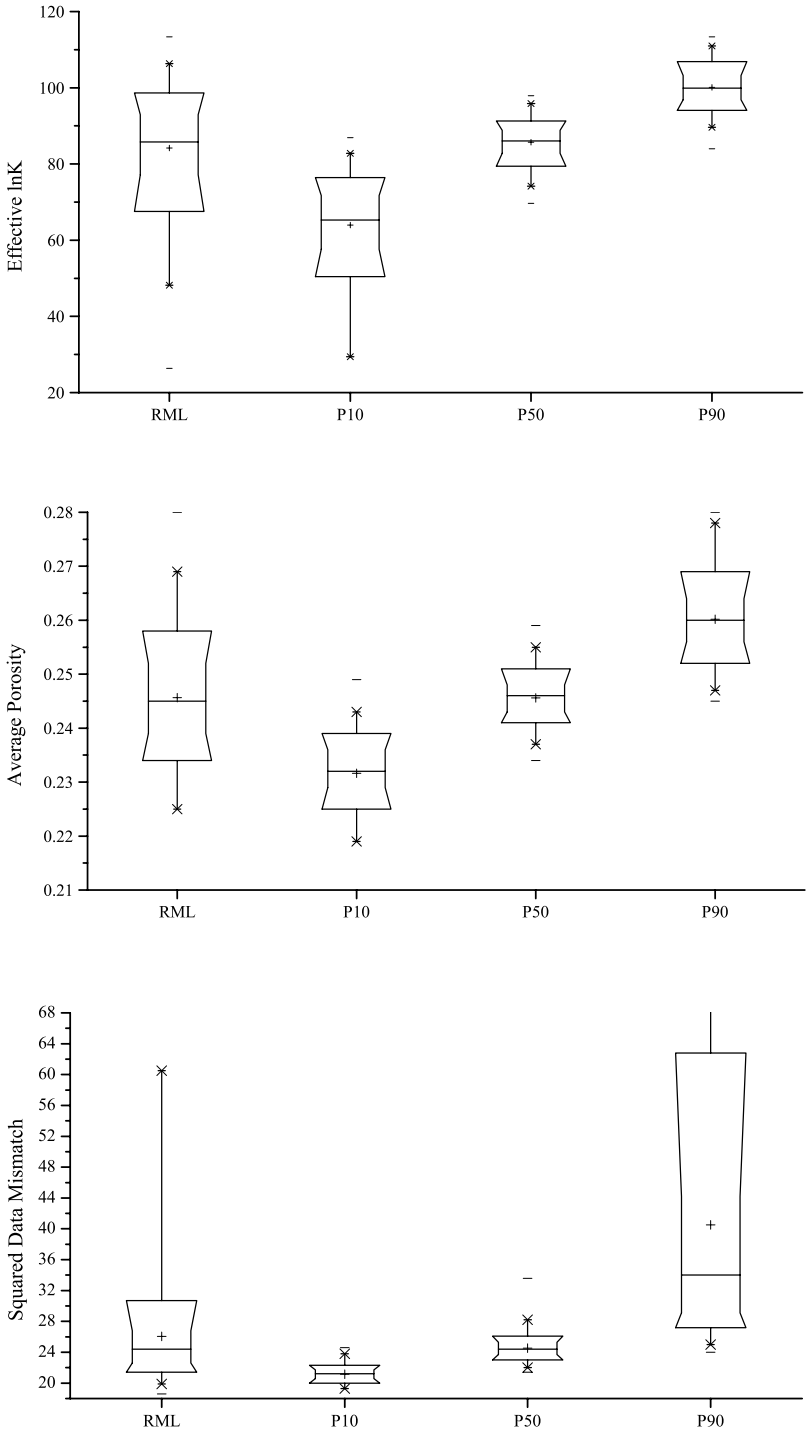


Figure 7.2: Distributions of P10, P50 and P90 of the 5000 RML realizations. The whole distribution is shown for comparison.

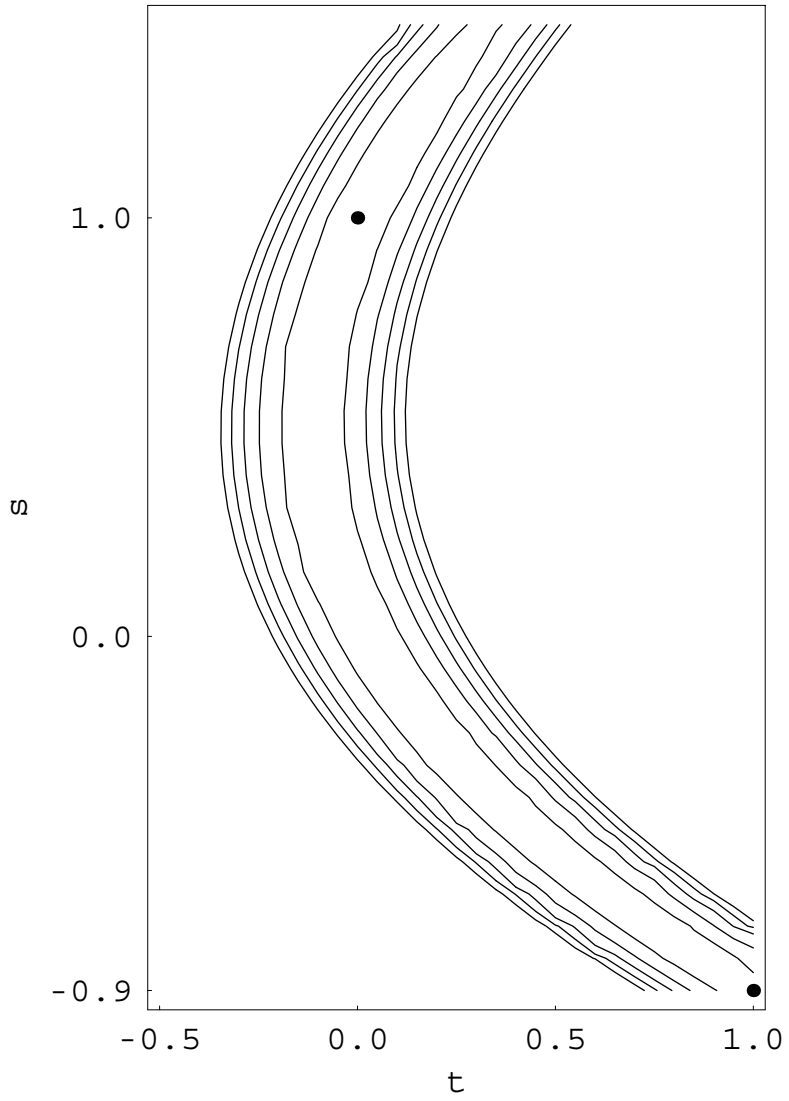


Figure 7.3: The posteriori pdf for the single-phase flow problem appears to have a plateau instead of a single peak. The minima shown as black dots are connected by a valley.

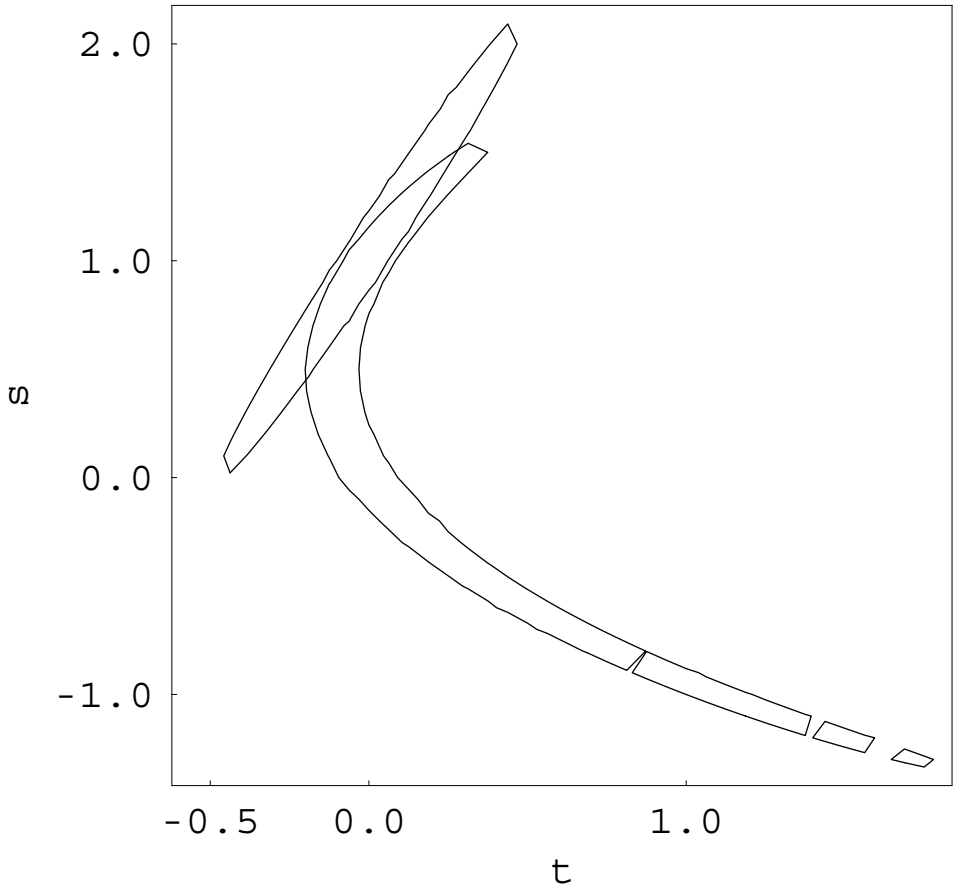


Figure 7.4: The posteriori pdf for the single-phase flow problem appears to have a plateau instead of a single peak. The minima shown as black dots are connected by a valley.

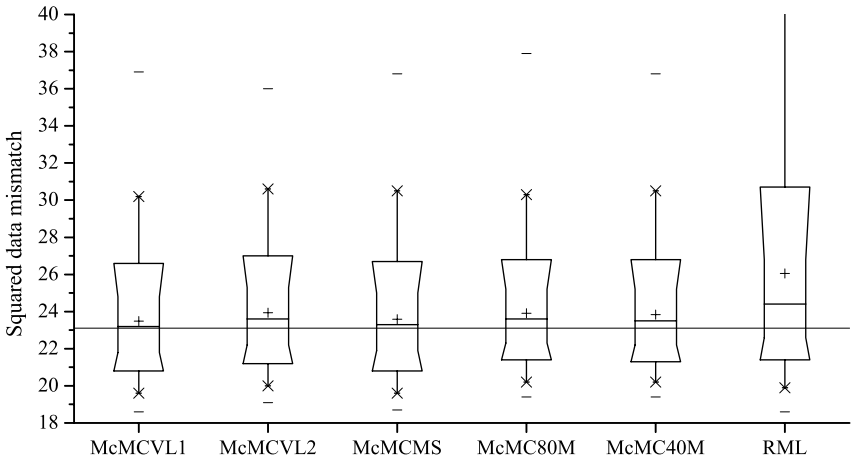


Figure 7.5: Distributions of conditional realizations of squared data mismatch from five different Markov chains. The distribution from randomized maximum likelihood is shown for comparison. McMCVL1 is the very long chain (320 million iterations) starting from the first RML realization; McMCVL2 is the 320 million iterations long chain starting from the second RML realization; McMCMS means multiple short chains (each of which is 2 million iterations in length); McMC80M means one chain of 80 million iterations; McMC40M means one chain of 40 million iterations.

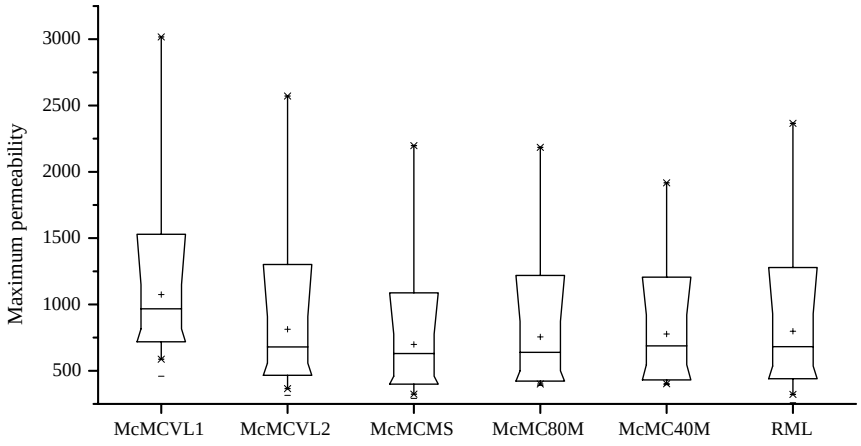


Figure 7.6: Distributions of conditional realizations of the maximum permeability from five different Markov chains. The distribution from randomized maximum likelihood is shown for comparison. McMCVL1 is the very long chain (320 million iterations) starting from the first RML realization; McMCVL2 is the 320 million iterations long chain starting from the second RML realization; McMCMS means multiple short chains (each of which is 2 million iterations in length); McMC80M means one chain of 80 million iterations; McMC40M means one chain of 40 million iterations.

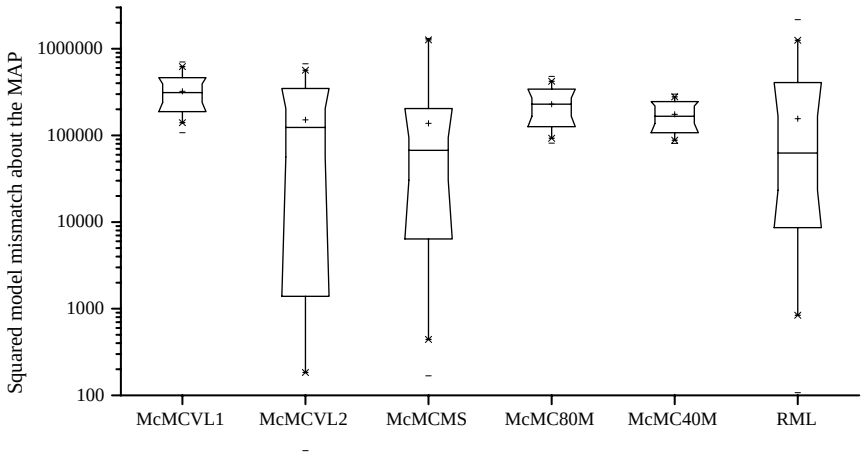


Figure 7.7: Distributions of conditional realizations of the squared model mismatch about the MAP estimate from five different Markov chains. The distribution from randomized maximum likelihood is shown for comparison. McMCVL1 is the very long chain (320 million iterations) starting from the first RML realization; McMCVL2 is the 320 million iterations long chain starting from the second RML realization; McMCMS means multiple short chains (each of which is 2 million iterations in length); McMC80M means one chain of 80 million iterations; McMC40M means one chain of 40 million iterations.

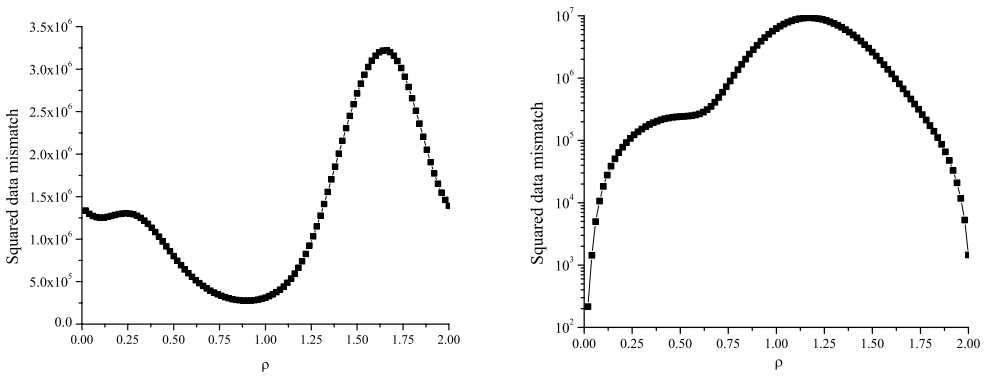


Figure 7.8: The shape of squared data mismatch function at the 1st (left) and 1000th (right) iteration by gradual deformation algorithm.

# CHAPTER VIII

# CONCLUSIONS

Two standard sampling methods and five approximate methods were evaluated in this work. The rejection algorithm was too inefficient for this highly nonlinear problem, as no relatively simple proposal distribution could be found with an acceptable acceptance rate. An extremely large number of realizations is required by the Markov chain Monte Carlo algorithm to be confident with the validity of the resulting distribution. Unfortunately, this is usually computationally inapplicable for most test problems. LMAP realizations do not honor production data, so we could not use it to predict future production. The method of gradual deformation provides acceptable sample distributions for uncertainty estimation. Although efficiency was not the primary focus of this investigation, it was clear that the method of gradual deformation was less efficient for generating realizations than other approximate methods. The method of randomized maximum likelihood produced distributions of reservoir properties that were compatible to the distributions from McMC, which is known to reflect the true distribution with sufficient number of realizations. From this study, it appears that, of the methods considered here, generating realizations using the randomized maximum likelihood method is the only practical alternative that provides acceptable assessment of uncertainty.

| block | True Model | | MAP Model | |
|---|---|---|---|---|
| | $lnk$, md | $\phi$ | $lnk$, md | $\phi$ |
| 1 | 3.54 | 0.247 | 4.673 | 0.256 |
| 2 | 3.17 | 0.150 | 4.862 | 0.263 |
| 3 | 4.14 | 0.207 | 5.137 | 0.272 |
| 4 | 5.76 | 0.175 | 5.424 | 0.281 |
| 5 | 4.69 | 0.234 | 5.609 | 0.287 |
| 6 | 4.14 | 0.280 | 5.588 | 0.281 |
| 7 | 4.47 | 0.277 | 5.558 | 0.274 |
| 8 | 5.10 | 0.265 | 5.466 | 0.264 |
| 9 | 4.19 | 0.265 | 4.850 | 0.238 |
| 10 | 2.88 | 0.172 | 3.719 | 0.198 |
| 11 | 2.30 | 0.143 | 3.428 | 0.183 |
| 12 | 5.10 | 0.235 | 4.643 | 0.192 |
| 13 | 5.24 | 0.252 | 6.063 | 0.254 |
| 14 | 3.99 | 0.255 | 5.680 | 0.226 |
| 15 | 4.78 | 0.248 | 4.419 | 0.215 |
| 16 | 3.48 | 0.198 | 4.534 | 0.223 |
| 17 | 3.66 | 0.222 | 4.212 | 0.219 |
| 18 | 4.85 | 0.229 | 3.928 | 0.225 |
| 19 | 2.99 | 0.284 | 4.146 | 0.251 |
| 20 | 5.02 | 0.310 | 4.542 | 0.266 |

Table 8.1: The true permeability and porosity fields.

| Time (Days) | True Pressure (psia) | | | Observation Pressure (psia) | | |
|---|---|---|---|---|---|---|
| well location | 7 | 13 | 18 | 7 | 13 | 18 |
| 0.0004 | 3500.0 | 3462.3 | 3500.0 | 3500.6 | 3462.5 | 3500.2 |
| 0.0012 | 3500.0 | 3404.9 | 3500.0 | 3500.3 | 3404.6 | 3500.0 |
| 0.0020 | 3500.0 | 3361.1 | 3500.0 | 3499.8 | 3361.3 | 3499.3 |
| 0.0040 | 3500.0 | 3276.2 | 3500.0 | 3498.8 | 3275.0 | 3498.4 |
| 0.0080 | 3500.0 | 3142.2 | 3499.3 | 3498.4 | 3142.0 | 3498.6 |
| 0.0120 | 3499.7 | 3028.5 | 3496.8 | 3499.1 | 3028.6 | 3497.3 |
| 0.0200 | 3497.7 | 2834.6 | 3482.8 | 3498.3 | 2835.0 | 3483.5 |
| 0.0360 | 3484.6 | 2516.1 | 3420.2 | 3485.1 | 2517.0 | 3421.0 |
| 0.0600 | 3445.0 | 2128.3 | 3273.2 | 3446.7 | 2130.1 | 3275.0 |
| 0.1016 | 3341.7 | 1595.0 | 2954.2 | 3344.0 | 1598.2 | 2956.7 |

Table 8.2: True Pressure data and observed pressure.

Bibliography

Alabert, F., The practice of fast conditional simulations through the LU decomposition of the covariance matrix, *Mathematical Geology*, **19**(5), 369–386, 1987.

Alabert, F. G., Constraining description of randomly heterogeneous reservoirs to pressure test data: A Monte Carlo study, SPE-19600, in *64th Annual SPE Tech. Conf.*, pp. 307–321, 1989.

Barker, J. W., M. Cuypers, and L. Holden, Quantifying uncertainty in production forecasts: Another look at the PUNQ-S3 problem, *SPE Journal*, **6**(4), 433–441, 2001.

Bi, Z., *Conditioning 3D Stochastic Channels to Well-Test Pressure Data*, Ph.D. thesis, University of Tulsa, Tulsa, Oklahoma, 1999.

Bonet-Cunha, L., D. S. Oliver, R. A. Rednar, and A. C. Reynolds, A hybrid Markov chain Monte Carlo method for generating permeability fields conditioned to multiwell pressure data and prior information, *SPE Journal*, **3**(3), 261–271, 1998.

Bréfort, B. and V. Pelcé, Inverse modeling for compressible flow. Aplication to gas reservoirs, in *2nd European Conference on the Mathematics of Oil Recovery*, pp. 331–334, 1990.

Chib, S. and E. Greenberg, Understanding the Metropolis-Hastings algorithm, *The American Statistician*, **49**(4), 327–335, 1995.

Chu, L., M. Komara, and R. A. Schatzinger, An efficient technique for inversion of reservoir properties using iteration method, *SPE Journal*, **5**(1), 71–81, 2000.

Chu, L., A. C. Reynolds, and D. S. Oliver, Computation of sensitivity coefficients for conditioning the permeability field to well-test data, *In Situ*, **19**(2), 179–223, 1995.

Clifton, P. M. and S. P. Neuman, Effects of kriging and inverse modeling on conditional simulation of the Avra Valley Aquifer in southern Arizona., *Water Resour. Res.*, **18**(4), 1215–1234, 1982.

Davis, M., Production of conditional simulations via the LU decomposition of the covariance matrix, *Mathematical Geology*, **19**(2), 91–98, 1987.

de Marsily, G., G. Lavedan, M. Boucher, and G. Fasanino, Interpretation of interference tests in a well field using geostatistical techniques to fit the permeability distribution in a reservoir model, in *Geostatistics for Natural Resources Characterization, Part 2*, pp. 831–849, D. Reidel, 1984.

Deutsch, C. V., *Annealing Techniques Applied to Reservoir Modeling and the Integration of Geological and Engineering (Well Test) Data*, Ph.D. thesis, Stanford University, Stanford, California, 1992.

Deutsch, C. V., Conditioning reservoir models to well test information, in *Geostatistics Tróia '92*, pp. 505–518, Kluwer Academic Publishers, Dordrecht, The Netherlands, 1993.

Dietrich, C. R. and G. N. Newsam, Efficient generation of conditional simulations by Chebyshev matrix polynomial approximations to the symmetric square root of the covariance matrix, *Mathematical Geology*, **27**(2), 207–228, 1995.

Farmer, C. L., Numerical rocks, in *Mathematics of Oil Recovery*, pp. 437–447, Clarendon Press, Oxford, 1992.

Floris, F. J. T., M. D. Bush, M. Cuypers, F. Roggero, and A.-R. Syversveen, Methods for quantifying the uncertainty of production forecasts: A comparative study, *Petroleum Geoscience*, **7**(SUPP), 87–96, 2001.

Gelman, A. and D. B. Rubin, Inference from iterative simulation using multiple sequences, *Statistical Science*, **7**(4), 457–472, 1992.

Geyer, C. J., Practical Markov chain Monte Carlo, *Statistical Science*, **7**(4), 473–483, 1992.

Gilks, W. R., S. Richardson, and D. J. Spiegelhalter, Introducing Markov chain Monte Carlo, in *Markov Chain Monte Carlo in Practice*, (edited by W. R. Gilks, S. Richardson, and D. J. Spiegelhalter), pp. 1–19, Chapman & Hall, New York, 1996a.

Gilks, W. R., S. Richardson, and D. J. Spiegelhalter (eds.), *Markov Chain Monte Carlo in Practice*, Chapman & Hall, New York, 1996b.

Gómez-Hernández, J. J., A. Sahuquillo, and J. E. Capilla, Stochastic simulation of transmissivity fields conditional to both transmissivity and piezometric data. 1. Theory, *Journal of Hydrology*, (203), 162–174, 1997.

He, N., *Three Dimensional Reservoir Description by Inverse Theory using Well-Test Pressure and Geostatistical Data*, Ph.D. thesis, University of Tulsa, 1997.

Hegstad, B. K. and H. Omre, Uncertainty assessment in history matching, in *5th International Geostatistics Congress*, 1996.

Hegstad, B. K. and H. Omre, Uncertainty in production forecasts based on well observations, seismic data and production history, Tech. Rep. Statistics No. 17/1999, Norwegian University of Science and Technology, 1999.

Hird, K. B. and M. G. Kelkar, Conditional simulation method for reservoir description using spatial and well performance constraints (SPE-24750), in *1992 SPE Annual Technical Conference and Exhibition*, pp. 887–902, 1992.

Holden, L., R. Madsen, A. Skorstad, K. A. Jakobsen, C. B. Tjølsen, and S. Vik, Use of well test data in stochastic reservoir modelling, SPE 30591, in *Proceedings of the SPE annual Technical Conference and Exhibition*, 1995.

Holden, L., Ø. Skare, H. Omre, and H. Tjelmeland, Sampling algorithms for Bayesian history matching, *preprint*, 1–29, 2001.

Hu, L. Y., M. L. Ravalec, G. Blanc, F. Roggero, B. Noetinger, A. Haas, and B. Corre, Reducing uncertainties in production forecasts by constraining geological modeling to dynmaic data, in *Proceedings of the 1999 SPE Annual Technical Conference and Exhibition*, pp. 1–8, 1999.

Journel, A. and C. J. Huijbregts, *Mining Geostatistics*, Academic Press, New York, 1978, 600 p.

Kitanidis, P. K., Quasi-linear geostatistical theory for inversing, *Water Resour. Res.*, **31**(10), 2411–2419, 1995.

LaVenue, A. M. and J. F. Pickens, Application of a coupled adjoint sensitivity and kriging approach to calibrate a groundwater flow model, *Water Resour. Res.*, **28**(6), 1543–1569, 1992.

Li, R., *Conditioning Geostatistical Models to Three-Dimensional Three-Phase Flow Production Data by Automatic History Matching*, Ph.D. thesis, University of Tulsa, Tulsa, Oklahoma, 2001.

Liu, N., S. Betancourt, and D. S. Oliver, Assessment of uncertainty assessment methods, *Proceedings of the 2001 SPE Annual Technical Conference and Exhibition*, 1–15, 2001.

Oliver, D. S., Multiple realizations of the permeability field from well-test data, *Soc. Petrol. Eng. J.*, **1**(2), 145–154, 1996a.

Oliver, D. S., On conditional simulation to inaccurate data, *Math. Geology*, **28**(6), 811–817, 1996b.

Oliver, D. S., Notes on sampling, 2000, unpublished notes.

Oliver, D. S., Five things I dislike about pilot points, Sept. 13–15, 1999, unpublished talk at the Statoil Research Summit, Conditioning Reservoir Models and Forecasts to Dynamic Data, Trondheim, Norway.

Oliver, D. S., L. B. Cunha, and A. C. Reynolds, Markov chain Monte Carlo methods for conditioning a permeability field to pressure data, *Mathematical Geology*, **29**(1), 61–91, 1997.

Oliver, D. S., N. He, and A. C. Reynolds, Conditioning permeability fields to pressure data, in *European Conference for the Mathematics of Oil Recovery, V*, pp. 1–11, 1996.

Oliver, D. S., A. C. Reynolds, Z. Bi, and Y. Abacioglu, Integration of production data into reservoir models, *Petroleum Geoscience*, **7**(SUPP), 65–73, 2001.

Omre, H., Stochastic reservoir models conditioned to non-linear production history observations, Tech. Rep. Statistics No. 3/2001, Department of Mathematical Sciences, Norwegian University of Science & Technology, Trondheim, Norway, 2001.

RamaRao, B. S., A. M. LaVenue, G. de Marsily, and M. G. Marietta, Pilot point methodology for automated calibration of an ensemble of conditionally simulated transmissivity fields, 1. Theory and computational experiments, *Water Resour. Res.*, **31**(3), 475–493, 1995.

Rao, C. R., *Linear Statistical Inference and Its Applications*, second edn., John Wiley & Sons, New York, 1973.

Ripley, B. D., *Stochastic Simulation*, John Wiley & Sons, New York, 1987.

Roggero, F. and L. Y. Hu, Gradual deformation of continuous geostatistical models for history matching, *SPE 49004, Annual Technical Conference*, 1998.

Romero, C., A. G. J.N. Carter, and R. Zimmerman, A modified genetic algorithm for reservoir characterisation, *SPE 64765*, 2000.

Sagar, R. K., B. G. Kelkar, and L. G. Thompson, Reservoir description by integration of well test data and spatial statistics, SPE-26462, in *Proccedings of the 68th Annual Technical Conference of the SPE*, pp. 475–489, 1993.

Scheuer, E. M. and D. S. Stoller, On the generation of normal random vectors, *Technometrics*, **4**, 278–281, 1962.

Sen, M. K., A. D. Gupta, P. L. Stoffa, L. W. Lake, and G. A. Pope, Stochastic reservoir modeling using simulated annealing and genetic algorithm, in *Proceedings from the 67th Annual Technical Conference and Exhibition of the Society of Petroleum Engineers*, pp. 939–950, 1992.

Zhang, F., A. C. Reynolds, and D. S. Oliver, Model errors inherent in conditioning a stochastic channel to pressure data, (SPE-62987), in *2000 SPE Annual Technical Conference and Exhibition*, pp. 167–176, 2000.

Zimmerman, D. A., G. de Marsily, C. A. Gotway, M. G. Marietta, C. L. Axness, R. Beauheim, R. Bras, J. Carrera, G. Dagan, P. B. Davies, D. P. Gallegos, A. Galli, J. Gomez-Hernandez, S. M. Gorelick, P. Grindrod, A. L. Gutjahr, P. K. Kitanidis, A. M. Lavenue, D. McLaughlin, S. P. Neuman, B. S. Ramarao, C. Ravenne, and Y. Rubin, A comparison of seven geostatistically based inverse approaches to

estimate transmissivities for modeling advective transport by groundwater flow, *WRR*, **34**(6), 1373–1413, 1998.

# APPENDIX A

Plots in this appendix show all the property sequences from the chain of 40 million models. The initial model was a RML realization. Among the eight property sequences, no evidence of a transition period is shown at the beginning of the chain.

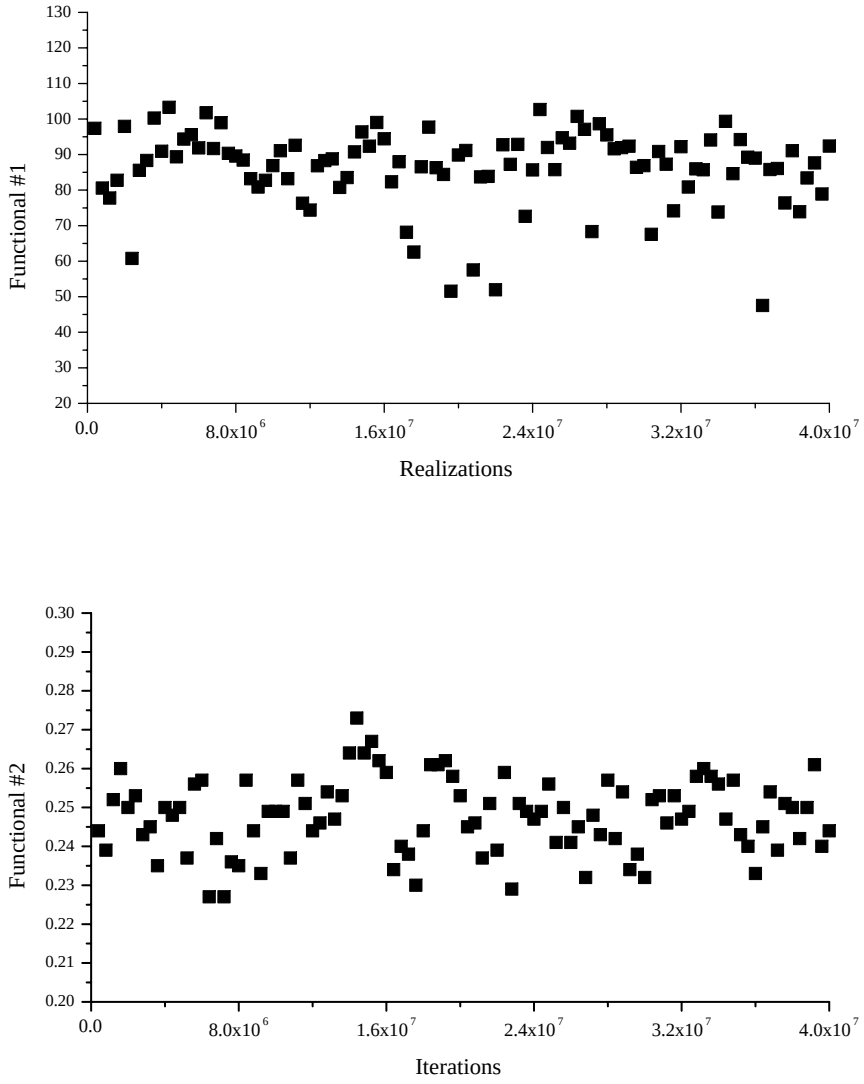


Figure A.1: Every 40,000th model from the chain of 40 million models was used to generate effective permeability and average porosity. The initial model was a RML realization. No evidence of a transition period is shown at the beginning of the chain.

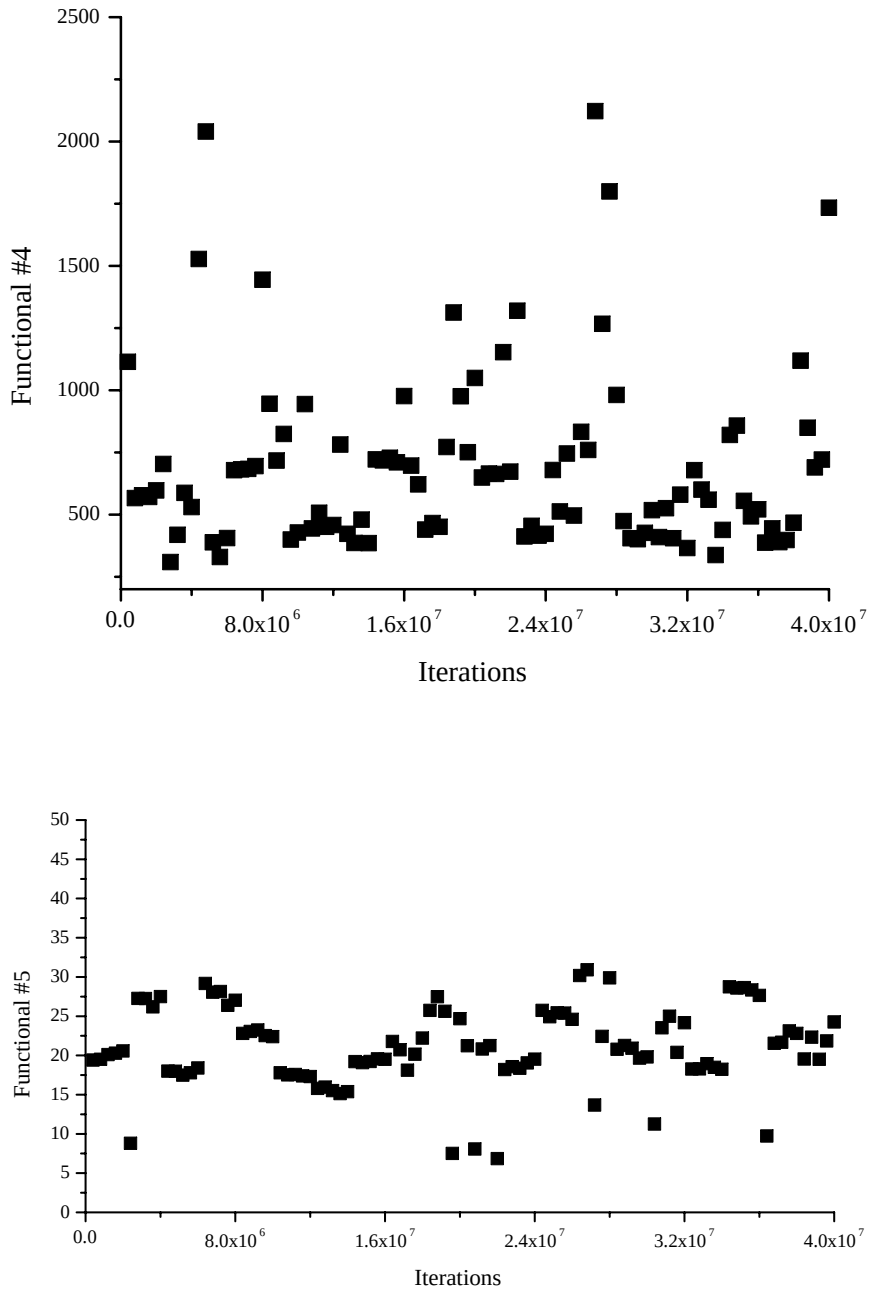


Figure A.2: Every 40,000th model from the chain of 40 million models was used to generate the maximum permeability and the minimum permeability. The initial model was a RML realization. No evidence of a transition period is shown at the beginning of the chain.

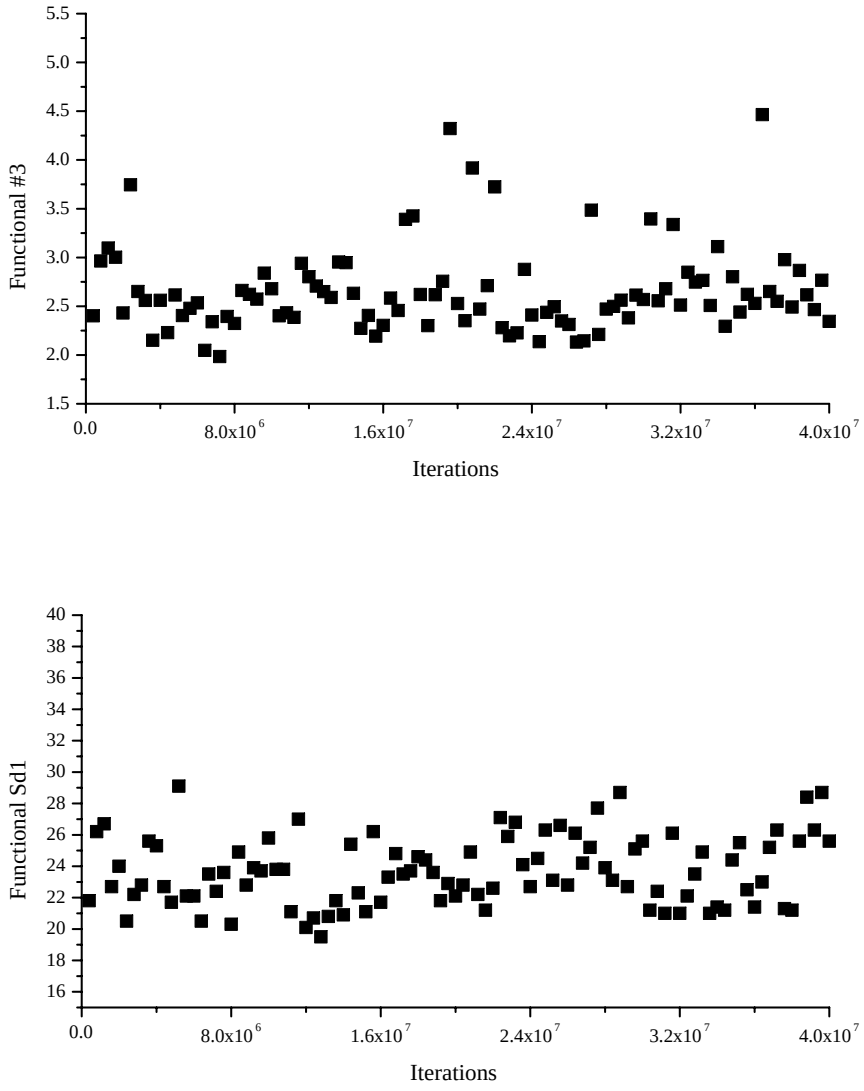


Figure A.3: Every 40,000th model from the chain of 40 million models was used to generate travel time and squared data mismatch. The initial model was a RML realization. No evidence of a transition period is shown at the beginning of the chain.

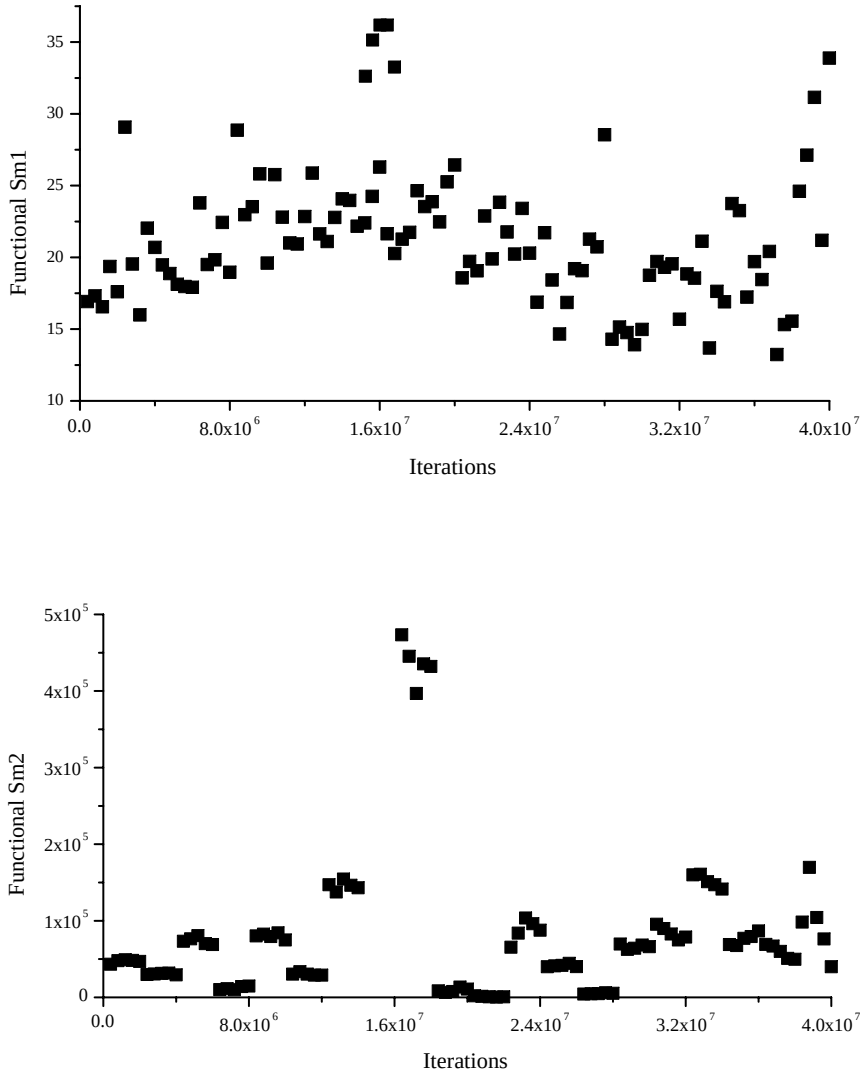


Figure A.4: Every 40,000th model from the chain of 40 million models was used to generate the squared model mismatch about the prior model and about the MAP estimate. The initial model was a RML realization. No evidence of a transition period is shown at the beginning of the chain.

# APPENDIX B

In this appendix, histograms of the maximum permeability, the minimum permeability, the model mismatch about the prior model and the model mismatch about the MAP estimate from each of the six Markov chains are put together for comparison. "McMC 40E6" indicates that the sequence is composed with 20 Markov chains, and each of which has 2 million iterations. "McMC 4E7" is the sequence of 40 million realizations in a single chain. "McMC 4E7 2nd" used the second realization of RML method as the initial element. Here the "320MM1ch" is the very long chain starting from the first realization of RML method.

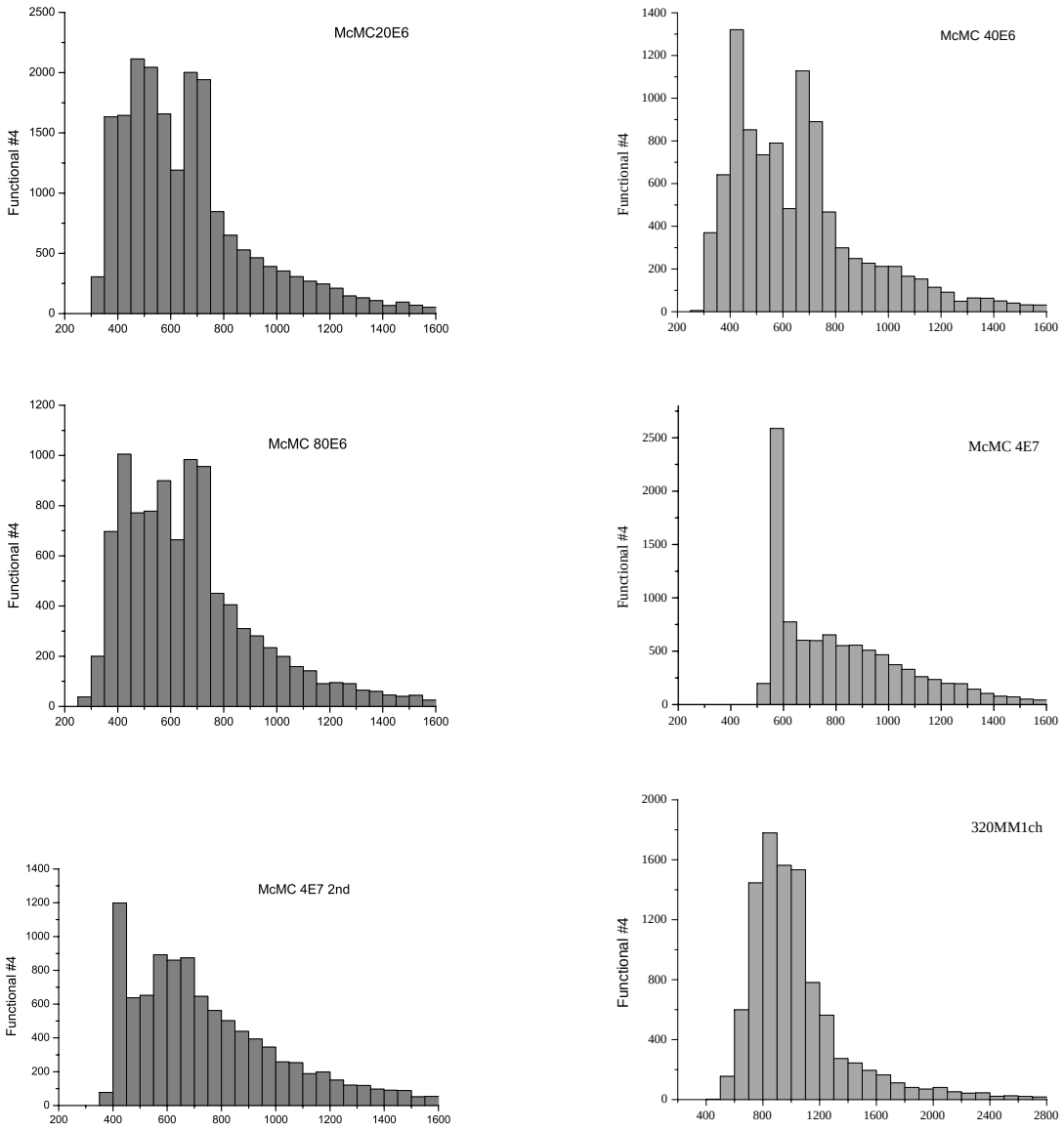


Figure B.1: The comparison of histograms of maximum permeability from a variety of McMC sequences with different length and number of chains.

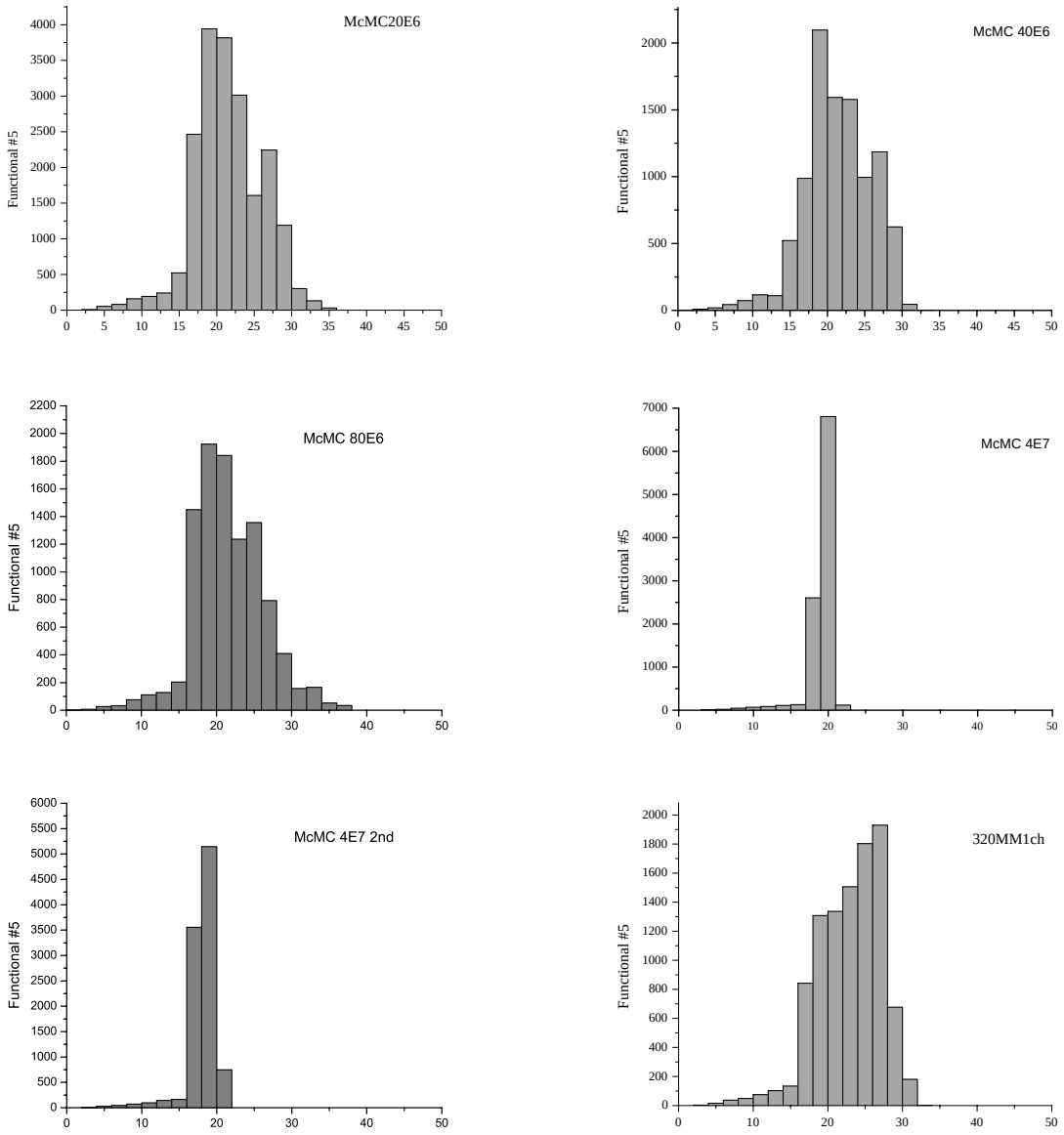


Figure B.2: The comparison of histograms of minimum permeability from a variety of McMC sequences with different length and number of chains.

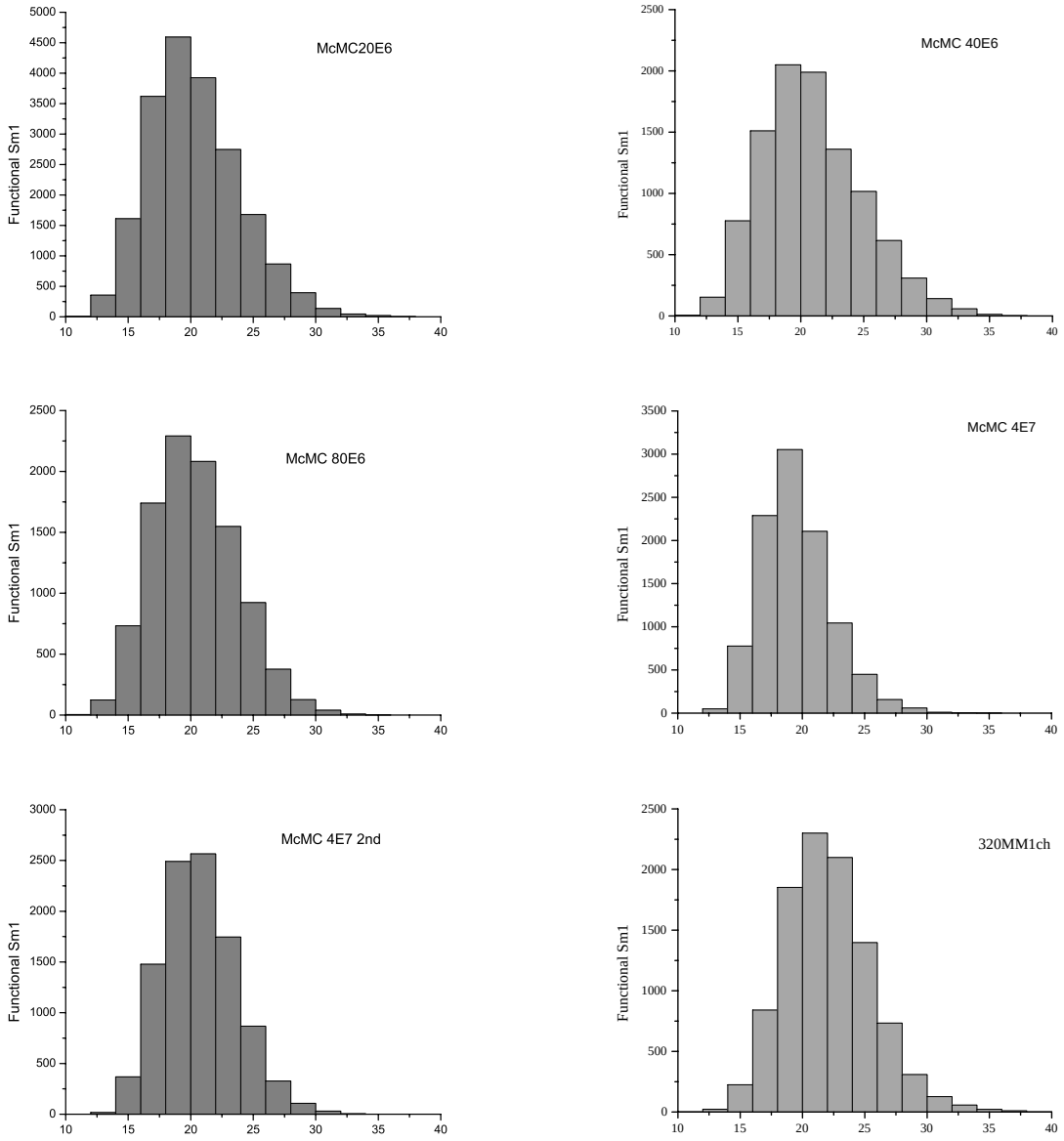


Figure B.3: The comparison of histograms of squared model mismatch about the prior model from a variety of McMC sequences with different length and number of chains.

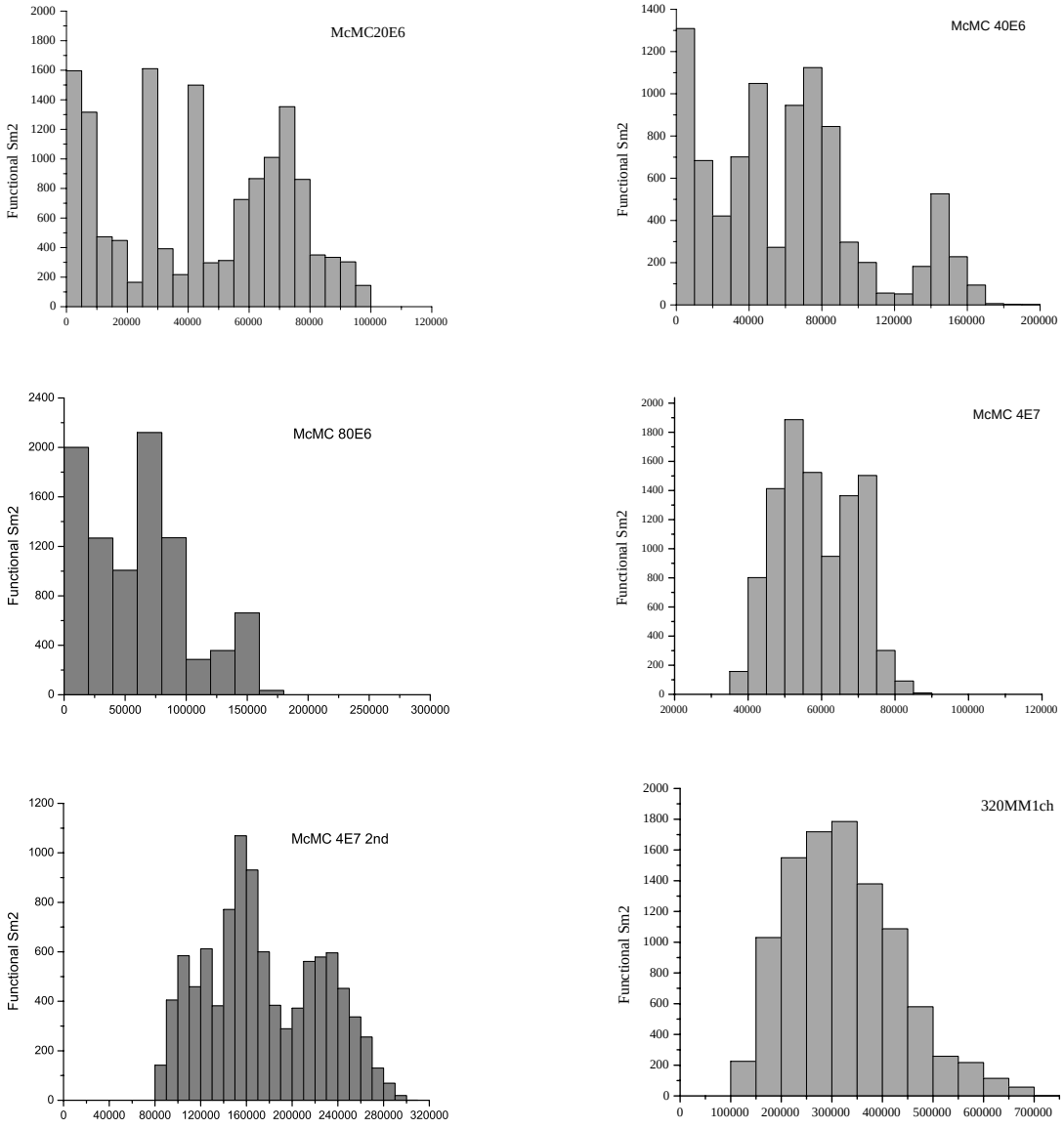


Figure B.4: The comparison of histograms of squared model mismatch about the MAP estimate from a variety of McMC sequences with different length and number of chains.

# APPENDIX C

Histograms of the realizations from all the approximate methods are shown in this appendix. Four pilot point methods have been applied in the test problem to generate model realizations. "PP6" is the pilot point method with full objective function and 33% pilot point density. "PP9D" indicates the method with only squared data mismatch in the objective function and 45% pilot point density.

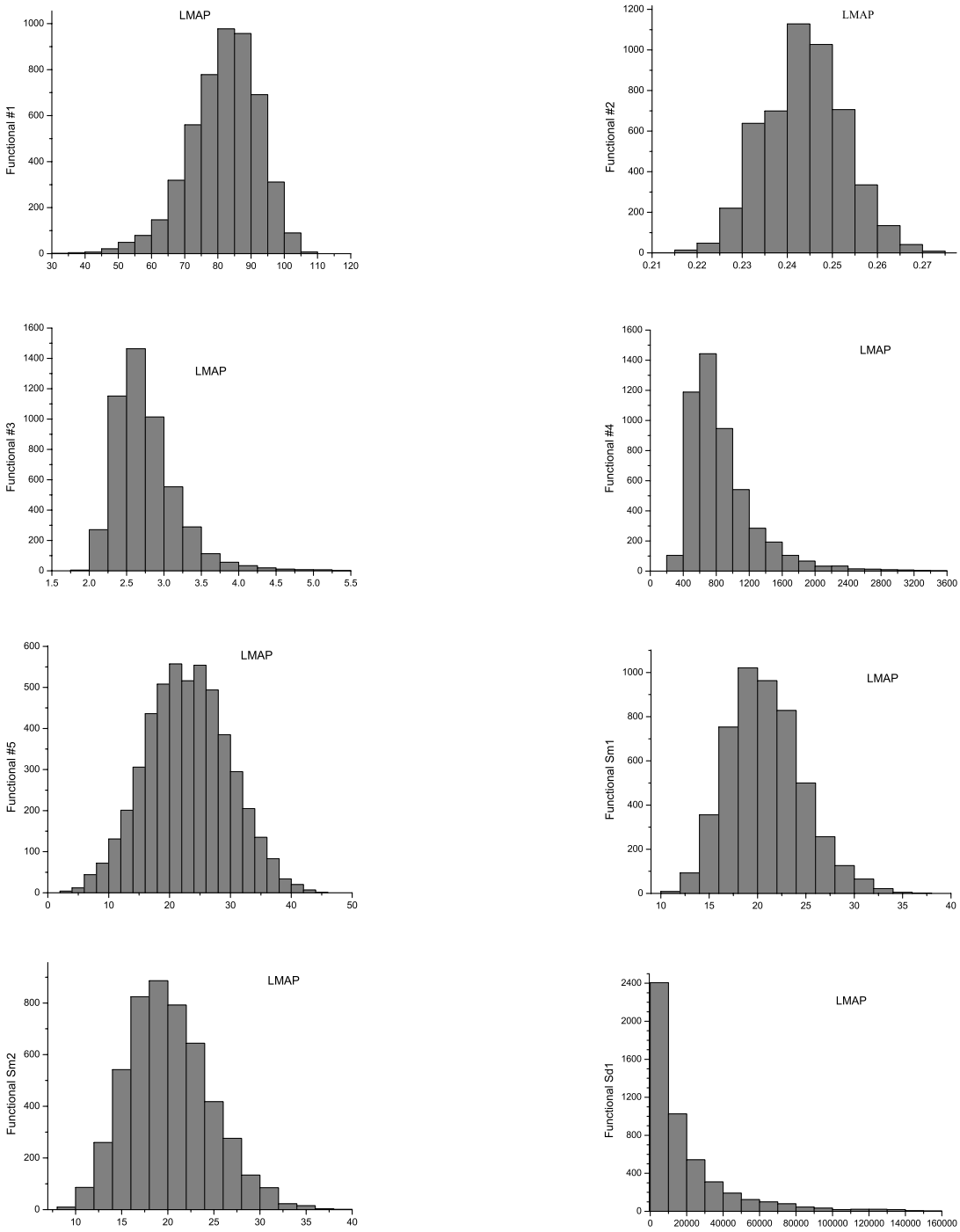


Figure C.1: Histograms for the properties of 5000 LMAP realizations sampled from the test problem.

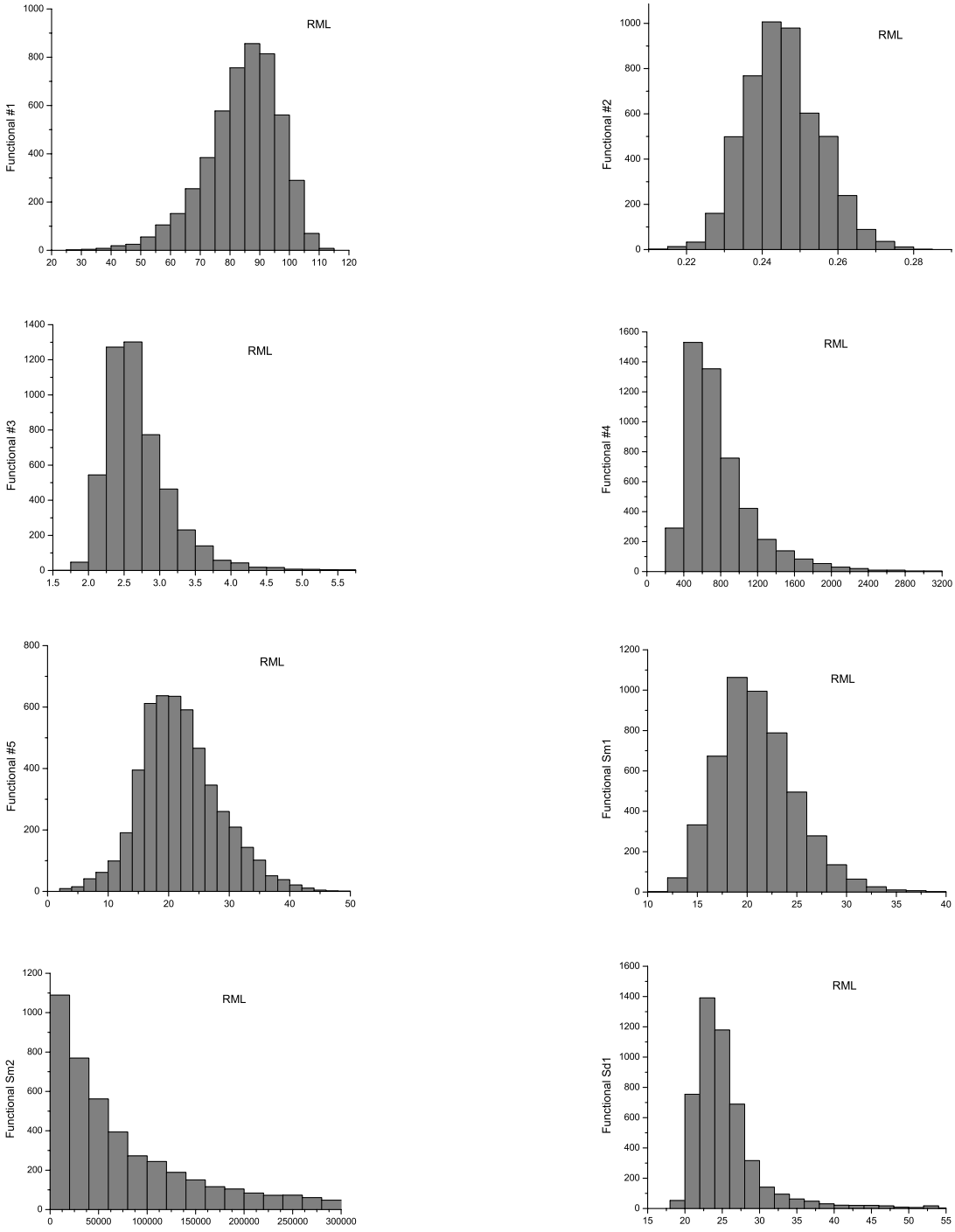


Figure C.2: Histograms for the properties of 5000 RML realizations sampled from the test problem.

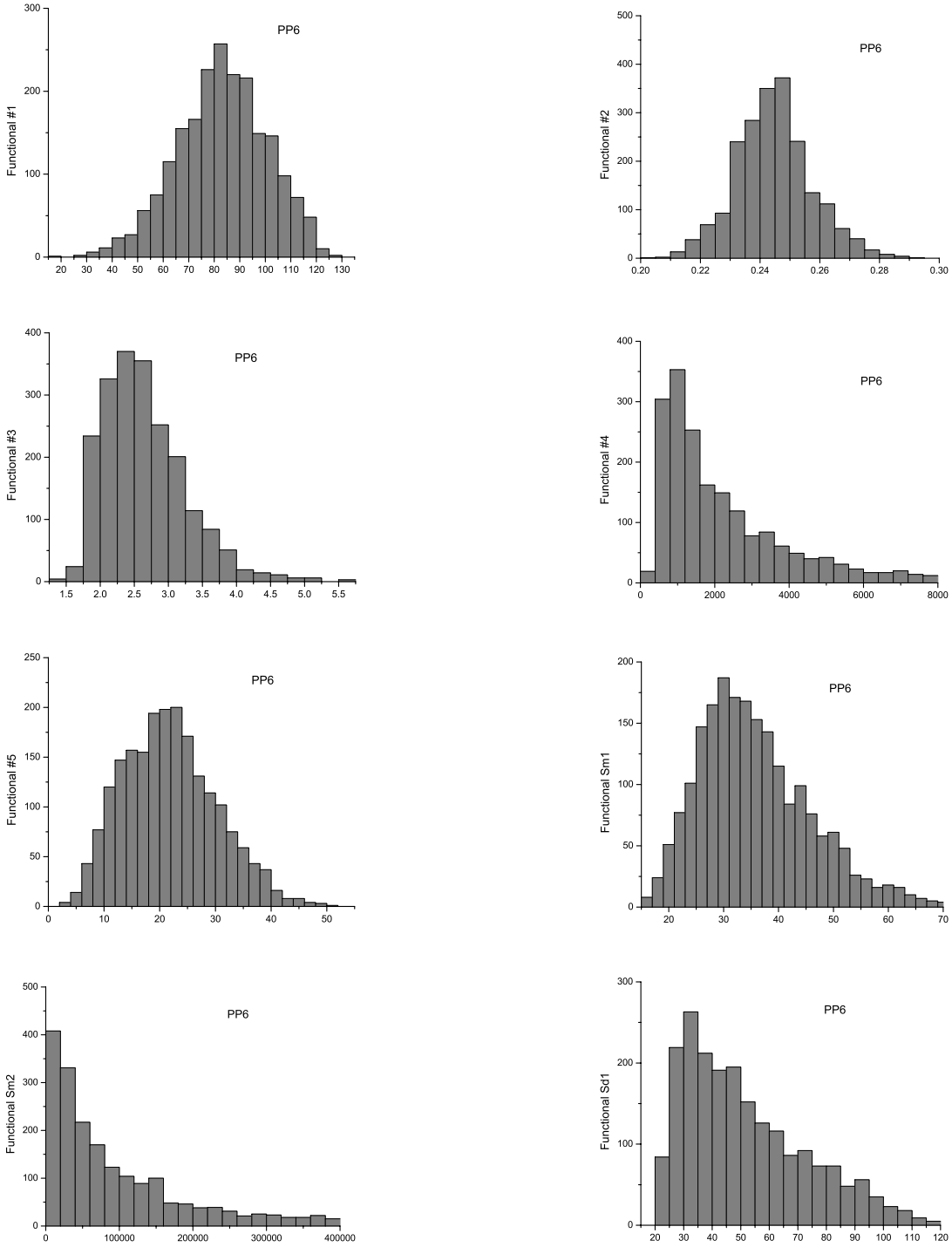


Figure C.3: Histograms for the properties of 5000 realizations sampled from the test problem by the pilot point method with six pilot point locations in the field and using a full objective function.

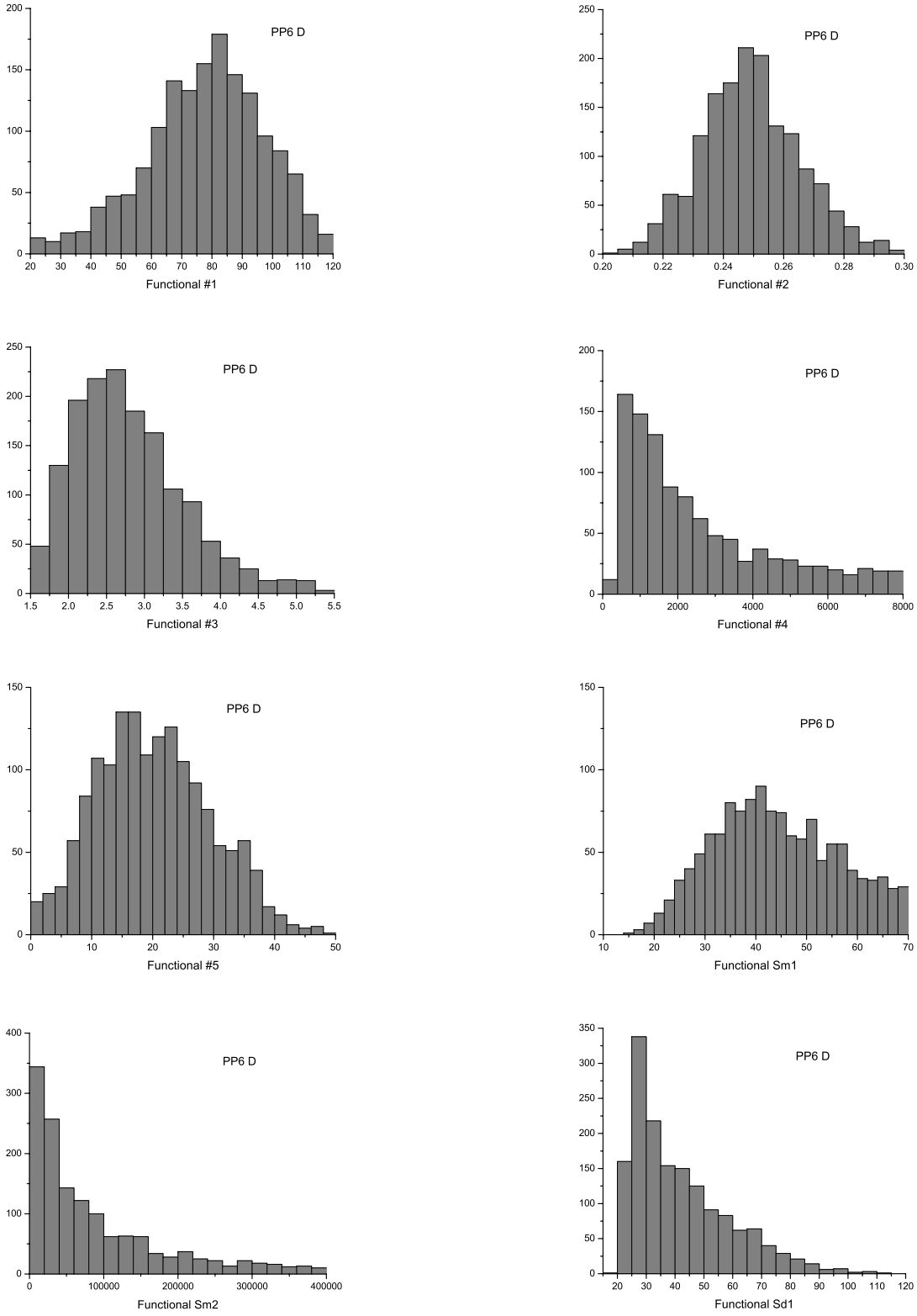


Figure C.4: Histograms for the properties of 5000 realizations sampled from the test problem by the pilot point method with six pilot point locations in the field and using the objective function with only squared data mismatch part.

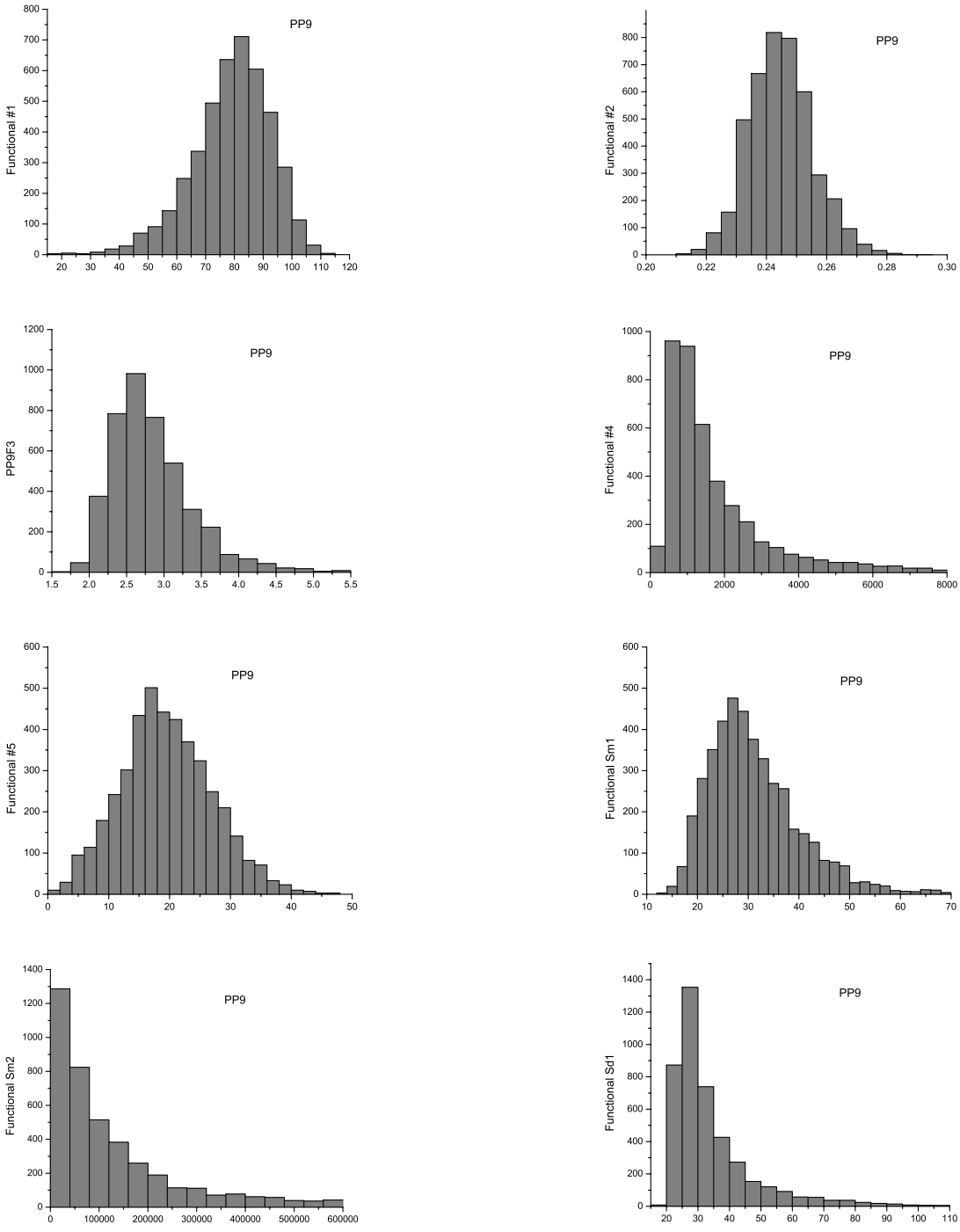


Figure C.5: Histograms for the properties of 5000 realizations sampled from the test problem by the pilot point method with nine pilot point locations in the field and using a full objective function.

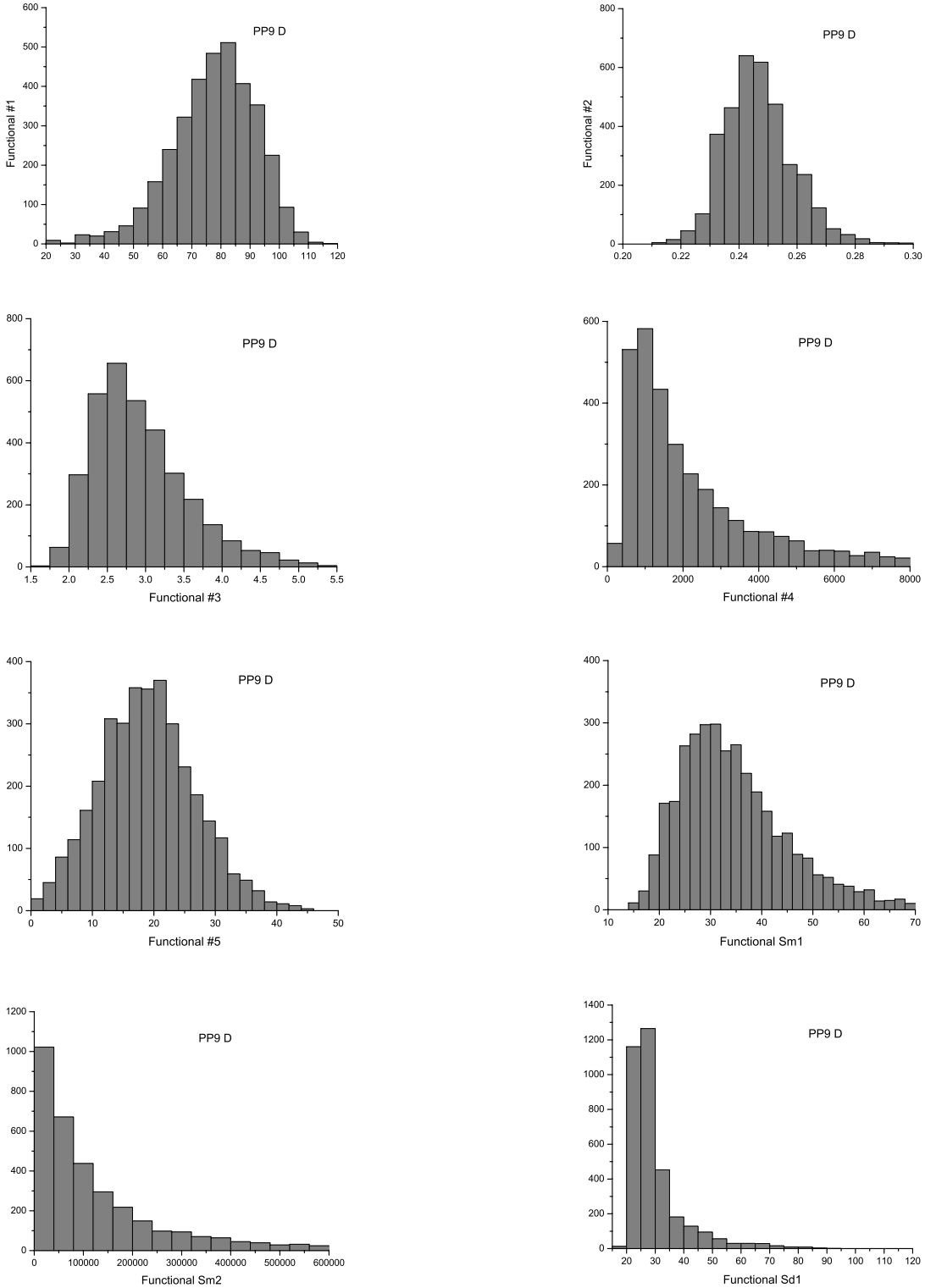


Figure C.6: Histograms for the properties of 5000 realizations sampled from the test problem by the pilot point method with nine pilot point locations in the field and using the objective function with only squared data mismatch part.

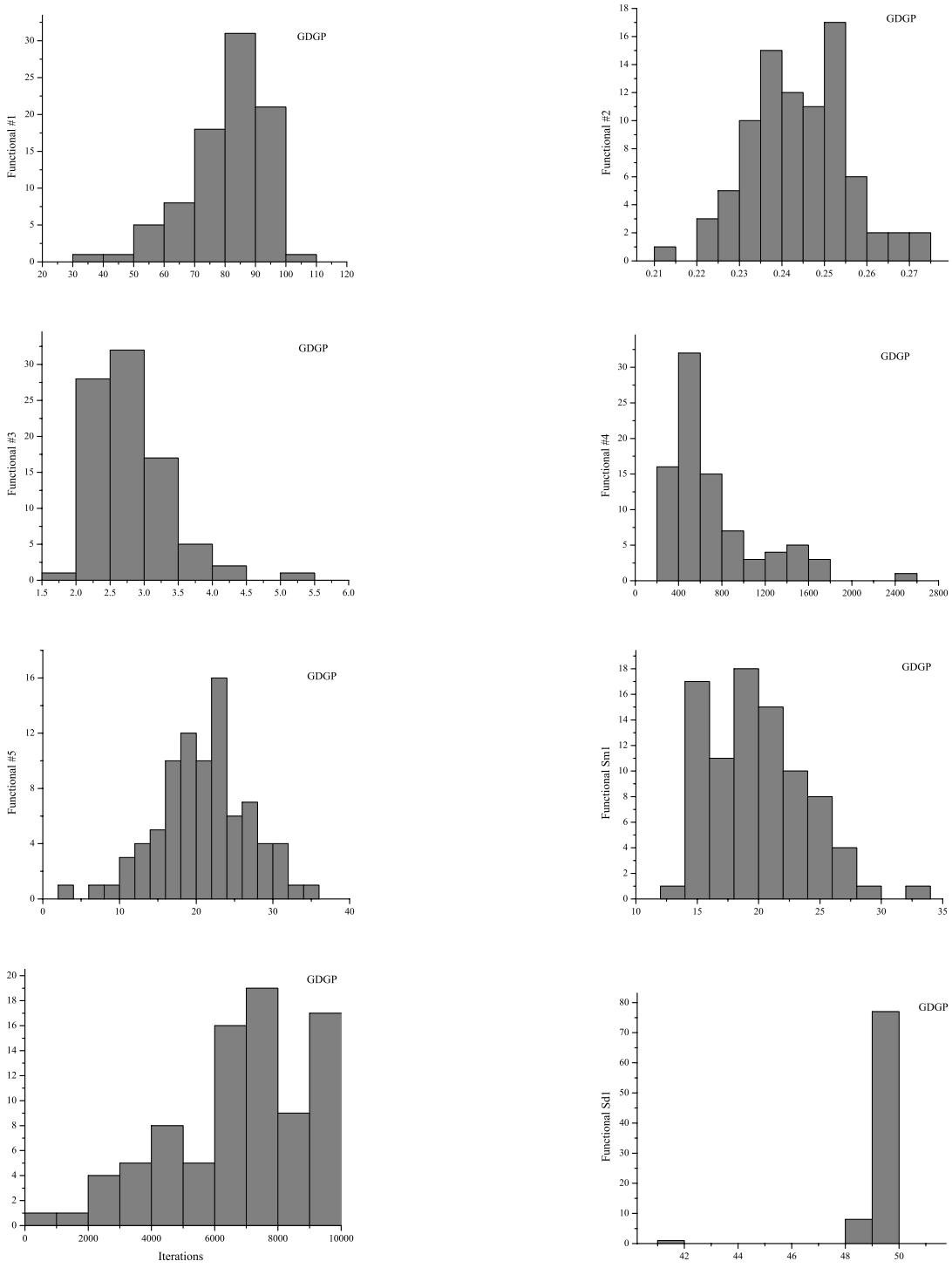


Figure C.7: Histograms for the properties of realizations sampled from the test problem by the gradual deformation method with global perturbation.

# APPENDIX D

Histograms of the realizations from all the approximate methods for each of the property are shown in this appendix together with the distribution from the second very long Markov chain for a better comparison of the sampling ability of each approximate method.

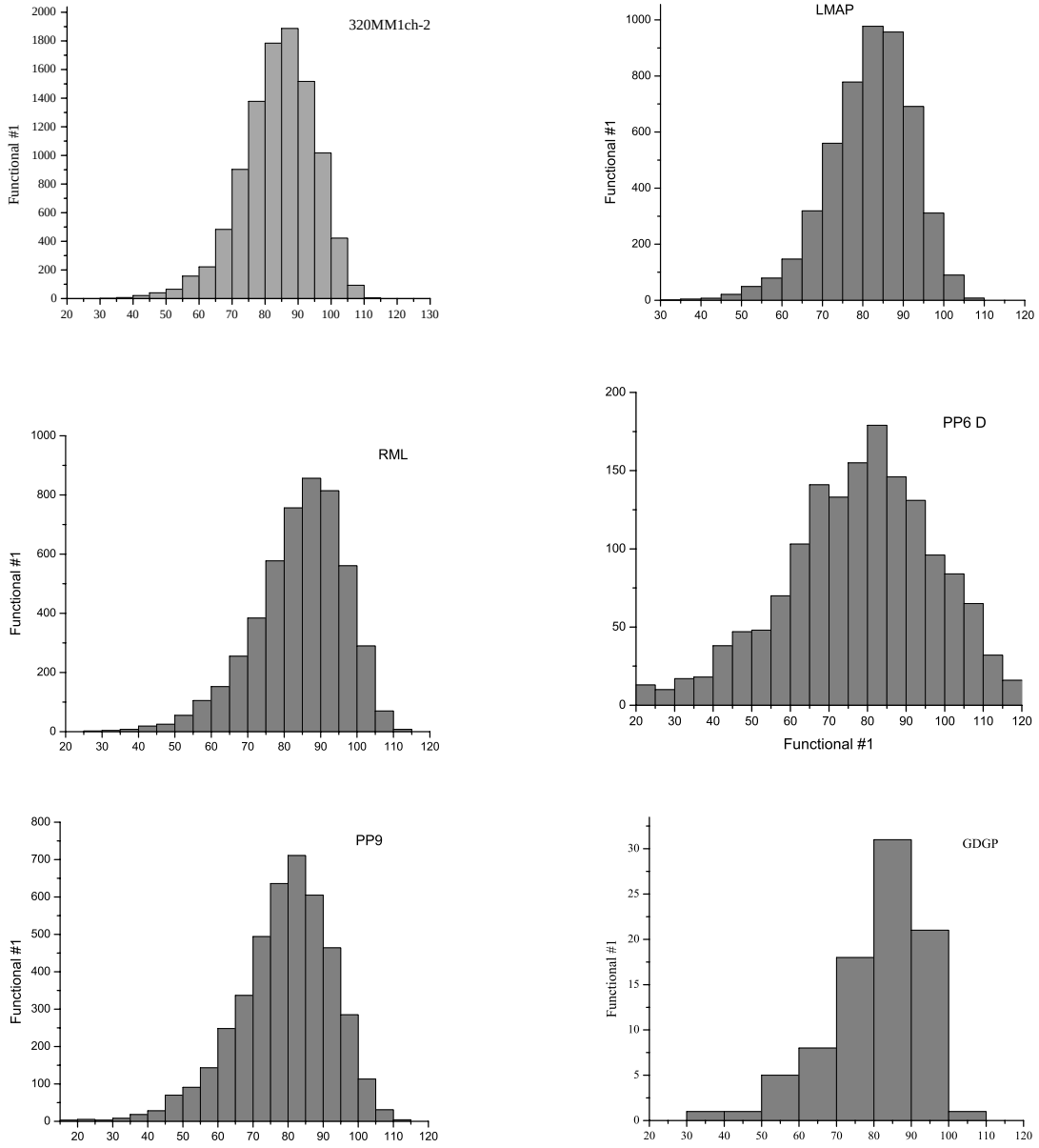


Figure D.1: The comparison of histograms of effective permeability from a variety of sampling methods.

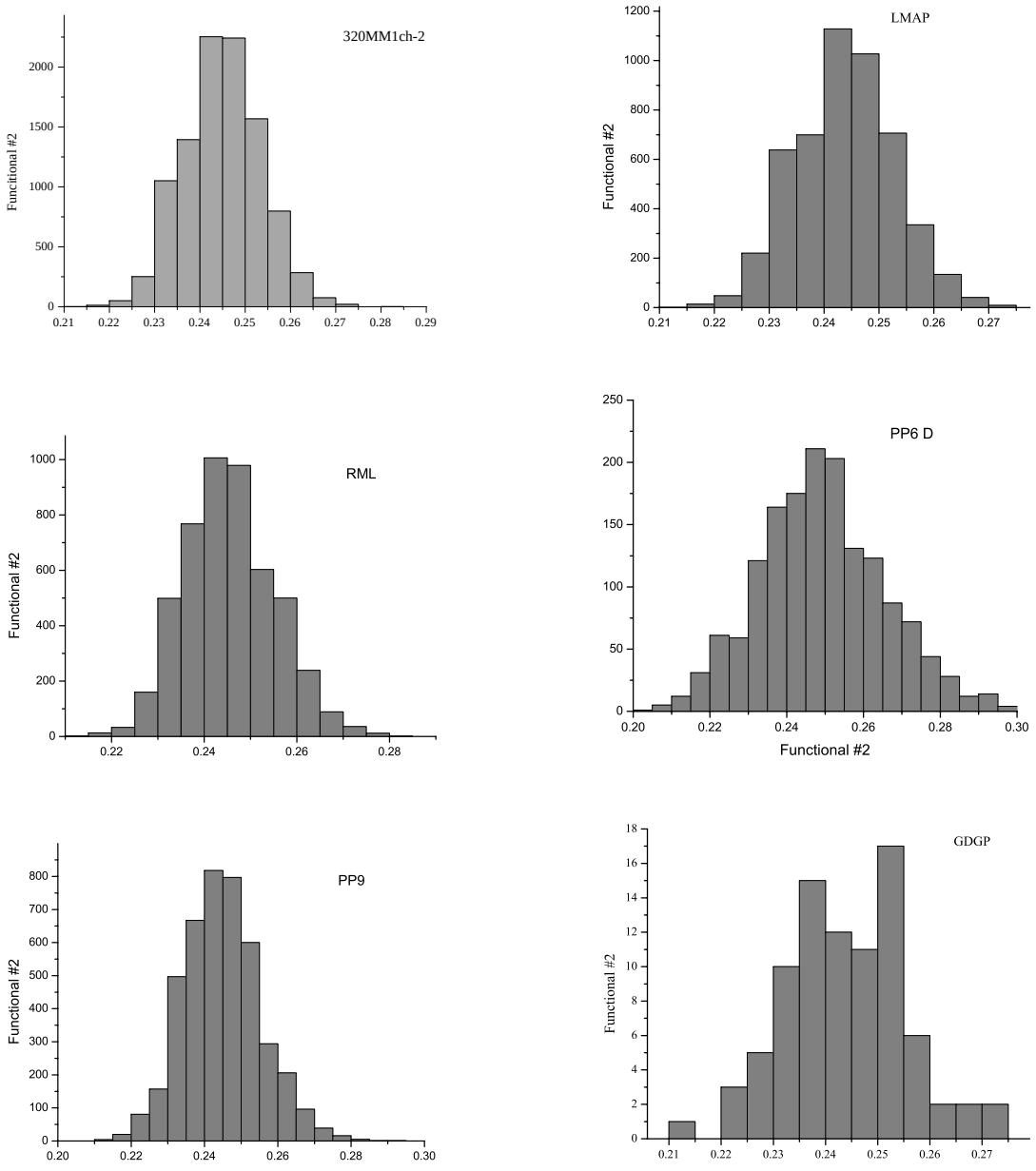


Figure D.2: The comparison of histograms of average porosity from a variety of sampling methods.

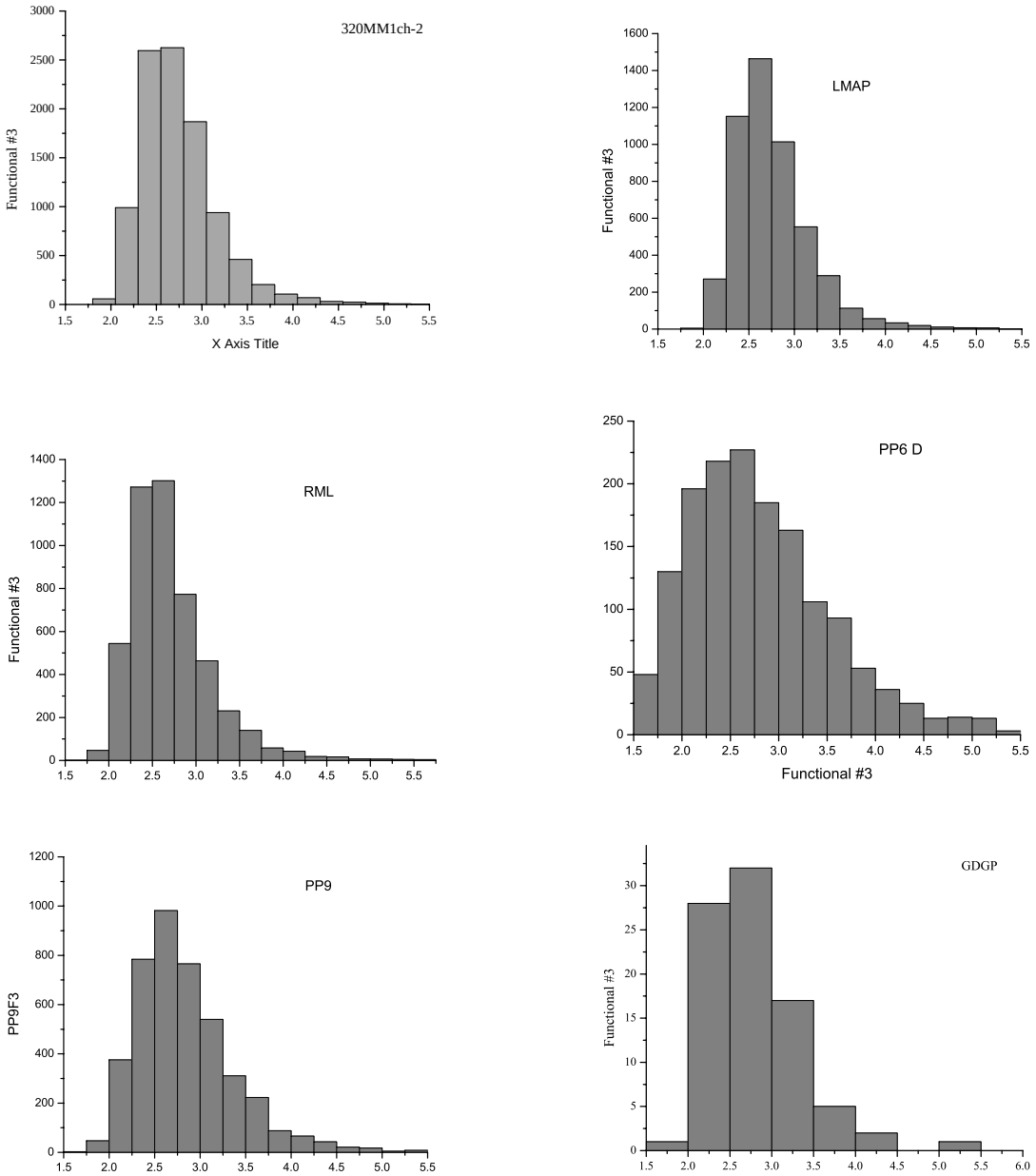


Figure D.3: The comparison of histograms of travel time from a variety of sampling methods.

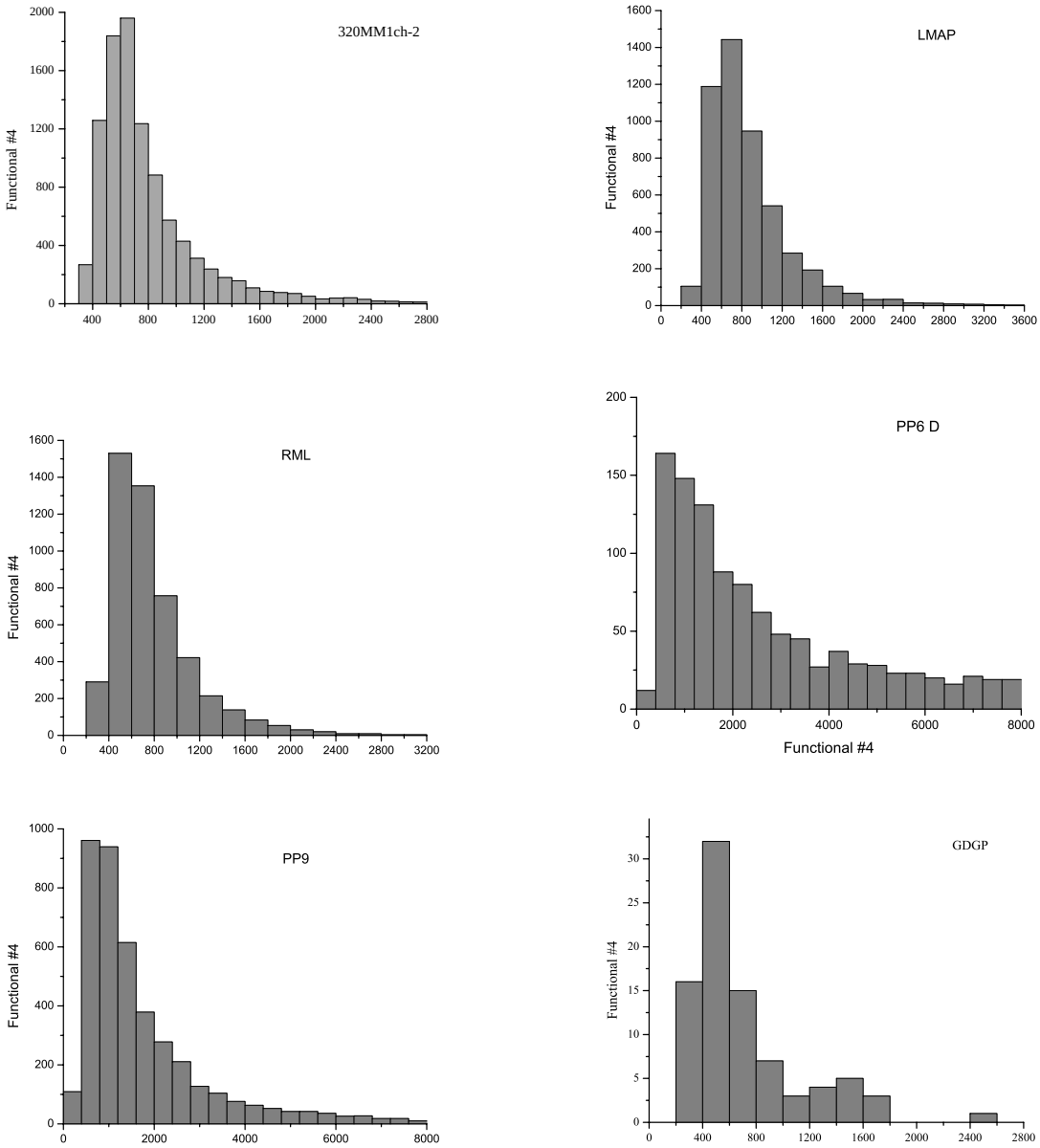


Figure D.4: The comparison of histograms of maximum permeability from a variety of sampling methods.

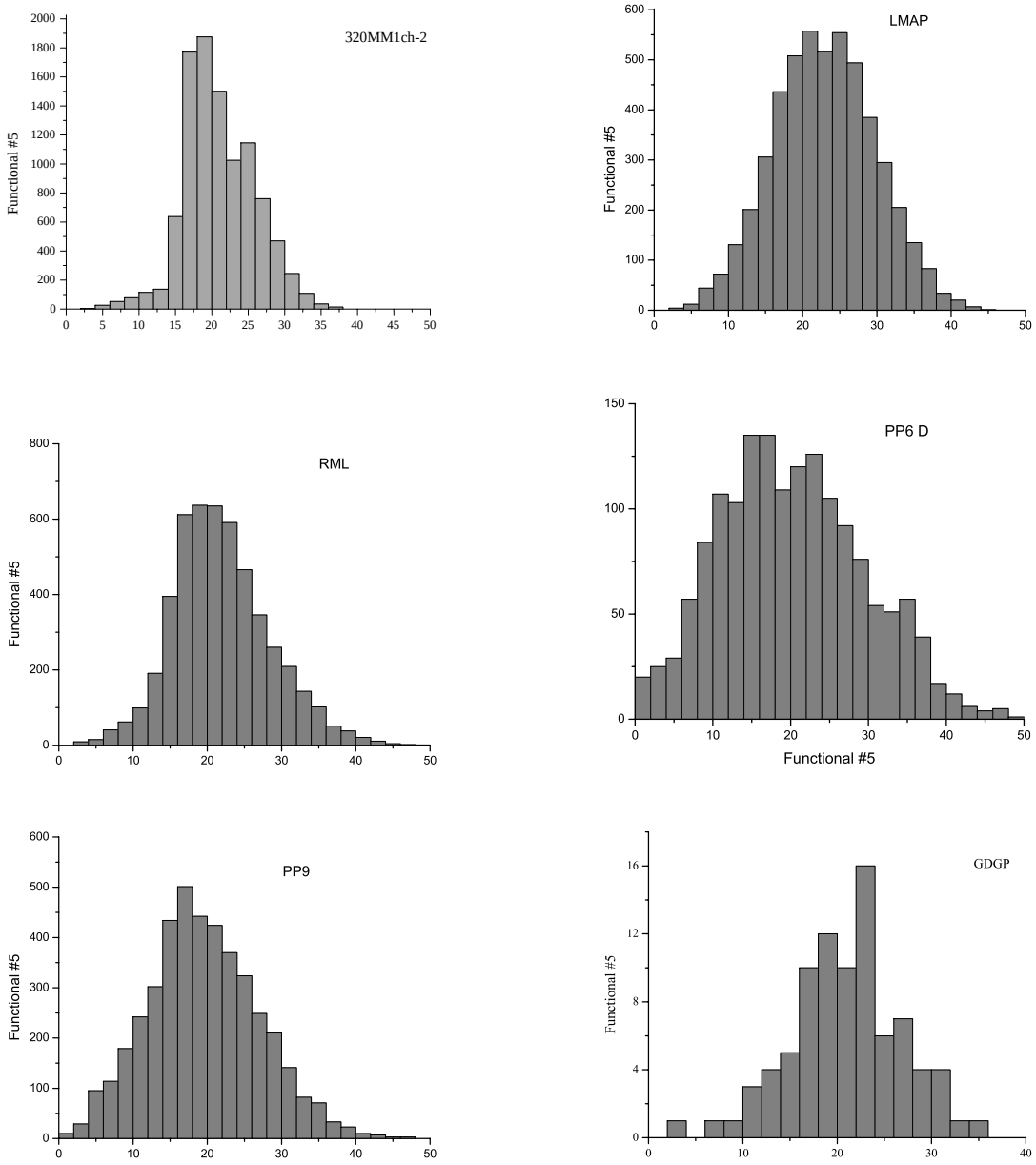


Figure D.5: The comparison of histograms of minimum permeability from a variety of sampling methods.

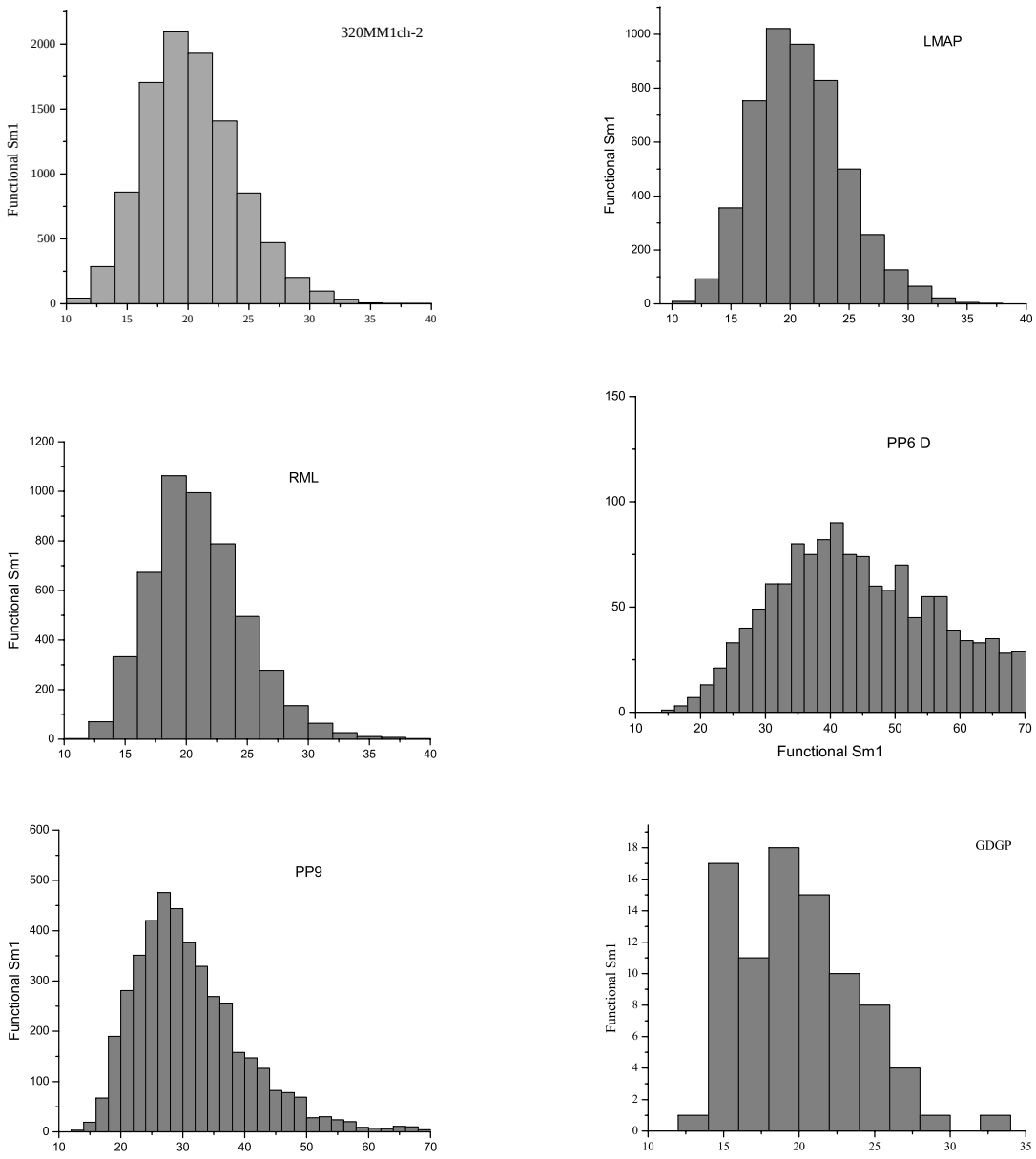


Figure D.6: The comparison of histograms of squared model mismatch about the prior model from a variety of sampling methods.

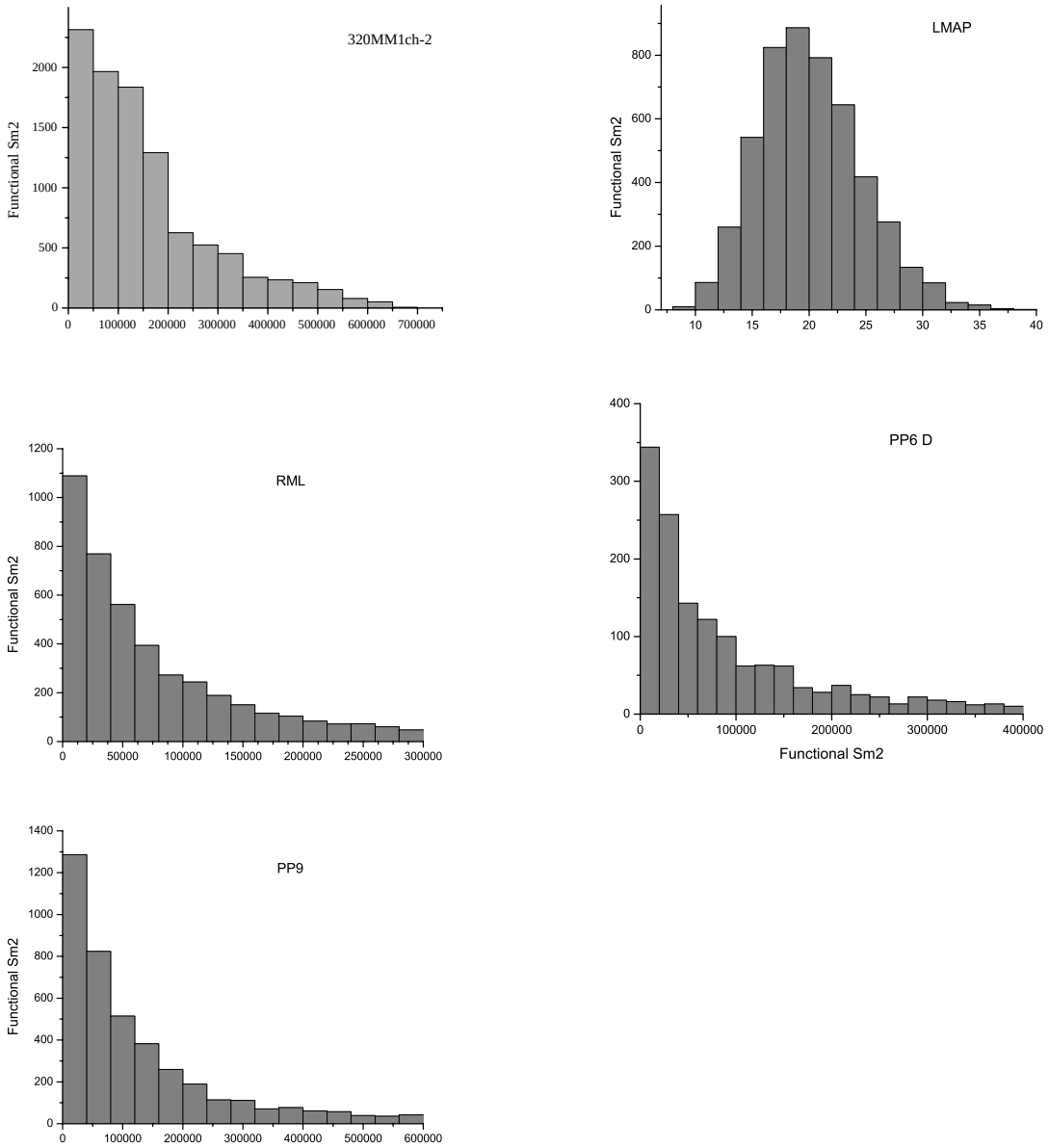


Figure D.7: The comparison of histograms of squared model mismatch about the MAP estimate from a variety of sampling methods.

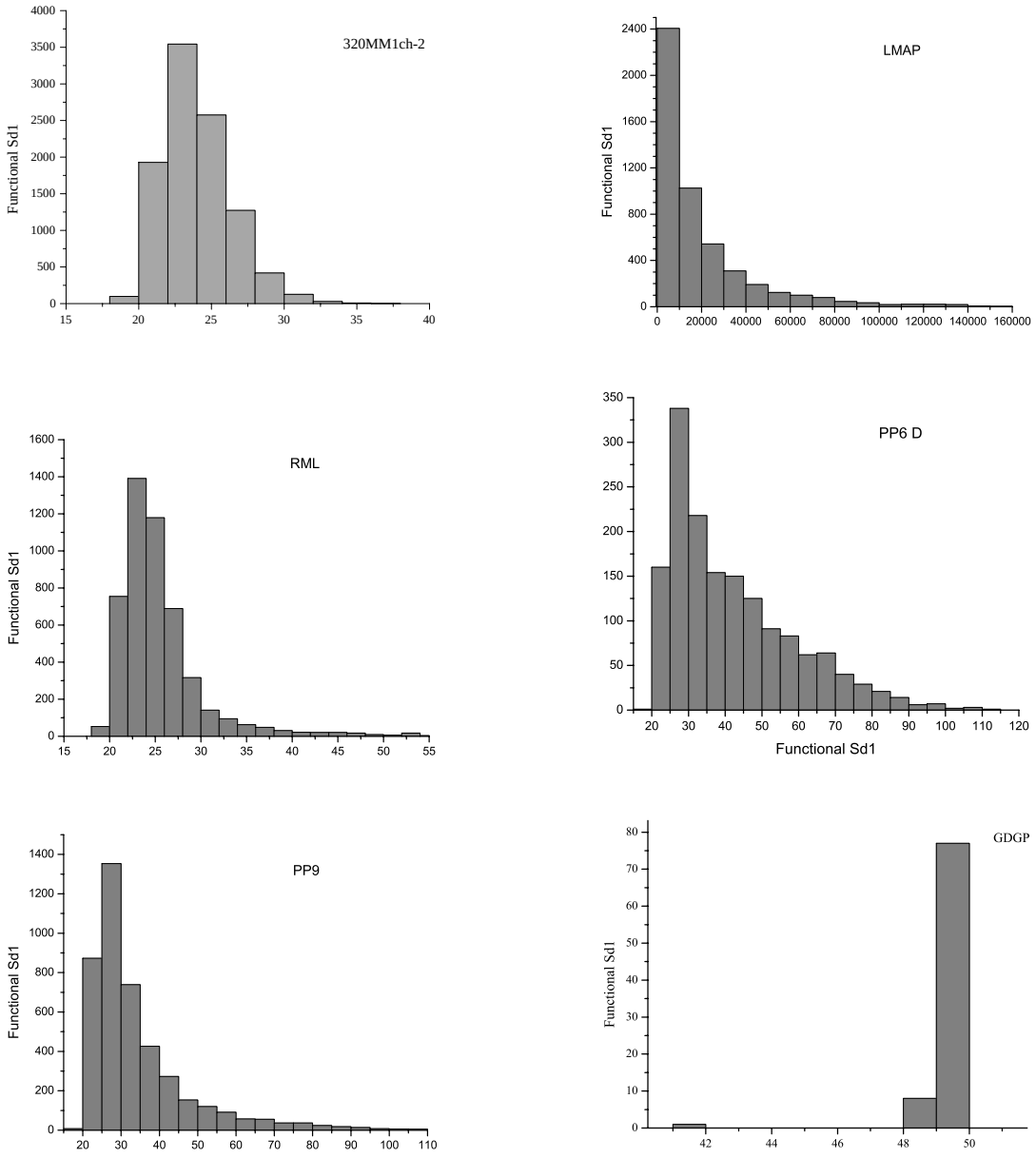


Figure D.8: The comparison of histograms of squared data mismatch from a variety of sampling methods.